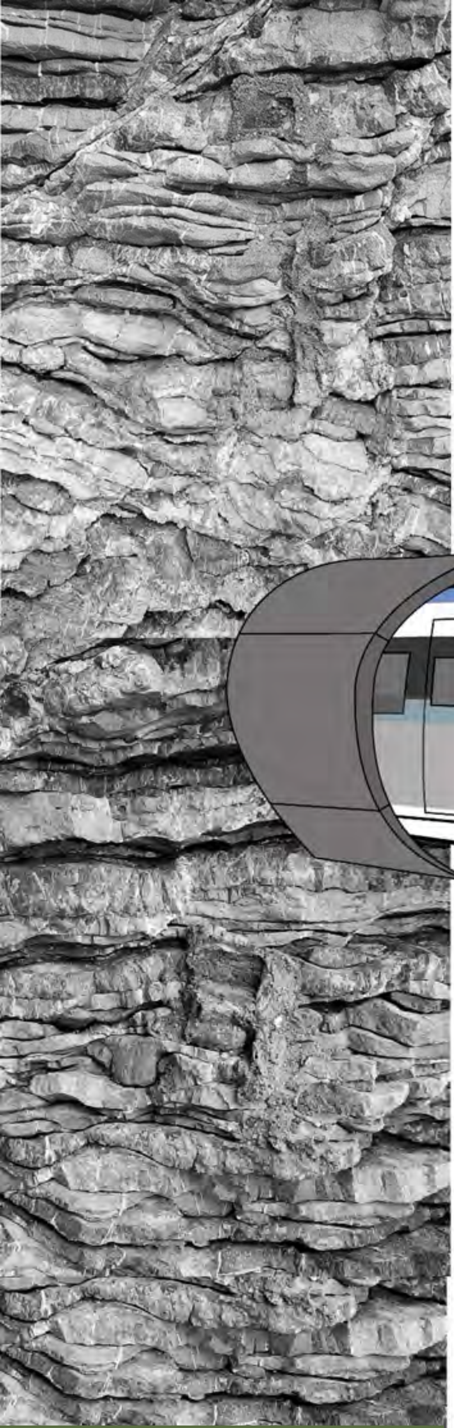

Feasibility Study of a High-Speed Metro in the Vaud Alps

Rocco Wennubst Pedrini, MSc

Prof. Michel Jaboyedoff

Sofie ten Bosch, MSc

Annik Schaufelberger, MSc

Dr. Elena Ravera

Prof. Lyesse Laloui

Avec les contributions de :

Prof. Jean-Luc Épard

Ing. Jean-Paul Dudt

UNIL | Université de Lausanne

ISTE Risk-group

EPFL | École Polytéchnique de Lausanne

LMS

clim⟷act

Funded by

Table of Contents

Table of Figures

Table of Tables

1 Introduction

Creating a high speed metro with innovative technology would allow the Vaud Alps to form one unique station, thanks to the rapid green mobility. The high speed VAlp Metro concept strives to render the daily commute attractive and feasible, promoting decentralized living and daily workforce travels. In around 30 minutes Aigle will be connected to Chateau d'Oex! Additionally, the tunnel can serve multiple functions, such as transporting goods, high tension power lines, fiber optics and more. The integrated product vision includes renewable energy infrastructure for both the excavation and operational phase, responding to Switzerland's mission of green electrical self-sufficiency by 2050.

In view of the ambitious pioneer concept, the current feasibility study is conceived by Prof. Laloui's LMS group of EPFL and Prof. Jaboyedoff's Risk-group at UNIL. The combined knowledge base provides an integral study approach.

The VAlp Express (CLIMACT project) outcome report investigates the location's geology in 3D, and refines geotechnical consideration, and proposes a small diameter twin-tube tunnel design. The technological innovations proposed in the study are a rapid-aerodynamic rubber tyred metro, re-uptake of tunnelling spoil, and aeolian and solar plants in the Vaud alps. Thereafter the energy predictions, carbon-dioxide evolution and cost-time models are proposed for the lightweight mountain metro. Finally, the next steps are proposed to concretize the integrated project proposal. A ten-year Gantt chart is envisioned to execute the VAlp Express mountain metro.

2 Metro Technology

A rubber-tyred metro is a form of rapid transit system that uses a mix of road and rail technology. The vehicles run on rubber tires guided along rolling pads for traction. Additionally, traditional railway steel wheels with deep flanges guide the vehicles through conventional switches and provide support in case a tyre fails. Most rubber-tired trains are purpose-built and designed for the system on which they operate.

2.1 Current Use

A rubber-tyred metro is proposed due to the gradients of the metro line. This technology uses a mix of both road and rail technology and is also used in the currently steepest metro in the world, the M2 in Lausanne. The vehicles run on rubber tires guided along rolling pads for traction. Additionally, traditional railway steel wheels with deep flanges guide the vehicles through conventional switches and provide support in case a tyre fails. Most rubber-tired trains are purpose-built and designed for the system on which they operate, which should also be done for this case. The large gradients and high speeds expected in the VAlp metro design can be met with this existing driverless technology.

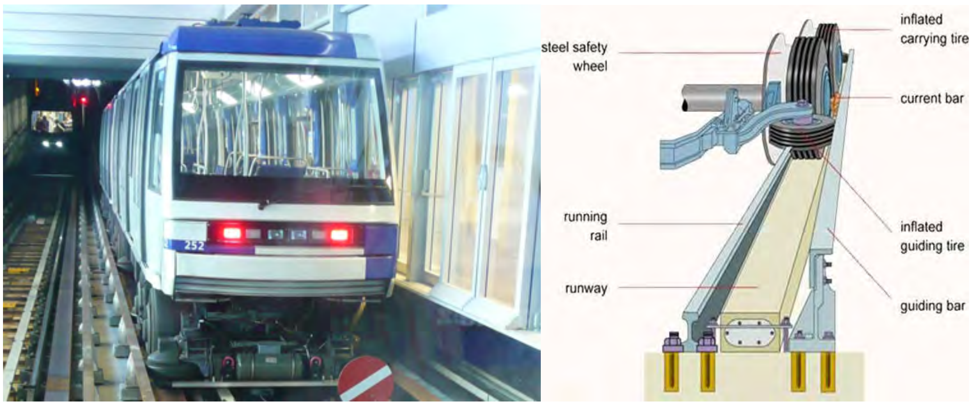

Figure 1 - The rubber-tyred Lausanne M2 metro (TL, 2021) and the rubber-tyred traction technology (railsystem.net).

Using a rubber-tyred metro technology has certain advantages compared to conventional steel rolling stock. The vibration damping guarantees passenger comfort, leading to a smooth mobility experience. Benefitting from large traction, faster accelerations and shorter braking distances can be achieved, allowing trains to be signalled closer together. This feature allows the vehicle to climb or descend steeper than what would be feasible with conventional rail tracks.

On the other hand, the technology's higher friction and increased rolling resistance causes a higher energy consumption of the system . Heat is generated in the tunnel, and must therefore be dissipated or recuperated. The system also generally has higher construction and maintenance costs as it requires ad-hoc technology.

2.2 Future Innovation

The rubber tyred metro rolling stock and systems are designed specifically for a project. Doing so greatly benefits the innovative VAlp concept; the technology can be optimally designed and adapted for the current project. For example, the research and development team could collaborate alongside rubber-tyred metro technology leaders Siemens and Alstom. These entities should be contacted to design the VAlp innovation.

To achieve a rapid green mountain metro line, the following aspects are important optimization and design considerations:

- *Aerodynamics of the vehicles and the metro line*

  The cross sectional blockage should be minimized and the impact of the aerodynamics in the tunnel has to be evaluated. Reduced pressure loading on the infrastructure should be a priority and this also leads to increased passenger comfort.

- *Light-weight rolling stock*

  There should be an optimization to have feasible light-weight rolling stock for the project leading to a decrease in rail wear and maintenance costs for the project.

- *Energy efficiency of the metro line*
  The energy consumption of the metro line should be reduced as much as possible. In a reference project, the Lille MEL in 2019 a proposed high-performance traction equipment solution from Alstom was targeted to reduce energy consumption of the metro with 20% (Alstom, 2019).

- *Targeted velocities*
  To keep with travel times between 10 to 15 minutes high velocities have to be reached in certain sections of the metro line, especially between Les Diablerets and Chateau d'Oex. This has to be considered during the design of the metro system.

3 Geology Overview

The VAlp Metro is located in the Vaudoise Alps, crossing Penninique and Ultra-Helvetic (UH) nappes alike. The tunnel initially crosses the Ultra Helvetic nappes, comprised of Triassic gypsum, cornieule, flysch and dolomite-limestone series. Moving North-East, the Niesen formations are crossed, consisting of varying limestone, sandstone and flysch lithologies. Finally, as the tunnel moves northward towards the final station, the Penninique nappes of Brianconais origin are crossed. These consist or shallow or distal limestone lithologies, which are cross cut by faults in the pre-alpine domain.

3.1 Tectonic Legend

Hereafter, a tectonic legend summarizes the formations crossed by the VAlp Metro line. In the scope of this study, smaller scale formations are grouped according to similar geotechnical characteristics. The rock types and stratigraphy are compiled by homogenizing the tunnel alignment lithological descriptions of the geological atlas 1:25'000 (12445 Chateau d-Oex, 1265 Les Mosses, 1285 Les Diablerets and 1284 Monthey).

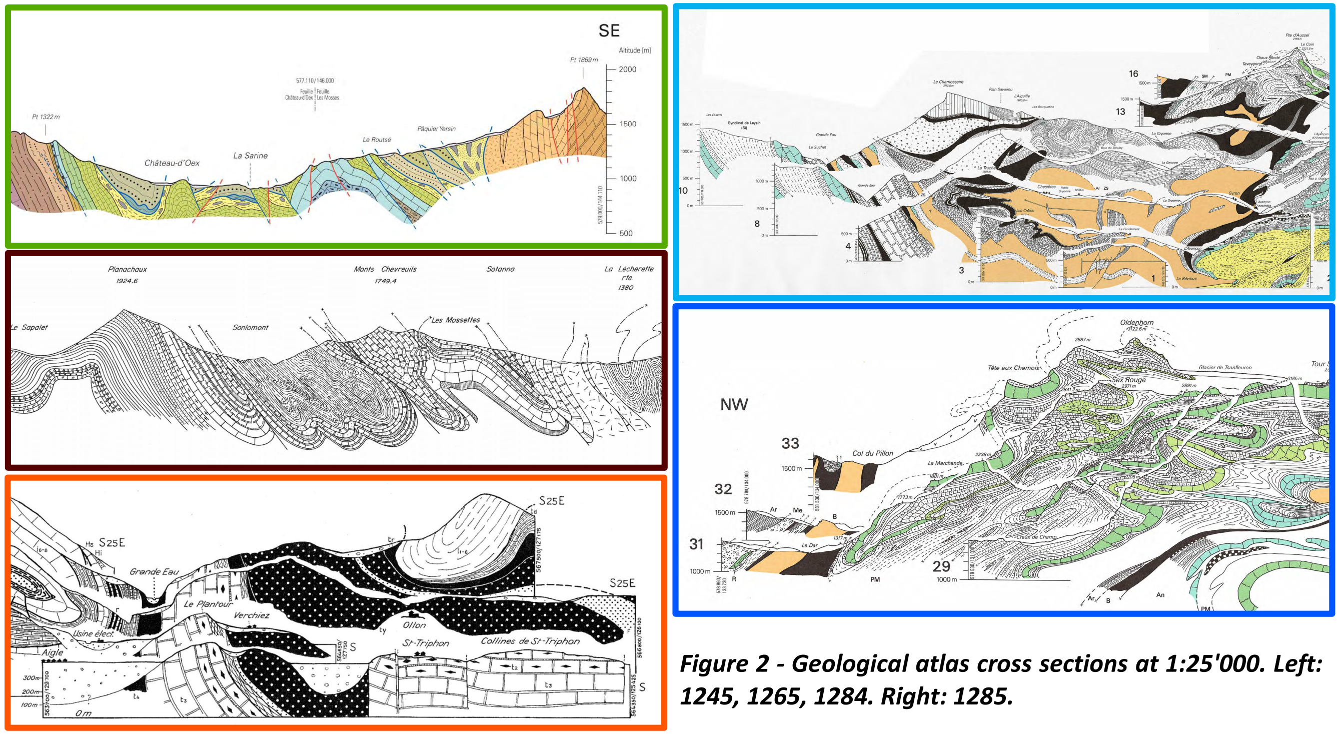

Figure 2 - Geological atlas cross sections at 1:25'000. Left: 1245, 1265, 1284. Right: 1285.

Table 1 - Tectonic legend of the study location.

Unit	***Formation***	***Rock Type*** *(relevance to geotechnical rock quality)*	***Variability*** *(along metro)*	***Additional notes***
Nappes Penniques	Nappe de la Simme Nappe de la Dranses Formation de Biot	f_H : Base de grèso-calcaire, avec alternance d'argilites. Après marnes grises à lamelles, avec intercalations de calcaire et grès.	Bancs de Δ0.5m, épaisseure 200-500m	Grès faiblement cimenté, donc a faible résistance mécanique.
	Nappe de la Bréche	Flysch, pelites, et couches rouges calco-marneuses	Bancs de Δ0.1m, épaisseure 20-60m	Mécaniquement similaire à la Nappe de la Simme
	Prealpes Medianes Plastiques (**PMP**) *+ Serie Profonde interne*	$i_{7\text{-}8}$: Calcaire massif du malm, trias calcaire a gros bancs e_3 : Couches Rouges, calcaire fins avec argiles et marnes schisteuses	Bancs de Δ10m, épaisseure 20-60m Bancs de Δ0.1m	Série proximale de dépôt, donc variabilité stratigraphique le long du tunnel. Présence de failles verticales !
	Prealpes Medianes Rigides (**PMR**)	$t_{2\text{-}3}$: Calcaire gris massif à gros bancs. Présence de silez et calcaire dolomitique. $i_{6\text{-}8}$: Calcaire massif, compact et uniforme.	Bancs de Δ10m, épaisseure 200m Épaisseure 150m	Le sommet stratigraphique définie par les faibles Couches à Mitilus, formé par alternance de calcaires et marnes bitumineuses.
	Zone Submediane	f : Gypse, cornieules, calcaire, dolomie et schiste.	Bancs de Δ4m,	Zones indifférenciées à haute variabilité !
	Nappe du Niesen (avec Lias d'Oidoux)	$f_{g\text{-}s,m,z,c}$: Flysch gréso-schisteux laminé, conglomérat massif sans ciment, calcaire détritique sableux zoogénique, flysch conglomératique à bancs fins de calcaires blancs t : Dolomie claire et argilites, avec 10m de cornieules bréchiques initiales	Épaisseures de 50-100m, 50-80m, 20-40m, 10-80m Bancs de Δ10-20m, épaisseure 130m	Conglomerat mal classé (rond et anguleux) Base triassique peu favorable !

	Flysch Priabonien	f_U: Flysch et calcaires marneux	Discontinue	Zones indifférenciées à haute variabilité !
Nappes Ultrahelvetiques (UH)	**Nappe du Meilleret**	f_{m4} : Conglomerat polygénique avec éléments cristallins f_{m3} : Calc-arénites a ciment silteux, calcaires gréseux f_{m2} : Arkoses à gros grain f_{m1} : Flysch indifférencié, contentant turbidites à conglomérats, grès fins, pélites et calc-arénites. f_m : Conglomérat basal a matrice silto-marneuse.	Bancs de Δ10m Épaisseures de 50m, 100m, 50m, 60-100m, 10m	Conglomerat polygénique mal classé (rond et anguleux) Base triassique peu favorable ! Conglomerat basal à faible cohésion !
	Nappe de Arveye Nappe du Sex-Mort	f_S : Cornieules, schistes argileux noires, marnes à calcaires gréseux, flysch	Discontinue, sauf les marnes 200m	Haute plasticité !
	Nappe de Bex	$t_{d,y}$: Anhydrite rubané ou bréchique, cimenté par NaCl Cornieules avec dolomie en bancs	Discontinue, sauf les bancs de dolomie Δ0.5m	Gypse par hydratation en surface. Haut risque de déformations de la matrice ! Formes karstiques / vides abondants !
	Nappe de Bex – Lias des Mines	$l_{1\text{-}6}$: Calcaire détritique basal, surmonté par un calcaire sombre dur à fossiles. $l_{1\text{-}6,s,c}$: Schistes et calcaires-schisteux, contenant zones finement micacés et pyriteuses	Bancs de Δ5m, épaisseures de 70m et 200m.	Calcaire gris très compètent
	Nappe d'Anzeinde	$i_{6\text{-}8}$: Calcaire bleuté siliceux $c_{1\text{-}4}$: Marnes à calcaire noduleux	Bancs de Δ0.5m, épaisseure 50m et 10m	
	Flysch de la Plaine-Morte (PM) Flysch parautochtone helvétique (H)	f_P : Flysch gréso-marneux, avec blocs sporadiques calcaires ou conglomératiques. Contient wyldflysch et schistes argileuses.	Lames de calcaire de <200m	Zones à haute variabilité !

VAlp EXPRESS

4 Geological Model

Geological maps, topographical models, dip data, cross sections and tectonic sketches were used as primary inputs for the three-dimensional geological model. Cross-checking of the horizon's limits was manually performed using specific point deep borehole data. Nonetheless, the study area's scale (>30km in length), relies on the model being a first order approximation of the region's structural geology. Future field exploration (deep boreholes and exploratory tunnels) can be used as additional input data to refine the same model.

4.1 Model Input

The 3D geological model is constructed using the MOVE program by Petroleum Engineering. Geospatial graphical information system performance is extended in the third z-dimension by combining GIS vector and raster inputs, with verticalized XY cross sections. Four geological maps are merged and prepared prior to import and workflow in move.

The following overview shows the combined surface (XY) input data. It contains the merged geological atlas raster, the polyline tectonic boundary vectors, and the lithological dip data points. Additional data used in the model (not pictured), include the catchment basin polygons, surface flow polylines, karst feature point locations and instability PLG.

Figure 3 - Surface model input data processed with QGIS.

The second overview shows the combined vertical plane (XZ) input data. It contains the merged topographical map raster, and the location of 52 cross sections. In red the ten Monthey sections, in blue the thirty-two Les Diablerets sections, in brown those of Les Mosses, in green the three cropped Chateau d'Oex ones. Finally, four ad-hoc cross sections are constructed for the study location.

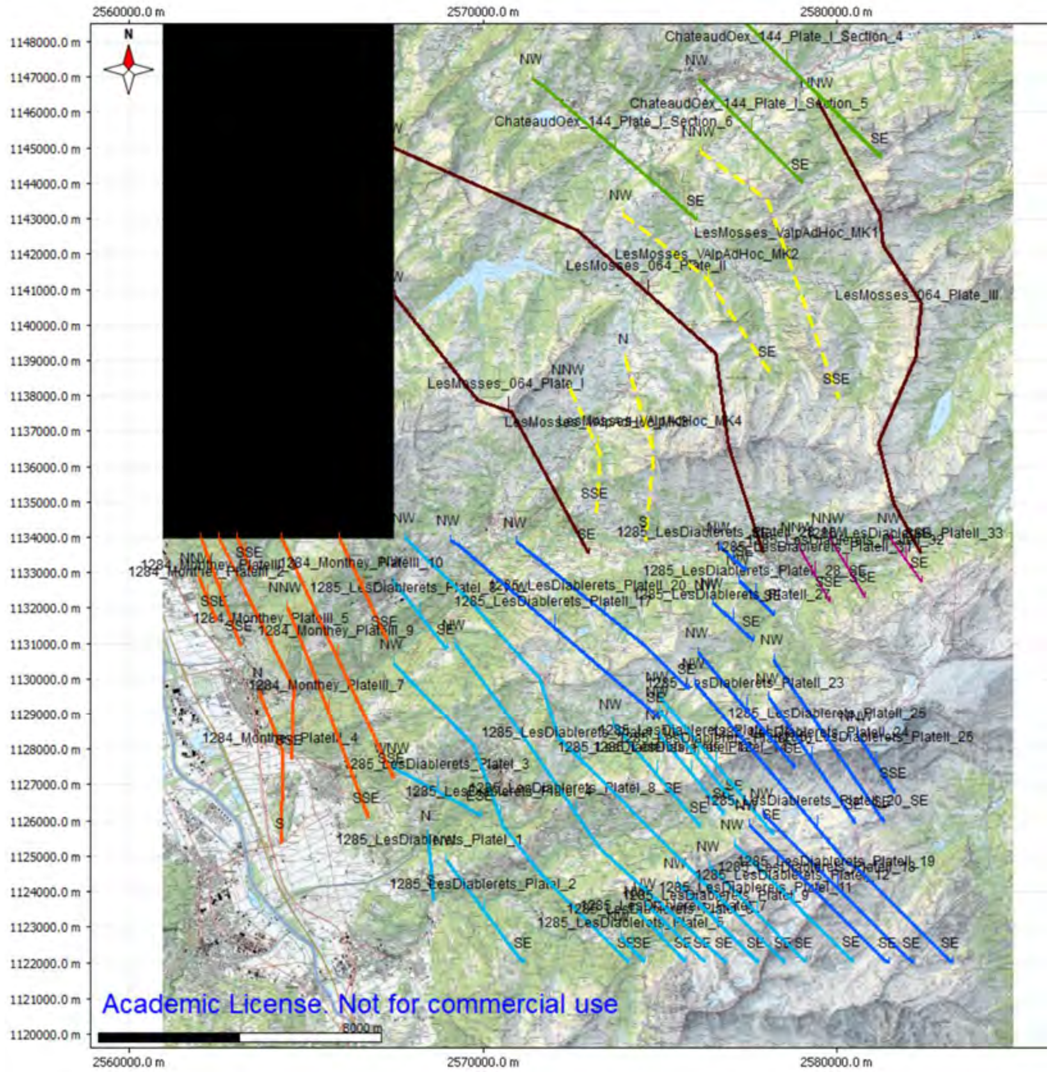

Figure 4 - Vertical input data processed with Adobe Illustrator, QGIS and MOVE (section tool).

The model is constructed in three phases. Firstly, all horizon (see 3.1 Tectonic Legend) limits are traced by a polyline tool on the 52 cross-sections. Secondly, the surfaces are linearly projected between each cross section. Abundant manual clipping of polylines is required to maintain realistic fold axes when projecting linearly between adjacent sections (eg. Arveye folds below Villars dip 30deg to the NE). Thirdly, the surfaces are modified by snapping/deforming planes according to surface-projected tectonic boundaries and point dip data.

Finally the two are joined in three dimensions by projecting and geo-referencing all data according to the LV96 coordinate system and the Swiss Digital Elevation Model (DEM) at a downsampled resolution of 2m.

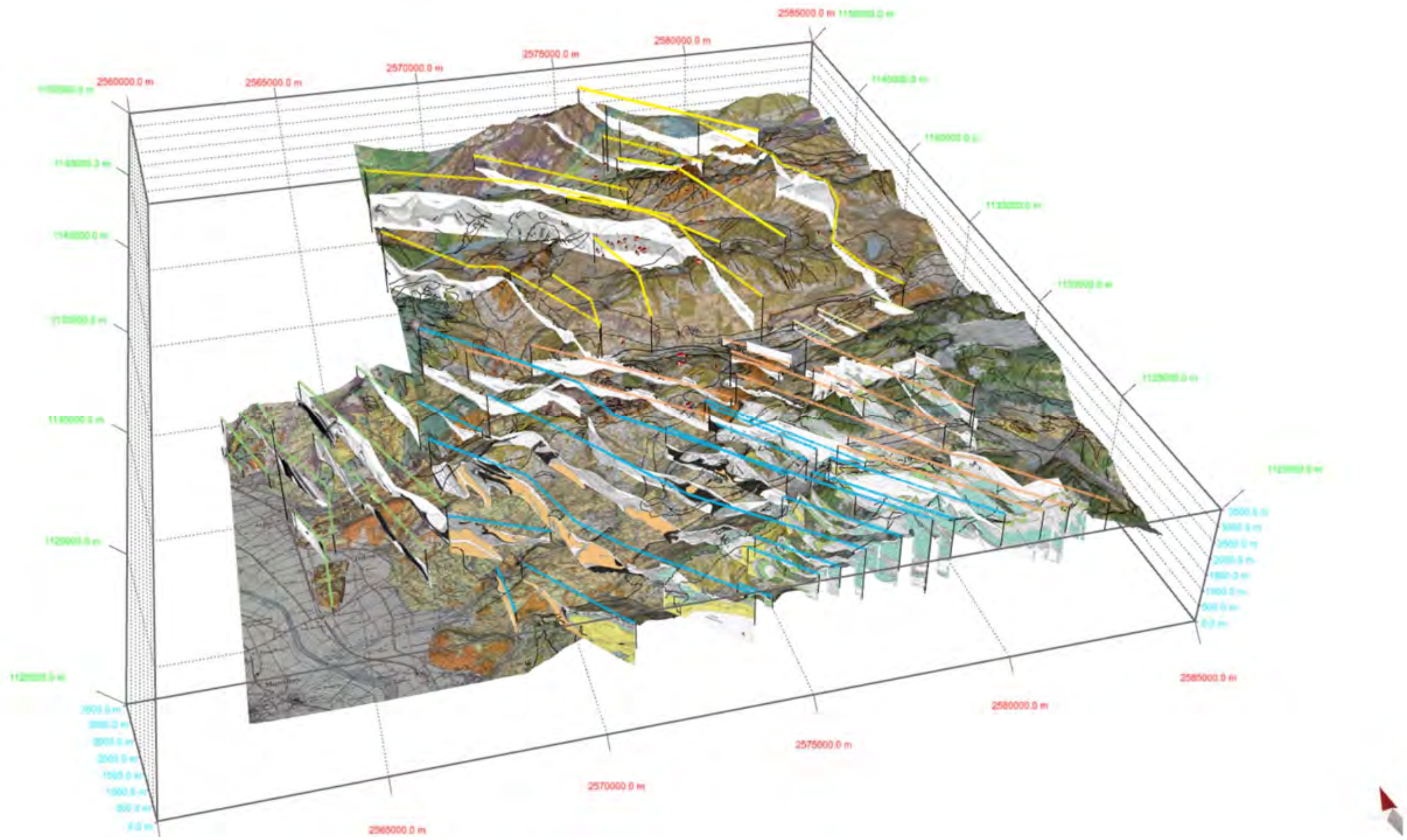

Figure 5 - Complete input data used to create the geological model in three dimensions, including geological cross sections and surface data.

4.2 Model Result

Stratigraphic limits are constructed over the ~30km study region. The horizon limits are defined by the coloured surfaces.

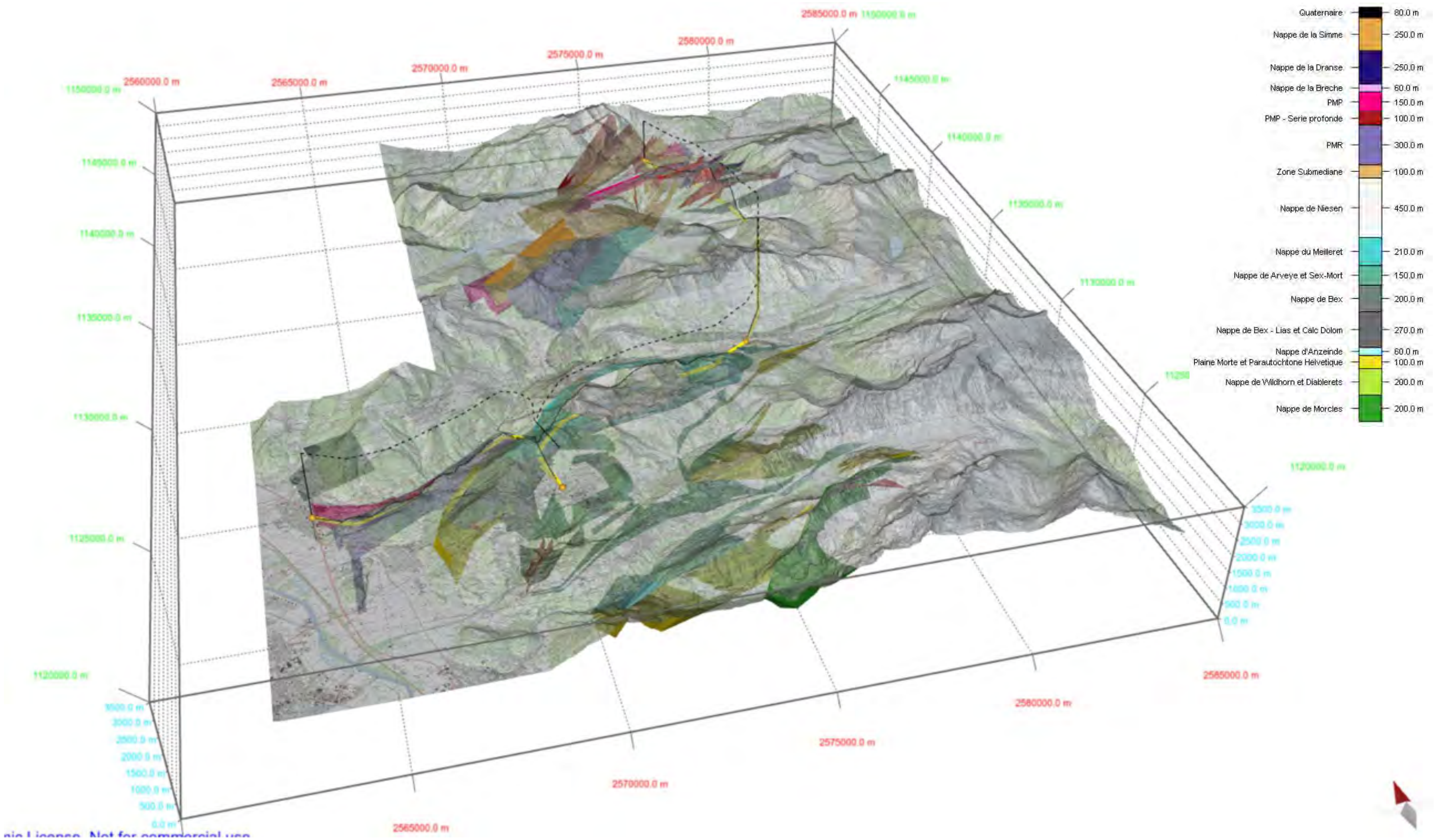

Figure 6 - 3D Geological model of stratigraphic boundaries, with overlain topographical map. Top view.

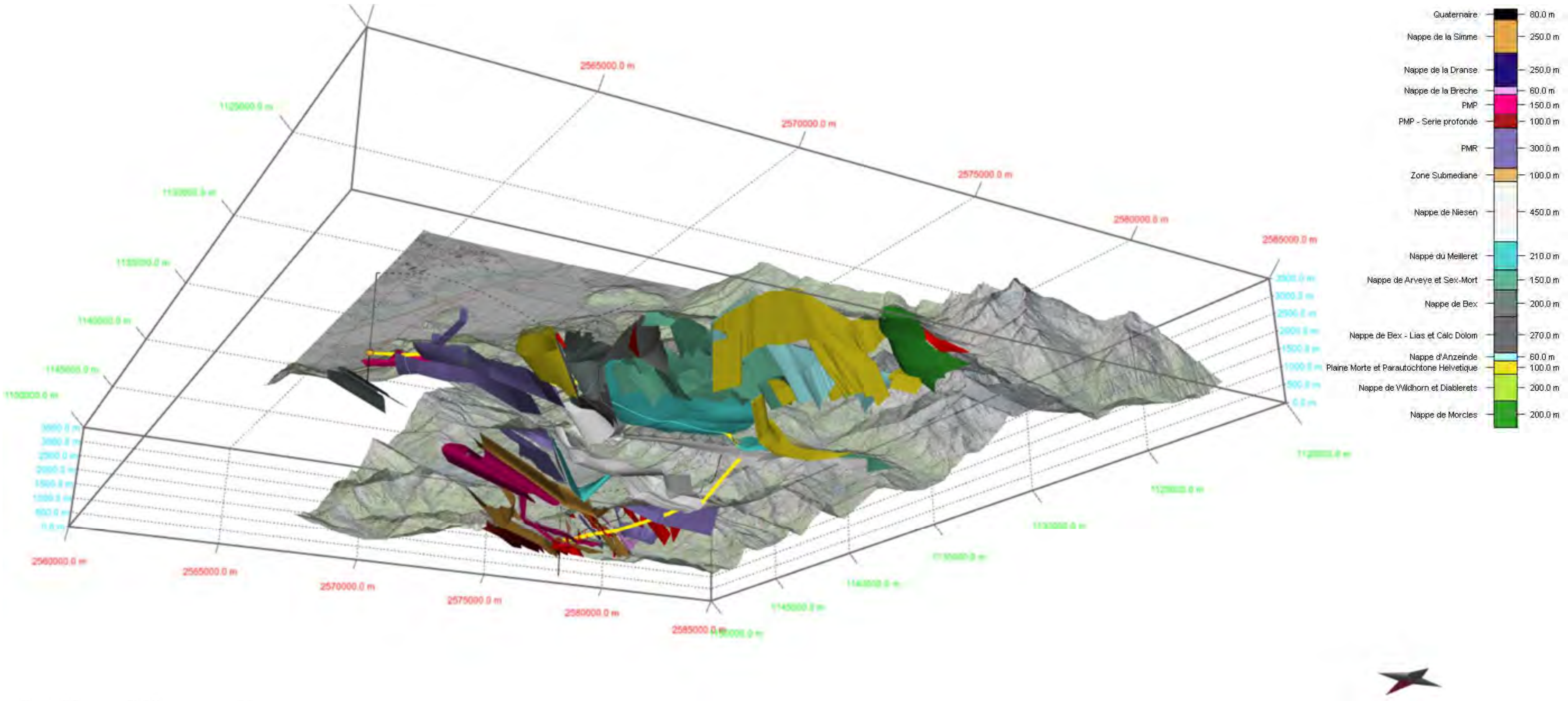

Figure 7 - 3D Geological model of stratigraphic boundaries, with overlain topographical map. Bottom view.

A dozen deep boreholes are used to cross check stratigraphic limits (Guichet Cantonal de Vaud). Nonetheless, the surface error is estimated to be in the decametric range at the surface, but may attain significant offsets at greater depths.

4.3 Future Calibration

The model file (.mov) can be easily calibrated to borehole data (Z-direction). Future development of the VAlp metro concept will require deep borehole exploration to reduce the subsurface uncertainty of stratigraphic limits. Additionally, such findings would provide in-situ rock quality (Q), information on discontinuity spacing and in-situ geotechnical parameters (point load, etc.).

Boreholes may be complemented by common geophysical exploration such as cross-hole seismic tomography. Such measures are especially useful to identify the location of weathered Triassic rock (near Villars), karstic void location and size, and fractured limestone-dolomite (near Aigle and Chateau d'Oex).

5 Tunnel Alignment

The 3D model is used to optimize the tunnel alignment between the four stops such that it:

- minimizes excavation in unfavourable rock
- reduces maximal gradients
- maintains ~30km length

This is done by iteratively creating a 3D polyline for the tunnelling route.

5.1 Overview

The resulting trace connects the four stops over a 34.25 kilometre tunnel. Two of those serve two way traffic from and to Villars, meaning the TBM will excavate ~32 kilometres.

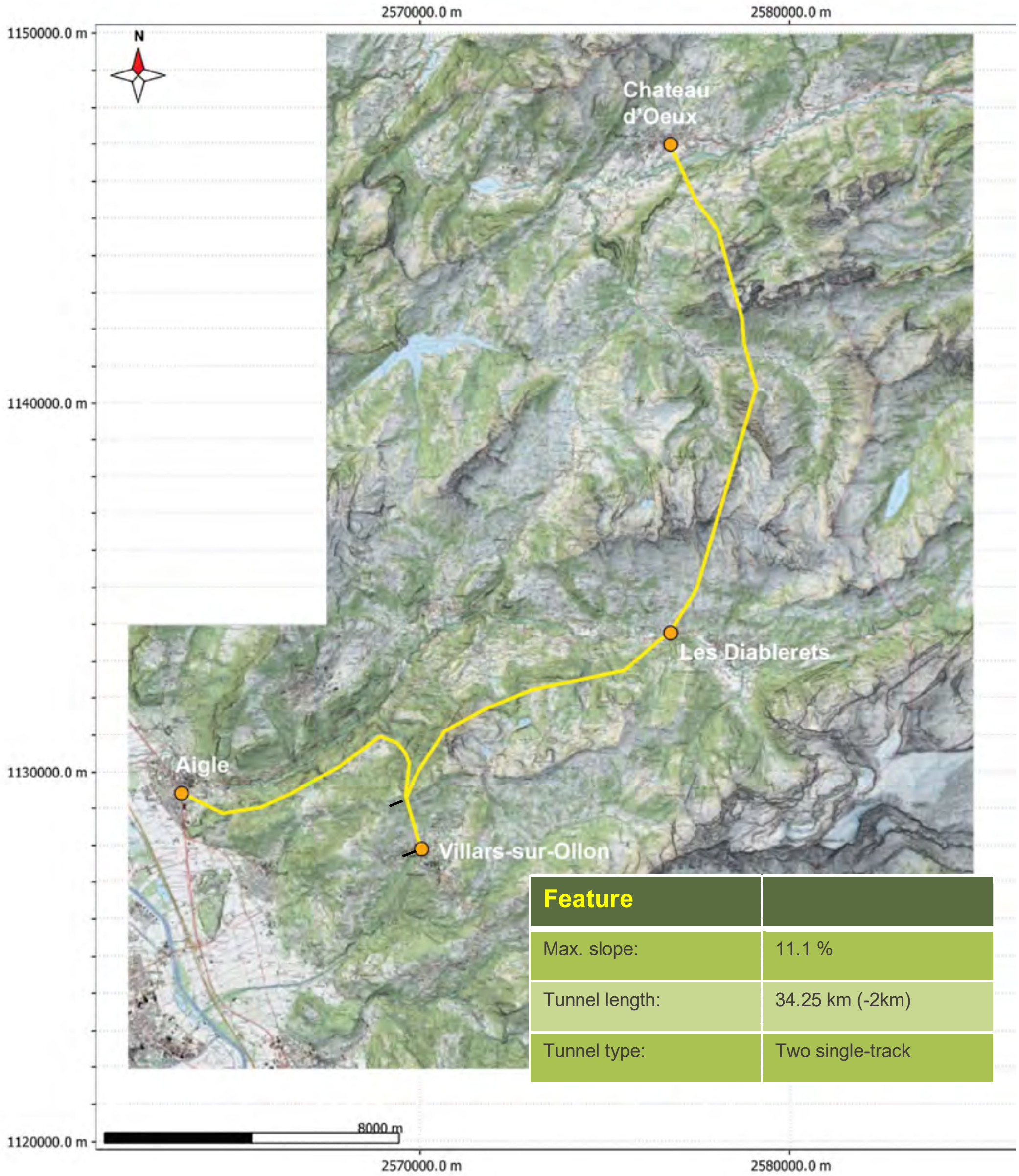

Figure 8 - Map view of the VAlp Metro connecting the vaud alps over a 34.25km line. Note the 2km long two-way tunnel section coming to and leaving Villars-sur-Ollon.

More precisely the tunnel alignment and stops are segmented in three segments connecting the four stations.

Table 2 - Length and gradients for the three tunnel segments connecting the Vaud Alps.

Stops	
Aigle - Villars	Length: 9.7km Gradients: 6.9%$_{avg,}$ 10.9%$_{max}$
Villars - Diablerets	Length: 10.0km Gradients: 4.2%avg, 11.1%max
Diablerets – Chateau d'Oex	Length: 14.6km Gradients: 1.5%avg, 7.2%max

5.2 Geological Cross-Section

The geological model and tunnel trace polyline are used to extract the geological cross-section for the VAlp Metrobetween Villars-sur-Ollon, Les Diablerets and Chateau-d'Oex. The DEM elevation data is exaggerated by a factor of two with respect to the horizontal distance.

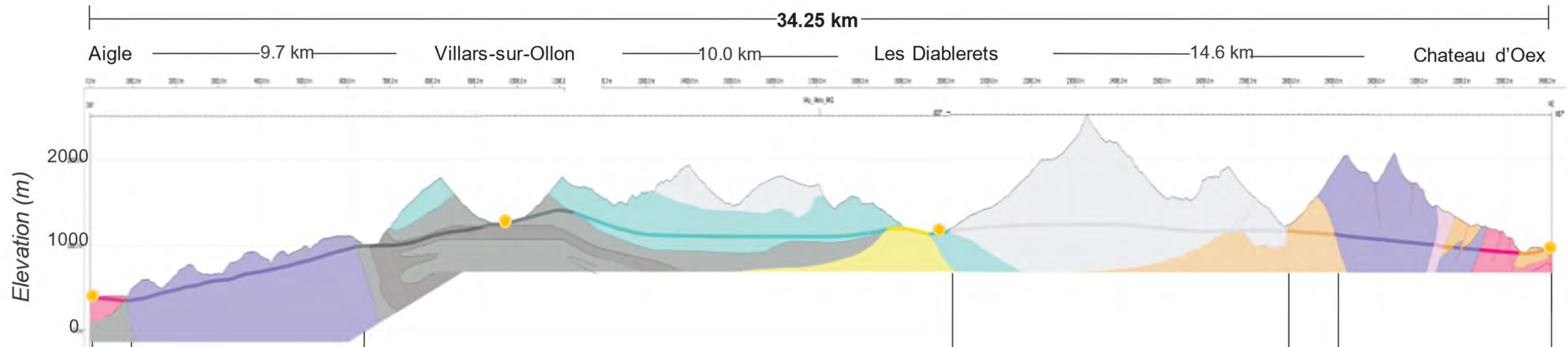

	Q.	Pennique	Ultrahelvetique					Pennique	UH	Pennique		
	Q.	PMR	Lias calc.	Trias	Meilleret	PM	M.	Niesen	Priab. flysch	PMR	B. S.	PMP
Type	conglom	massive limestone, dolom limestone, quartzite	limestone, detritic limestone, calc-shale	gypsum, anhydrite, dolomite	polyg conglomerate, calc-arenite, arkose, flysch, conglomerate	marly flysch, limest blocs, clayey slate		marly flysch, massif conglomerate, sandy limestone, clay and dolomite	See PMR	flysch, marl, limest and sandst intercal		limest, couches rouges
Dip	n.a.	60-90°	0-45°	0-30°	0-30°	30-90°		0-45°	45-90°	30-60°		0-30°
RMR	~70	100 - 50	81 - 41	60 - 0	100-41	60 - 21		81 - 41	100-50	81 - 41		100 - 50
Karst	no	no	no (?)	yes	no	no		no	no	no		no (?)
GC range	1-2	1-3	2-3	3-4	1-3	2-4		1-3	2-4	2-4		1-3

Table 3 - Tunnel details considering length and elevation gain along the studied tunnel alignment. Additional notes mention potential risks.

Formation	***Length*** *(km)*	***Max. Inclination*** *(°)*	*(%)*	***Final Altitude*** *(m)*	***Risks***	***Additional notes***
Quaternary	0.790	-3.3	-3.7	450	Water inflow, non-cohesive blocks	Morraine
Bex	0.070	-3.1	-3.4	450		
PMR	5.400	7.8	8.7	1000		Vertical massive limestone bands
Bex	0.330	2	2.2	1000	Swelling while hydrating anhydrite, cornieule cavities, mechanically weak	
Bex – Lias des Mines	0.660 0.620 0.440 0.970	0.7 6.2 9.8 4.7	0.8 6.9 10.9 5.2	1000 1075 1150 1225	Overlain by weaker lithologies of calc-schiste	Strong basal lithology (70m of detritic limestone to dark grey massive limestones)
Bex	0.400 1.420 0.320	2.7 7.3 -10	3.0 8.1 -11.1	1250 1425 1375	Swelling while hydrating anhydrite, cornieule cavities, mechanically weak	
Meilleret	1.780 2.600 2.870	-8.2 -0.4 1.7	-9.1 -0.4 1.9	1125 1100 1175	Uncemented basal conglomerate, calcium carbonate dissolution features, variability in lithological boundary unkown	Strongly cemented massive conglomerate
Plaine-Morte (PM)	0.980	-3.8	-4.2	1150		
Meilleret	0.570	0	0.0	1150	Lithological uncertainty	Undefined flysch, conglomerat or breche
Niesen	7.850	0	0.0	1150	Potential crossing of flysch UH formations for 400m at km. 6.4	Max. overburden 1275m, avg. overburden 600m
Flysch Indiff. (UH)	1.100	1.4	1.6	1200	Gypsum (at <50m from the surface), dissolution features	Potential vertical plumes of gypsum
PMR	2.300	-3.0	-3.3	1100		Sub-vertical massive limestone (first formation dipping 40-70° NW, second dipping 70-vert SE), then transitions to dolomite at km. 1.8
Brèche	0.250	-3.2	-3.6	1100		
Simme	0.200	-3.5	-3.9	1075		Flysch schisteux conglomératique

PMR	0.180	-3.5	-3.9	1075		Likely flysch marno-greseux a lentilles calcaires
Simme	0.060	-3.5	-3.9	1075		Extensive sub-vertical faulting separates lithologies
PMR	0.400	-3.5	-3.9	1050	Crosses clay bearing distal facies (Couches Rouges)	
PMP	0.920	-2.9	-3.2	900		Proximal facies of massive limestone, vertical faulting at km. 0.4 and 0.7
Simme	0.770	6.5	7.2	950		Sub-vertical faulting and potential PMP limestone between m. 60 and 170, vertical fault at km. 0.7

5.3 Spoil Utility

The reuse of excavated material is a primary practical and economic consideration of the pilot project. Quality and thus market value depends on the geology and TBM excavation method (EPBS or double-shield). The material reuse applicable for the afore specified sedimentary lithology can be used for:

1.) Limestone-dolomite aggregate production and backfilling material for infiltration zones (Rahimzadeh et al., 2018). The PMR and Trias limestone, quartzitic limestone and dolomite are deemed suitable. These aggregates have a market value of 14.-chf per metric ton.
Creating rapid basin infiltration systems (RIBS) to refill the water table in limitrophe communes is proposed. This is key in reaching the project's goal of sustainable living in the Vaud alps. Assuring water availability to extraction wells is critical in view of water scarcity induced by the rapid degradation of alpine glaciers (Sommer et al., 2020). Zones will be constructed following ad-hoc studies of the water tables along the tunnel alignment. Additionally, their impact will be monitored using moisture probes, monitoring wells and multi-level samplers with ports (Andres et al., 2013).
Good quality spoil = 5000m of the tunnel

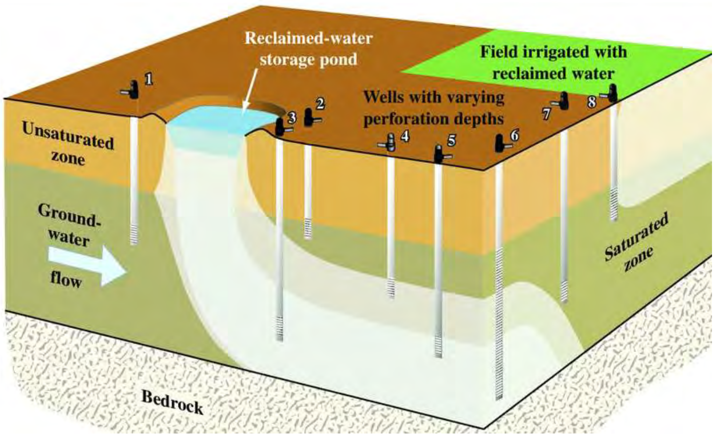

Figure 9 - Rapid infiltration basin systems (RIBS) built with coarse aggregates. They rapidly replenish the water table, counteracting the drawdown effects of water wells (Kaehler and Belitz, 2003).

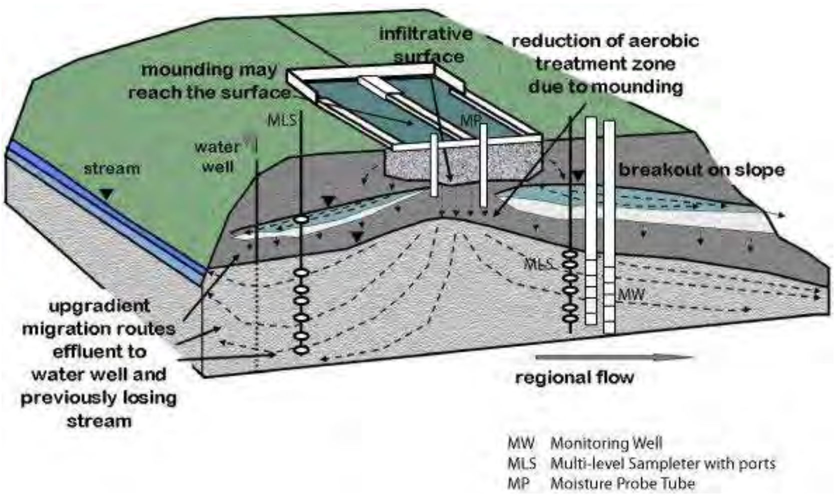

Figure 10 - Monitoring of RIBS via wells, moisture tubes and multi-level sampling (Andres et al., 2013).

2.) Crude gypsum-anhydrite from the Triassic nappes near Villars can be used for industrial production such as in cement and plaster production. This incentive counteracts the engineering geology hurdles in troublesome Triassic lithologies. The increase TBM cost and slow advance win karsted cornieules leads to good quality spoils with an economic value of 12.-chf per metric ton.
Good quality spoil = 2000m of the tunnel

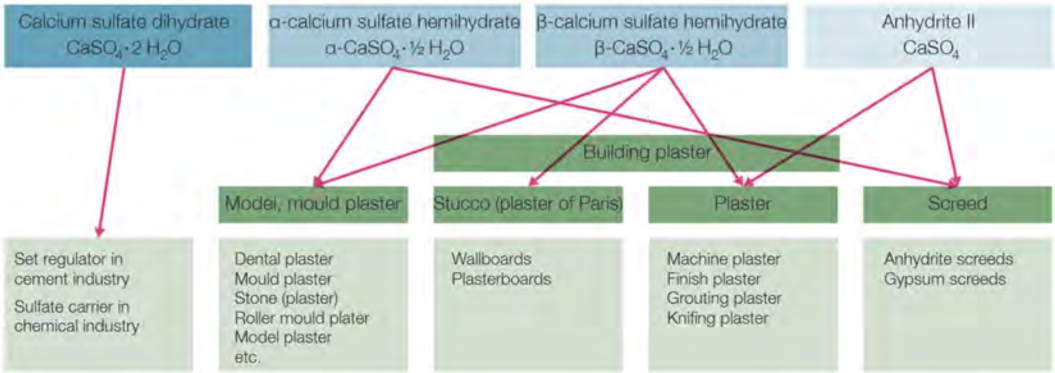

Figure 11 - Flow diagram showing the potential of gypsum re-uptake (Rubli, 2014)

3.) Shales, slate, flysch and low quality spoil from the Niesen formation, Brèche nappe and Ultra Helvetic excavation are usually disposed of. Nonethtless, recent developments have shown the great economic and logistical potential of using such spoils as lightweight filling materials for voids encountered along the tunnel alignment. A framework to recycling carbonaceous spoils is tested and verified by Zhang et al. (2022). This innovation can be pioneered alongside the EPFL material science division.

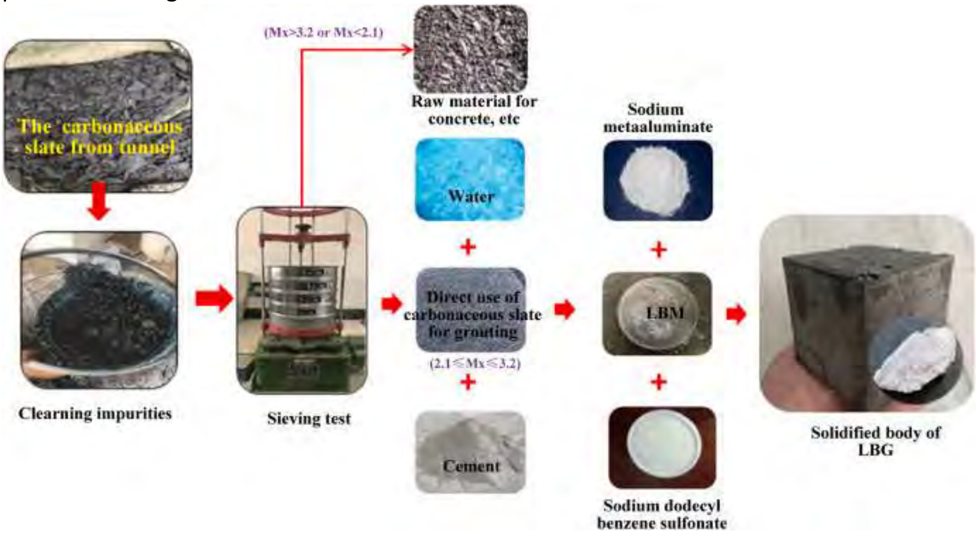

Figure 12 - Slate re-uptake to solidify and fill voids behind concrete segmental liners of a tunnel. The voids can be karstic voids, overbreaks or cavities. (Zhang et al., 2022)

Additionally, in line with the mission of the project presented, the clay rich formations can also be used to convert spoil into a soil. Mixing compost, fertilizers

These solutions are deemed more environmentally friendly and financially beneficial than disposal, but have to be further defined following a future detailed analysis of geological conditions and excavation method.

6 Geotechnical Considerations

The decision aid for tunneling tool (DAT) developed by the Massachusetts Institute of Technology (MIT) is used to provide a cost and time model for the location specific twin-tube tunnel excavation by TBM. Courtesy of Einstein (2018). Additionally, the considerations and model integration was iteratively improved in collaboration with Ing. Jean-Paul Dudt of EPFL. This methodology can be implemented with extremely detailed geotechnical profiles.

6.1 Influential Parameters for TBM Operation

Tunnelling performance, and thus TBM advance rates and costs are directly controlled by the rock quality and local conditions. For this desk study, the commonly used rock mass rating (RMR) classification is used to determine most influential parameters for tunnel construction. These parameters are then approximated according to literature values of common rocks, explicative notice insight, and map data.

The current desk study therefore focuses on the 6 most influential factors of classic tunnel design. Three states are assigned for each parameter, to allow sufficient permutations for each lithology, while not exceeding the detail level available for the desk study.

Table 4 - Most influential factors for the tunnel design during the desk study.

1. Rock Type	*state 1*	*state 2*	*state 3*
2. Jointing	none, 0-30°	0.06-0.2m, 30-60°	>0.2m, 60-90°
3. Groundwater State	dry	med. Inflow	large inflow
4. Overburden / Stress state	<500m	500-1000m	>1000m
5. Faults and Weak zones	<2.5	2.5 to 5	>5
6. Karsting	none	>100m apart	100-10m apart

2. The joint spacing and inclination descriptions for tunnelling quality are taken according to BSI standards (1999).

3. The reduction in joint shear strength and friction angle due to water pressure, is defined according to the RMR water reduction factor (Chapman et al., 2010). The groundwater states are defined by the approximate water pressures expected when excavating:

dry <1kg/cm^2

medium inflow 1-2.5kg/cm^2

large inflow 2.5-10kg/cm^2 *(1kg/cm^2=1bar)*

4. The primary stress conditions are defined by the overburden, and thus separated in ~500m intervals. Once excavating, arching occurs as stress redistributes around the tunnel void. Excessive stress conditions in running, swelling and squeezing conditions are extremely risky in TBM operation.

5. Sub-vertical faulting regimes, weak breccia and weathered zones (BSI 1991) are categorized according the Stress Reduction Factor (SRF) by Barton (2002). These are currently used in the RMR weakening parameter accounting for faults and weathered rock mass.

SRF <2.5 *none to single sheared competent rock at >50m depth*

SRF 2.5 to 5 *single shear at >50m competent rock, single shear zone containing clay*

SRF >5 *cornieule and gypsum, open joints with loose infill, single shear at <50m depth, multiple shear at >50m in competent rock*

6. Geomorphological features (doline, instabilities), hydrological and karstic maps are used to quantify the frequency of karstic features along the study region.

6.2 Ground Classes

Once each lithology and each permutation of influential factors are identified, the BSI standards are used to create simplified classes of fair, moderate, poor and very poor ground classes (GC). According to the RMR guidelines (Annex A.1) after Chapman et al. (2010), and the proposed project specific ground parameters, simplifying as a ground class for the DAT (Table 5).

Table 5 - Semi-quantitative ground classes defined for DAT cost-time model of the VAlp Express metro project.

1. Mechanical Properties	**v. good (I) /good (II)**	**fair (III)**	**poor (IV)**	**v. poor (V)**
RQD rating	100-75%	*75-50%*	50-25%	<25%
RMR	*100-81 / 80-61*	*41-60*	40-21	<21
UCS (MPa)	*>250 / 100-200*	*50-100*	25-50	<25
Point Load (MPa)	*>10 / 4-10*	*2-4*	1-2	n.a.
RM Cohesion (kPa)	*>400 / 300-400*	*200-300*	100-200	<100
RM Friction Angle (°)	*>45 / 35-45*	25-35	25-15	<15
VAlp Parameter	Limestone, Dolomitic Limestone, Quarzitic Limestone, Conglomerat, Arkose Sandstone	Limestone, Dolomitic Limestone, Marly Limestone, Conglomerat, Flysch, Arkose Sandstone, Schistes	Anhydrite, Dolomite, Calc-schiste, Marly Limestone, Flysch, Schistes	Gypsum, Anhydrite, Cornieueles, Dolomite, Schistes
2. Jointing	**V. Favorable / Favorable**	**Fair**	**Unfavorable**	**V. Unfavorable**
Condition Discont.	*Rough surfaces, <1mm separation, minimal weathering of walls*	*Slightly rough surfaces, <1mm Separation, Weathered walls*	Slick surfaces or gouge <5mm, 1-5mm Separation, Weathered	Soft gouge >5mm or Separation >5mm
Strike Perp. Tunnel	*Drive w. dip at 20-90°*	*Drive against dip at 45-90°, any dip 0-20°*	*Drive against dip at 20-45°*	-
Strike Parallel Tunnel	-	*Drive w. dip at 20-45°, any dip 0-20°*	-	*Dip 45-90°*
VAlp Parameter	none, 0-30°	0.06-0.2m, 30-60°	0.06-0.2m, 30-60°	>0.2m, 60-90°
3. Groundwater State	**Dry / Damp**	**Wet**	**Dripping**	**Flowing**
Inflow per 10m tunnel (L/min)	*None / <10*	*10-25*	*25-125*	*>125*
Joint water pressure / Primary stress (-)	*0 / <0.1*	*0.1-0.2*	*0.2-0.5*	*>0.5*
VAlp Parameter	dry	med. Inflow	med. Inflow	large inflow

4. Overburden / Stress state	**V. Favorable / Favorable**	**Fair**	**Unfavorable**	**V. Unfavorable**
VAlp Parameter	<500m	<500m, 500-1000m	500-1000m, >1000m	>1000m
5. Faults and Weak zones	**V. Favorable / Favorable**	**Fair**	**Unfavorable**	**V. Unfavorable**
Persistence (m)	*<3*	*3-10*	*10-20*	*>20*
Weathering		*Moderately weathered, hard fill*	*Highly weathered, soft fill*	*Decomposed*
Roughness	*Rough*	*Slightly rough*	*Smooth*	*Slickensided*
VAlp Parameter	SRF <2.5	SRF 2.5 to 5	SRF 2.5 to 5	SRF >5
6.Karsting	**V. Favorable / Favorable**	**Fair**	**Unfavorable**	**V. Unfavorable**
Weathering		*Moderately weathered, hard fill*	*Highly weathered, soft fill*	*Decomposed*
VAlp Parameter	none	>100m apart	100-10m apart	100-10m apart
Proposed GC	**GC 1**	***GC 2***	**GC 3**	**GC 4**

For each tunnel section, a Monte Carlo analysis stochastically varies the possible ground parameter permutations. The table is used as the primary guideline to attribute a specific cost and advance rate   for a given permutation.

It must be noted, that at the desk study phase, the input data for this feasibility study remains constricted in it's lack of detail.

Laboratory and in-situ geotechnical characteristics are key requirements to precisely predict the TBM's performance. Mechanical strength parameters must be detailed for each lithology (see 3.1 Tectonic Legend). For example unconfined compressive tests, triaxial loading, Vickers surface hardness, abrasiveness testing, linear and rotary rock cutting tests and Siever J-value miniature drill test. Geological (jointing, dip, RMR), geo-hydrological (trace and pumping tests) and geophysical exploration (seismic cross-hole tomography and resistivity) along the trace line is also needed to refine the project specific ground parameters.

7 Decision Aid for Tunneling (DAT)

The cost and temporal calculation was done using the decision aid for tunneling tool (DAT) developed by MIT's Einstein (1998). Since its initial conception, the tool has been often used as a decision support system, refined multiple times until deep learning models by Garcia et al. (2021). Courtesy of Sofie ten Bosch and Prof. Laloui' EPFL Laboratory of Soil Mechanics, the location specific ground classes and tunneling parameters are used as input for the model.

7.1 Software Inputs

For all nineteen lithological variations along the tunnel trace (Table 6), a range of ground classes ranging from good to very poor (GC1-4) were attributed to all ground parameter permutations (mechanical parameters, jointing, groundwater state, stress state, faults and weak zones, karsting). Courtesy of Sofie ten Bosch, the inputs were uploaded and run in the DAT simulation software (Einstein, 1998).

Table 6 - Nineteen lithological variations crossed in the modelled excavation route. The approximate length (variable parameter) and rock type variability are used as input for the stochastic DAT simulations.

Zones	TECTONIC UNIT	ROCK TYPE 1	ROCK TYPE 2	ROCK TYPE 3	ROCK TYPE 4	Length (m)
Zone1	x	Conglomerat	-	-	-	790
Zone2	Bex	Gypsum	Anhydrite	Cornieueles	Dolomite	70
Zone3	PMR	Limestone	Dolomitic Limestone	Quarzitic Limestone		5400
Zone4	Bex	Gypsum	Anhydrite	Cornieueles	Dolomite	330
Zone5	Bex – Lias des Mines	Limestone	Marly Limestone	Calc-schiste	-	2690
Zone6	Bex	Gypsum	Anhydrite	Cornieueles	Dolomite	2140
Zone7	Meilleret	Flysch	Arkose Sandstone	Marly Limestone	Conglomerat	7250
Zone8	Plaine-Morte (PM)	Flysch	Schistes	Limestone	Dolomite	980
Zone9	Meilleret	Flysch	Conglomerat	-	-	570
Zone10	Niesen	Flysch	Conglomerat	Calc-schiste	Limestone	7850
Zone11	Flysch Priabonien (UH)	Flysch	Marly Limestone	-	-	1100
Zone12	PMR	Limestone	Dolomitic Limestone	Quarzitic Limestone	-	2300
Zone13	Brèche	Flysch	Marly Limestone	-	-	250
Zone14	Simme	Flysch	Calc-schiste	Marly Limestone	-	200
Zone15	PMR	Limestone	Dolomitic Limestone	Flysch	-	180
Zone16	Simme	Flysch	Calc-schiste	Marly Limestone	-	60
Zone17	PMR	Limestone	Dolomitic Limestone	Flysch	-	400
Zone18	PMP	Limestone	Calc-schiste	-	-	920
Zone19	Simme	Flysch	Calc-schiste	Marly Limestone	-	770
	2. JOINTS	none, 0-30°	0.06-0.2m, 30-60°	>0.2m, 60-90°		
	3. GROUNDWATER	dry	med. Inflow	large inflow		
	4. OVERBURDEN	<500m	500-1000m	>1000m		
	5. FAULTS or WEAK ZONES	SRF <2.5	SRF 2.5 to 5	SRF >5		
	6. KARSTIC features	none	>100m apart	100-10m apart		

Additionally, the advance rates (AR) and cost per kilometer are chosen for a 9m wide TBM. A specific simulation of 82 tunneling projects, calibrated over 50'000 simulations, was used to define five ground classes ranging from very good to very bad (GC1-GC5) (Harran, 2018). In the VAlp tunnel, tunneling does not occur in massive, unfractured, dry, intrusive rocks, and thus the very good (GC1) is deemed as unsuitable for the current study. For this reason, only the good to very poor AR and cost predictions are used in our model.

Finally, the modelled TBM advance rate and cost are shown in Table 7. The values are adapted from the extended database and simulations of Harran (2018) for a 9m wide machine. The study's metro tunnel is likely to be 6.5m in external diameter, rendering the DAT model inputs a conservative estimate. However, Harran's (2018) database was calibrated upon of short tunnels (<10km), whereas the VAlp metro might further benefit from economies of scale over the 34.25km long excavation.

Table 7 - Advance rate and cost estimate used to model the tunnelling efforts of the VAlp Express.

AR in m/day			
TBM d=9m (2018)	*min*	*mean*	*max*
GC1 good	13	18	20
GC2 fair	8	12	15
GC3 bad	3	7	9
GC4 v.bad	1	2	3

Cost in Mchf/km			
TBM d=9m (2018)	*min*	*mean*	*max*
GC1 v.good	11	13	16
GC2 good	14	16	21
GC3 fair	20	23	29
GC4 bad	51	57	73

7.2 Software Results

Using the project specific lithologies over the 34.25km tunnel (Table 6), 4000 Montecarlo simulations were performed for varying ground parameters. This led to an time estimate between 8-15 years (Figure 13), and a cost estimate of a single tunnel 564-774 million EUR (Figure 14). Considering the VAlp Metro's two single shaft concept, the total cost of tunneling would amount to 1-1.5 billion EUR.

The updated simulation derived from the 3D geological model displayed in Figure 13 by a range of cost and time estimates.

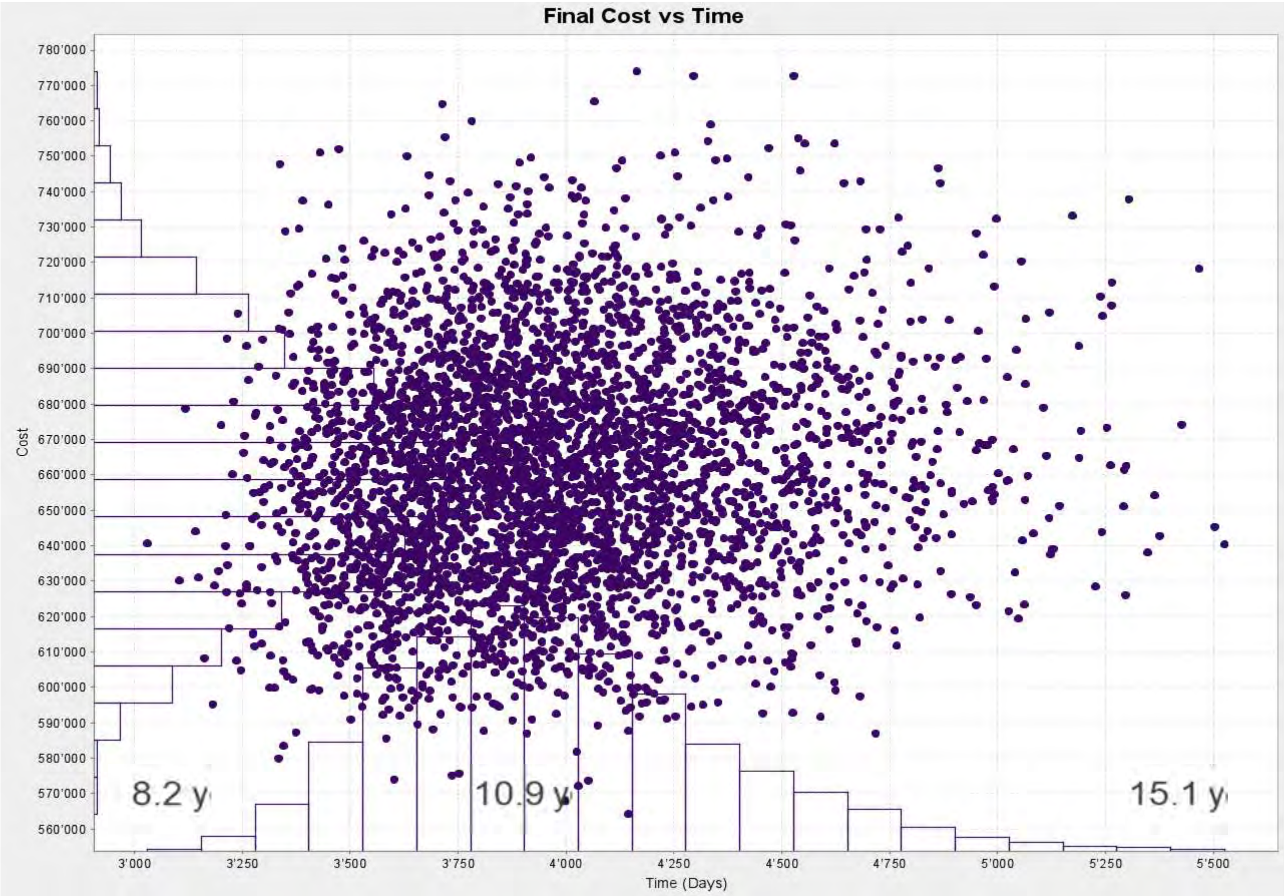

Figure 13 - Final cost (kchf) simulation using the geotechnical considerations along the tunnel alignement and the MIT decision aid for tunneling (DAT) tool introduced by Einstein et al. (1998) and updated over time (Moret and Einstein, 2016)

Additionally, the development of the excavation and advance rate shows in Figure 14 complex tunnelling conditions by TBM before Villars-sur-Ollon and before Les Diablerets. An average envelope is displayed in pink, alongside optimistic and pessimistic DAT results.

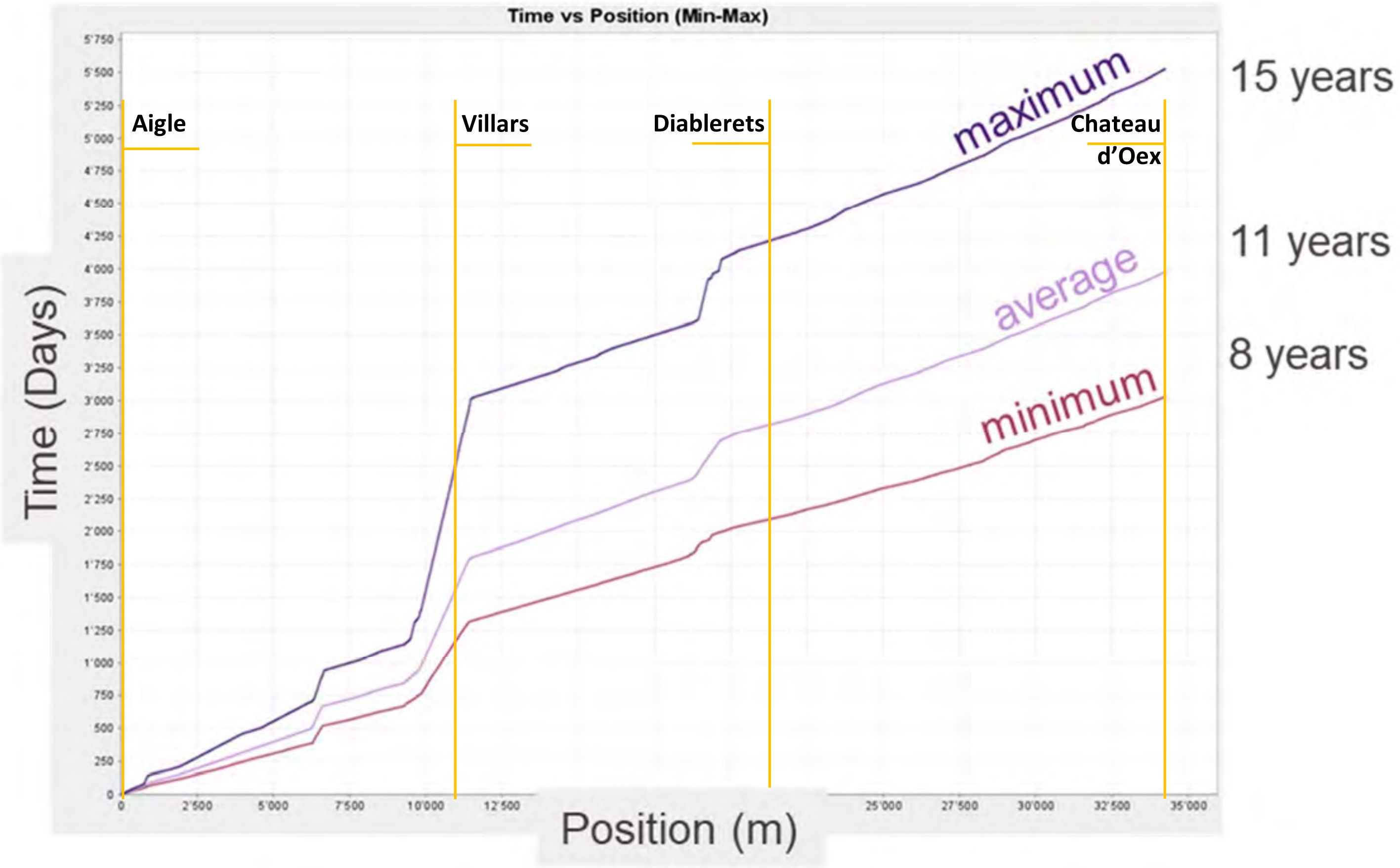

Figure 14 - Final advancement simulation for the current study using MIT's DAT tool introduced by Einstein et al. (1998) and updated over time (Moret and Einstein, 2016).

In view of the DAT output, the VAlp Metro tunnel is an innovative and impressive concept. Most European tunnels, excavated with 8-10m TBM, costed around 23.3-54.3 chf.-/km (HM Treasury, 2010). When accounting for the complete work (tunnel liner, cable placement, safety measures, etc), Flyvbjerg et al. (2008) estimate that rail tunnels cost from 60-100 million$/km. It is also noted that due to economies of scale, the costs are drastically reduced at lengths greater than 6km.

The VAlp Metro tunnel would be comparable in length to the renown Lotschberg (CH) and Koralm (AU) tunnels (Table 8). The DAT tunnelling cost estimate per kilometer matches the HM Treasury (2010) predictions, albeit being optimistic. The total cost remains well below that of existing tunneling projects. Development of the ad-hoc metro technology will likely match the current tunneling projects' costs.

Table 8 - Total cost estimation of long tunnels (adapted from Hilar and Srb, 2009).

Name	Count.	Date	Length (km)	Cost (Mchf.-/km)	Ø Diam Ext	Ø Diam Int	Tunnel Type	Speed (km/h)	
Mont Cenis	IT-FR	present	57.5	**158**		8.4	2 Single-tracks	250	*Geology*
Gothard Base	CH	2015	57	**114**	9.6	8.3		250	*flyshc, limestone, schiste, trias, gneiss and quartzite (slurry shield tbm)*
Lotschberg	CH	2006	34.6	**62**		8.4	2 Single-tracks	250	*crystalline rock 90%, sedim 10%. Sedrun poor area needed 13m wide excav (but 200m overburden)*
VAlp Metro	**CH**	**concept**	**34.3**	**16.5-22.6**	**6.5**	**5.9**	**2 Single-tracks**	**80-110**	*limestone, quartizitc limestone, flysch, marl, gypse, anhydrite, sandstone, conglomerat ,*
Koralm	AU	2016	32.8	**165**	9.9		2 Single-tracks	250	*gneiss, granite amphibolite*
Guadarrama	ESP	2007	28.4	**56**	10	8.5	2 Single-tracks	350	*gneiss, marble, mica-schist and amphibolite with faults. Portals of silt-sandstone*
Ceneri Tunnel	CH	2020	15.4	**117**	9	8.4	2 Single-tracks	200	*igneous metamorphic rock (gneiss, granite)*
Wienerwald	AU	2010	13.3	**13**	10.7		2 Single-tracks	250	*gneiss, orthgneiss*
Gothard Expansion	CH	present	7.9	**55**	12.2				*silt, clay, sandstone, marl*
M2 Lausanne	CH	2008	6	**200**			Single-track	60	*granite, gneiss, trias, calcschite, argilles*
Vue des Alpes (NE)	CH	1995	5	**70**			2 Single-tracks	cars	*molasse, conglomerat, sand*

The current DAT predictions are for a 9m external diameter TBM, which may be excessive for the lightweight, smaller TBM used in the metro concept (see Ceneri Tunnel). Likely, the blockage ratio for the VAlp Metro can be optimized in future studies. This would further reduce spoil and costs.

8 Hydro-Geothermal Model

The tunnels and stations designed in the scope of the project provide the potential for the extraction of geothermal energy. Integrating dry and wet energy geo-structures can be used to harness renewable energy along the VAlp metro line. This is especially desirable in the neighbouring communes at high altitude. New innovative projects, such as the Lausanne M3 metro line planned for 2030, strive to incorporate energy geostructures to harness excess heat. The thermal energy recovered from the ground, tunnels and stations can be used to heat nearby buildings (BG, 2021). This section explores a first order hydro-geothermal model to assess the heat potential along the metro line.

Later in the design phase, impermeabilization of the segmental tunnel liner is proposed. This would minimize the tunnels effect on the regional effective stress field, preventing undesirable drainage induce subsidence (Zangerl et al., 2023). Furthermore, no-flow conditions along the tunnel liner will minimize the metro’s modification of the water table; ensuring sustainable hydrological resources is imperative to regional well-being.

8.1 Model Input

8.1.1 Hydrogeological Cross-Section

Geo-hydrological maps are used to identify water protection zones, aquifer type, water courses and spring locations (*Figure 15*). The hydrological data, in conjunction with the geological cross-section (*5.2 Geological Cross-Section*), serve as inputs for the hydro-geological cross section at the regional scale. The Aigle-Villars section is not modelled, since it’s near subsurface alignment displays minimal geothermal potential.

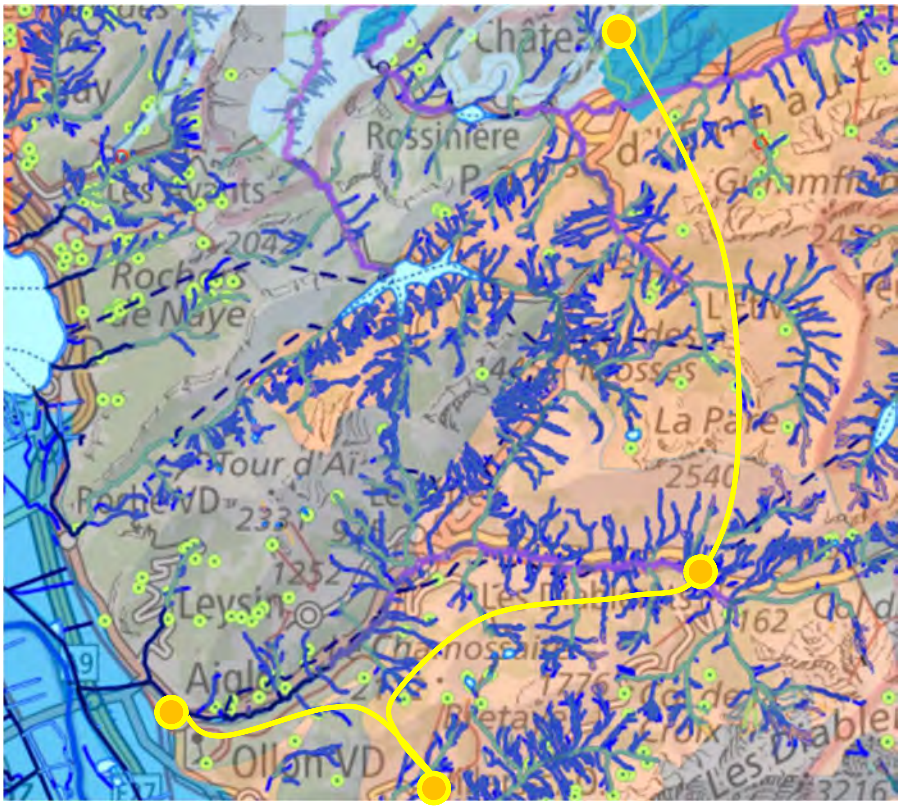

Figure 15 - Geo-hydrological maps courtesy of geo.admin.ch. Surfaces showing aquifer type (gray, pink) and water protection zones (blue). Polylines show streams (blue) and point springs (green). Permanent bodies of water, such as lake, are also shown (azure with blue outline).

Additionally, relevant boreholes less than 200-300 meters away from the tunnel alignment constrain the phreatic surface locations. Deep geothermal and geotechnical boreholes were used to identify the water table, whereas shallow hydrological infiltration tests were used to verify the modelled permeabilities. The hydro-geological cross section of Villars – Les Diablerets – Chateau d'Oex is shown in .

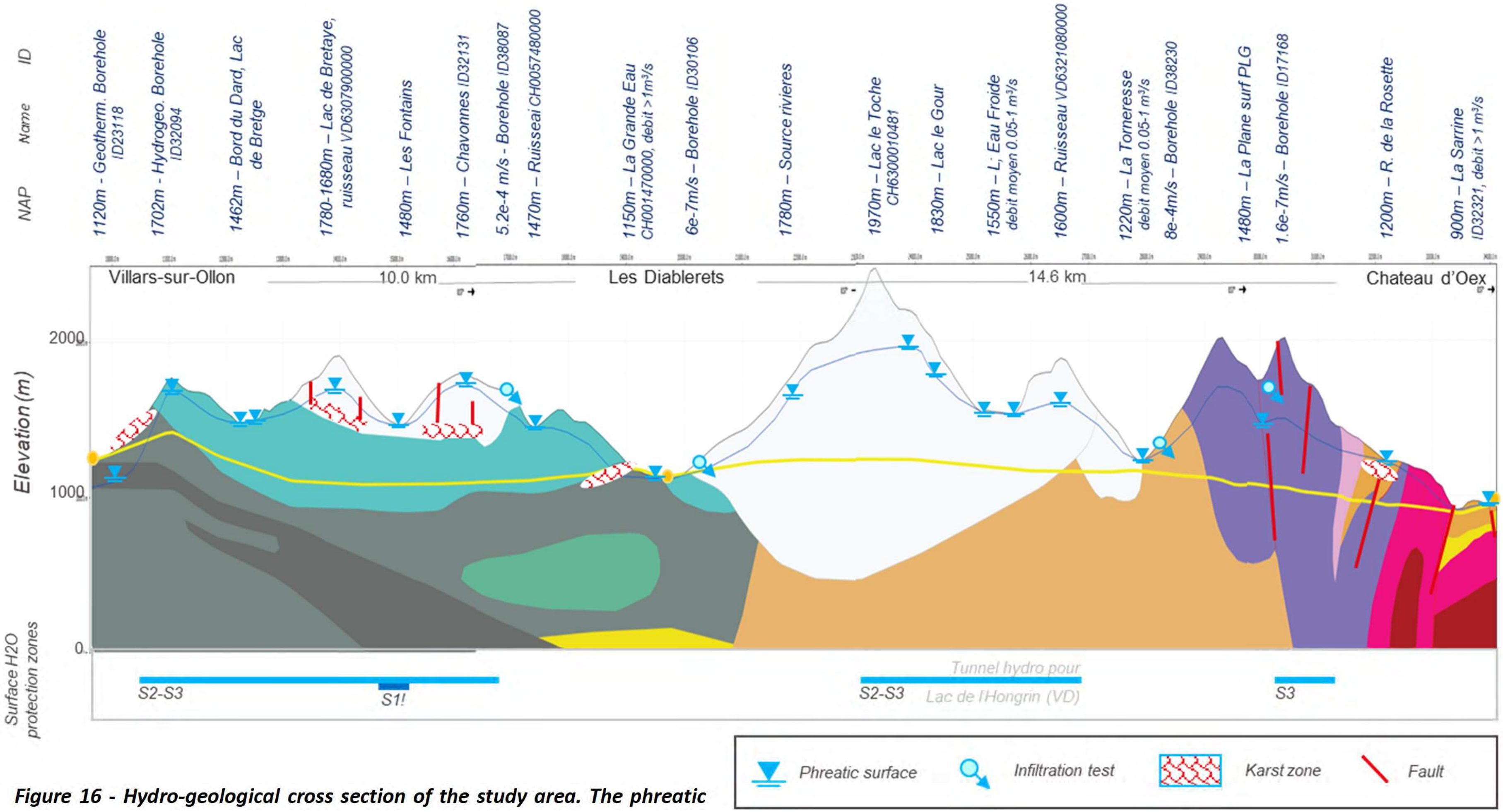

Figure 16 - Hydro-geological cross section of the study area. The phreatic surface is constrained by permanent bodies of water (lakes, rivers) and borehole data.

8.1.2 Boundary Conditions

The hydro-geothermal model is simplified to capture a first glace of flow basins and heat transfer along the VAlp metro line. For this reason, various assumptions are made to create ad-hoc a model capable of providing a quantifiable analysis at the regional scale.

A continuum conceptual model is envisaged to address the multiscale heterogeneity of the study domain (Marechal et al., 1999). The boundary conditions are described in *Figure 17*. Discharge and hydraulic gradients are solved for below the phreatic surface only (Sr = 1). Temperature gradients are modelled over the entire domain. Heat convection is coupled to the water's velocity field in the aquifer (Sr = 1), whereas it is assumed that air convection in the dry porous media does not occur.

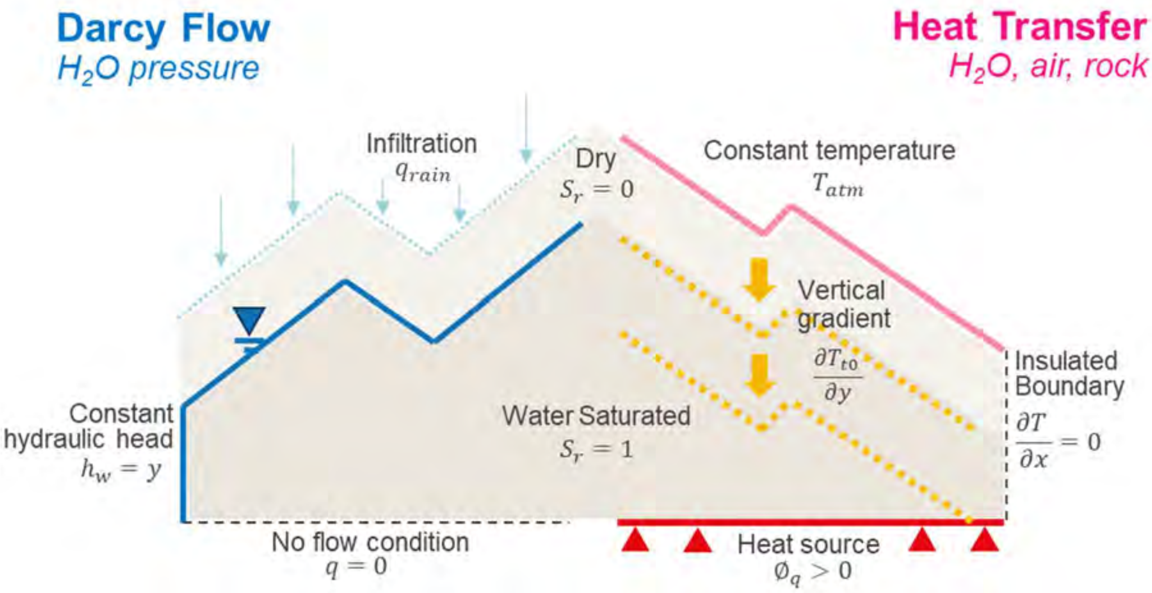

Figure 17 - Boundary conditions and initial states of the coupled hydro-geothermal 2D model. It is constructed by coupling Darcyan flow and Heat transfer in porous media governing equations in COMSOL Multiphysics software.

The governing equations are resolved in steady state, using quadratic discretization for Darcy's flow and linear discretization for Heat transfer equations. To do so, the parameters listed in *Table 9* are used.

Table 9 - Boundary model parameters of the coupled hydro-geothermal model.

Boundary Parameters	Value	References
Vertical geotherm	0.03 [°C/m]	*Bodmer (1982)*
Atmospheric temperature	10 [°C]	*Michelon et al. (2023)*
Heat source	30 [mW/m²]	*Marechal et al. (1999)*
Infiltration	Rainfall [mm/yr] equal to 5% of the surface node's altitude	*n.a.*

8.1.3 Material Properties

In the porous physical space, thermal conductivity and heat capacity are affected by the volume of fluids of the rock. Conduction and convection of thin structures (such as individual fractures) are not modelled at the scale of the regional scale. The rock mass is instead treated as an homogeneous medium in a given lithology. The material properties of the folded and complex geological structures are therefore assigned homogeneous and isotropic material properties from literature and infiltration tests. Additionally, major fault zones are modelled using an equivalent porous domain as per Marechal et al. (1999).

The material properties are therefore defined for four simplified lithologies, and an equivalent fault porous media. All porous media defined in *Table 10*Table 9 are water saturated below the water table, and air saturated above it.

Table 10 - Porous media material properties used as input for Darcyan flow and heat transfer coupling.

Lithologie	ρ_{solide} [g/cm^3]	K_{sat} [m/s]	Vol. Solide (1-Ø)	*Références*	k_s [Wm^{-1}K^{-1}]	Δk_s(100K) [Wm^{-1}K^{-1}]	C_p [Jm^{-3}K^{-1}]	*Références*
Calcaire-Dolomie	2.68	1e-8	0.9	*Earle (2019), Marechal et al. (1999*	3	0.8	2.4e6	*Cote et al. (2013),Selvadur RezaeiNiya's (2020), And Marquez et al. (2016)*
Evaporite	2.3	1e-7	0.8	*Earle (2019), Marechal et al. (1999*	4.5	n.a.	1.8e6	*Pouselliet al. (2021), And Marquez et al. (2016)*
Conglomérat	2.79	1e-8	0.85	*Earle (2019), Marechal et al. (1999*	3.2	1.4	2.2e6	*Dalla Santa et al. (2019)Selv and RezaeiNiya's (2020), A. Marquez et al. (2016)*
Flysch	2.5	1e-9	0.95	*Earle (2019), Marechal et al. (1999*	5.5	n.a.	2.4e6	*Labus and Labus (2018) An Marquez et al. (2016)*
Fault Zones	2.6	1^{e}-6	0.75	*Marechal et al. (1999*	3.5	0.8	2.2e6	*Cote et al. (2013),Selvadur RezaeiNiya's (2020), And Marquez et al. (2016)*

8.2 Results

The proposed model couples Darcyan flow and heat transfer in porous media. The boundary conditions and material parameters define the transfer of heat and fluid dynamics of the region.

Firstly, the steady state hydrological basins are shown in *Figure 18*, where the hydraulic head distribution (colored) and flow velocity streamlines (gray) are shown. Regional recharge divide is defined by the surface topography. It is noted that two regions contain significant upwards flow, notably the Diablerets valley floor. As expected, the highest expected water pressures occur below the areas of greatest overburden. This may be less problematic in lower permeability flysch formations north of Les Diablerets (*kilometer 12-16*), compared to faster flow rates encountered in the Chamosère conglomerates (*kilometer 4-7*).

Secondly, the regional geothermal gradient is computed according to the material properties and fluid flux (*Figure 19*). The colored domain discerns cooler purple areas and warm yellow zones. The lithospheric source of heating of the basal boundary heats by conduction, advection and diffusion the saturated aquifer. Notably, the advection free air saturated region remains very cold, close to the atmospheric temperature. In fact, water flow dominates the heat distribution of the system. Fast flowing lithologies and vertical flow cool the Villars and Diableret valleys significantly.

Additional hydraulic head distribution, zooms of geothermal plots, and a modified fractured model are included in annex *15.1 Hydro-Geothermal Models*.

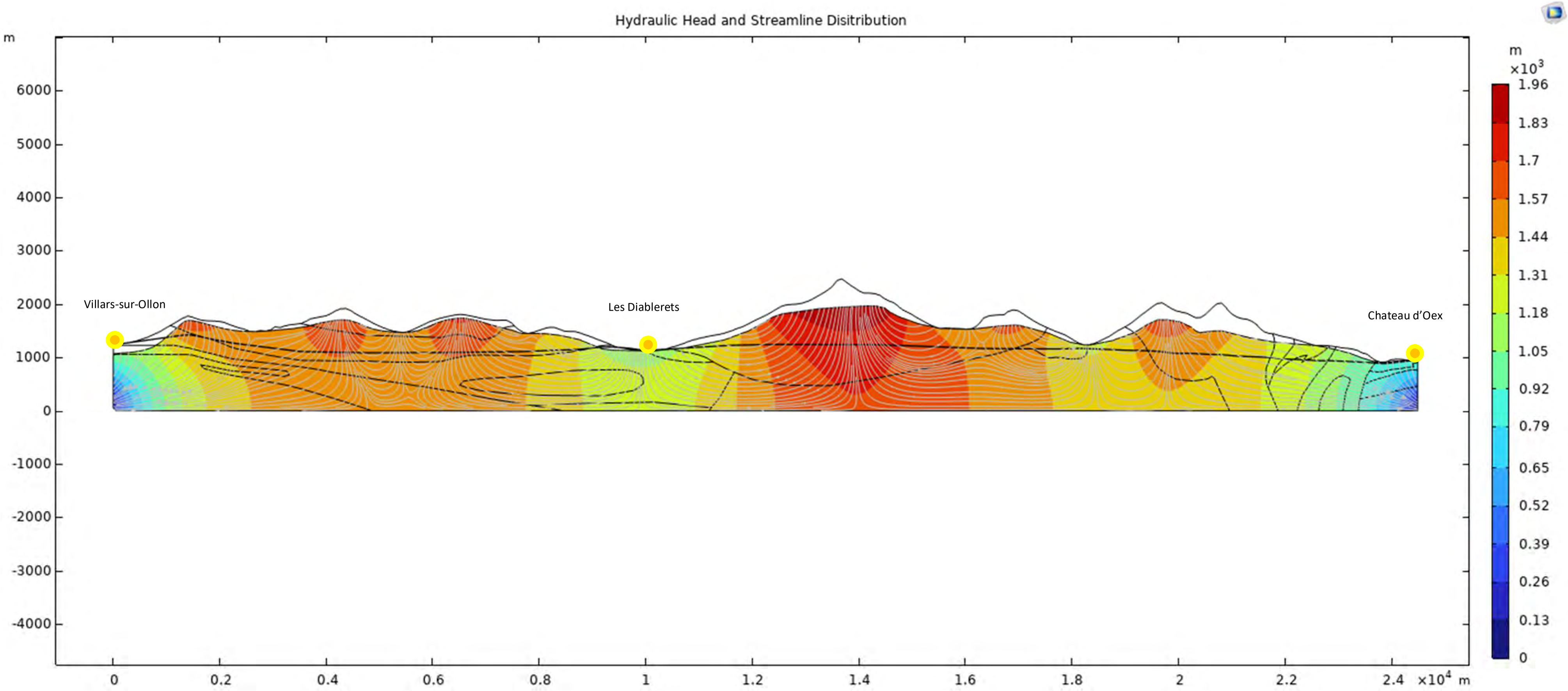

Figure 18 - Hydrological regional model from Villars to Chateau d'Oex. The hydraulic head distribution is colored accordingly, whereas the gray streamlines show flow directions and regional-local basin splits.

0

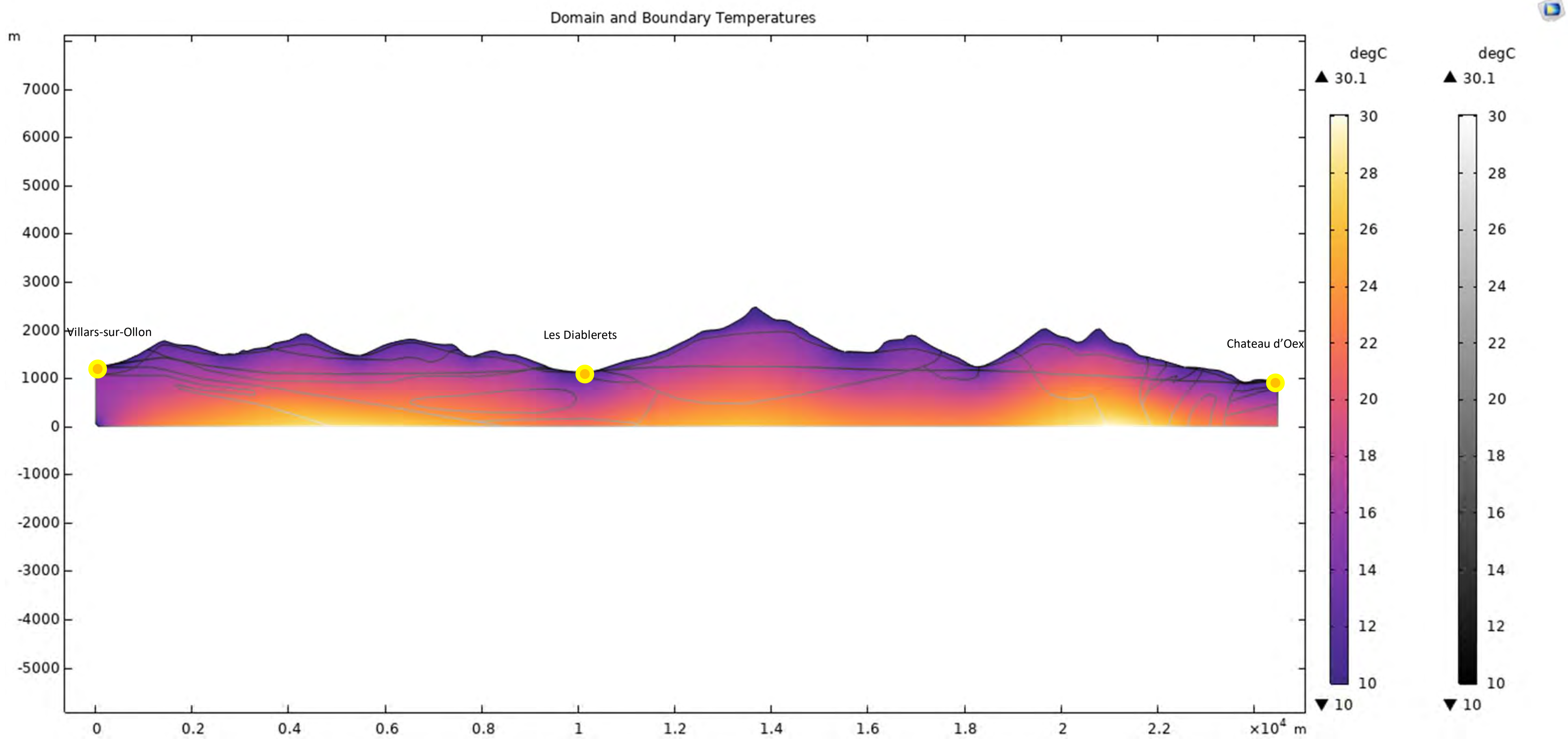

Figure 19 - Geothermal field along the tunnel alignment between Villars and Chateau d'Oex. The grayscale indicates the temperature at geological, aquifer and tunnel geometrical boundaries.

More precisely, the Meilleret conglomerats between Villars and Les Diablerets detailed in *Figure 20*. High infiltration rates are expected below the fractured Niesen limestone, and may even be underlain by karstic lithologies. Maximal temperatures of 18.5°C are modelled. Nonetheless, the region is expected to be further cooled by preferential flow in the discontinuous surface geology.

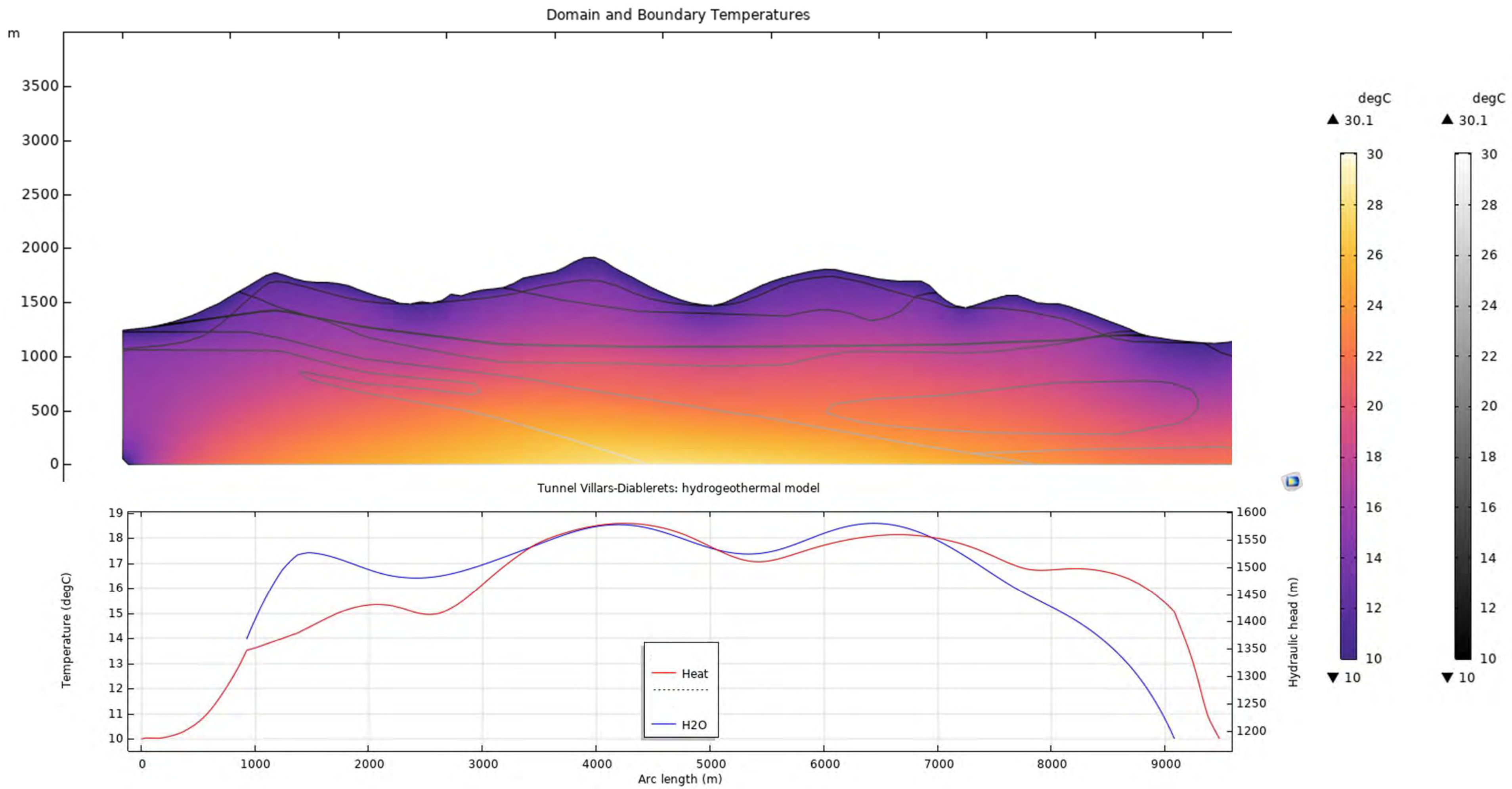

Figure 20 - Geothermal and hydraulic head distribution along the tunnel liner walls in the Meilleret formation north-west of Villars.

VAlp EXPRESS

More precisely, the section with greatest overburden in the limestone-flysch Meilleret formation is detailed in *Figure 21*. High water pressures are calculated below the mountain's peak, coinciding with maximal temperatures of 19°C. This zone is expected to be the least influenced by regional faults or Triassic karsting.

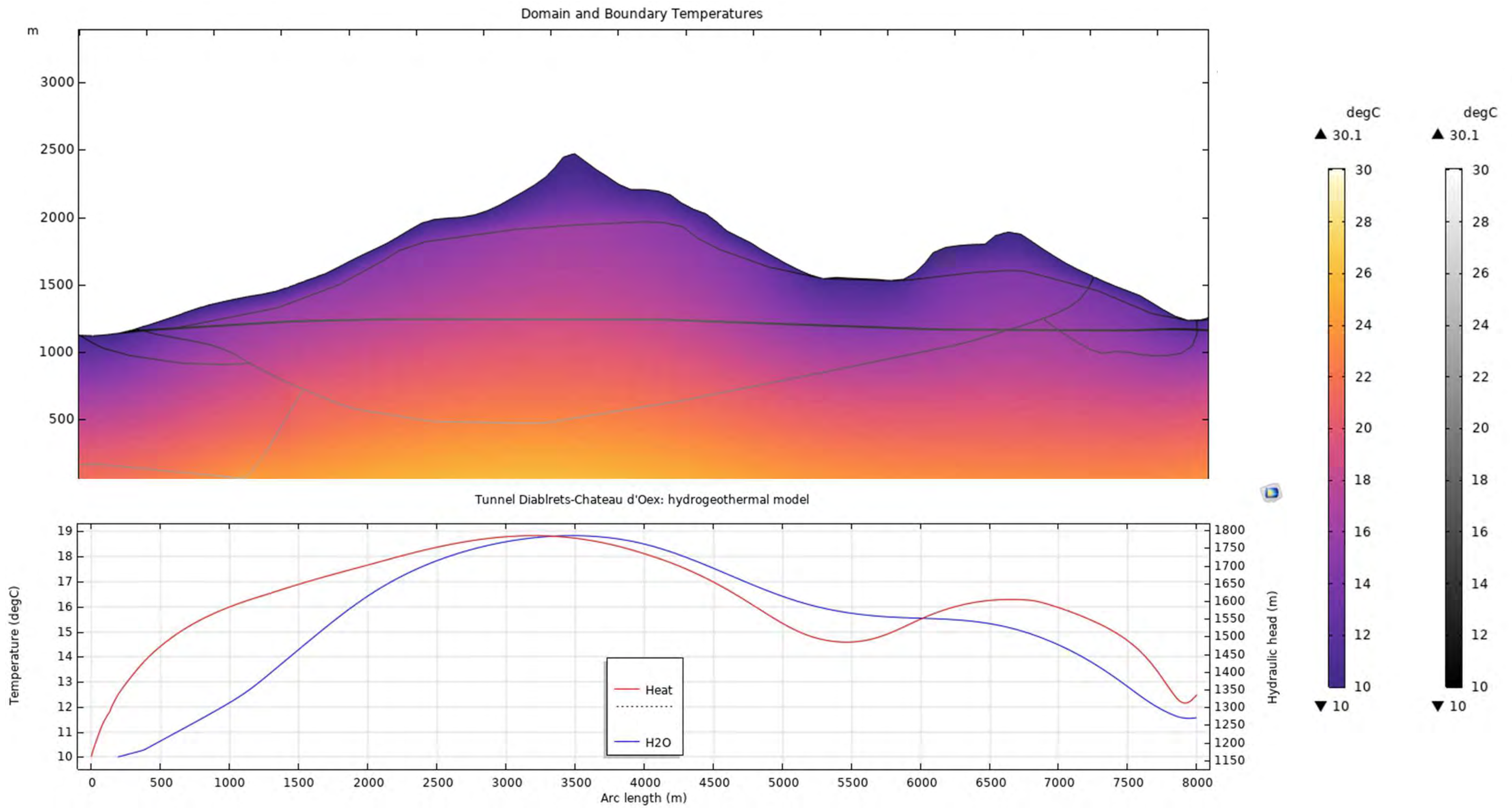

Figure 21 - Geothermal and hydraulic head distribution along the tunnel liner walls in the Niesen formation north of Les DIablerets.

To investigate the role of regional faults and karstic formations in the Triassic evaporites, a second model is run. Tectonized zones are modelled using an apparent hydraulic conductivity. An equivalent permeability approach allows rapid inclusion of faults in the governing model. It is shown that the steady state resolution of the proposed model is extremely sensitive to fluid flow (see annex). Low viscosity, rapid flowing water, drastically cools the domain. For this reason, it is envisaged that the continuum model of a faulted regime is very pessimistic, and may lead to an overconservative estimation of geothermal energy sources. Future work should improve geothermal modelling of fracture and karstic cooling by including field characterization (geometry) and time-dependant resolutions. For example, Hokr et al. (2016) implemented discrete fracture elements in a continuum porous media to model steady state and transient flow in fractured rock.

8.3 Energy Geostructures

The VAlp tunnel excavation provides an opportunity to access climate-friendly heating to the limitrophe communes. The embedded infrastructure can be thermally activated to exchange heat with the surrounding soil (Houhou and Laloui, 2022). As shown in the hydro-geothermal model, the VAlp metro shows promise for low enthalpy geothermal activation. This section explores how the tunnel's large surface area can actively exchange heat with the tunnels convective air and the surrounding soil.

8.3.1 Tunnel Liner Technology

The excavation by tunnel boring machine and use of impermeable segmental liners allows for integration of energy activated geostructures. Including absorbed pipes directly in tunnel liners require far lower investments than standard borehole heat exchangers and doublets. High overburden areas with sufficient groundwater circulation improve the exploitable energy potential. Recent developments of ground heat exchangers (GHEs) in pre-cast segmental tunnel liners were pioneered in 2010 in the Austrian Jenbach tunnel (Frodl et al., 2010). Thereafter, others such as engineers designing Torino's Line 1 metro, successfully thermally activated 120m^2 of the tunnel liner (Barla and Isana, 2018). They found that heat losses are minimized when coiling the pipe system perpendicular to the tunnel axis (*Figure 22*). Water pipes are prepared and placed in cast concrete segments, which are placed behind a TBMs cutterhead.

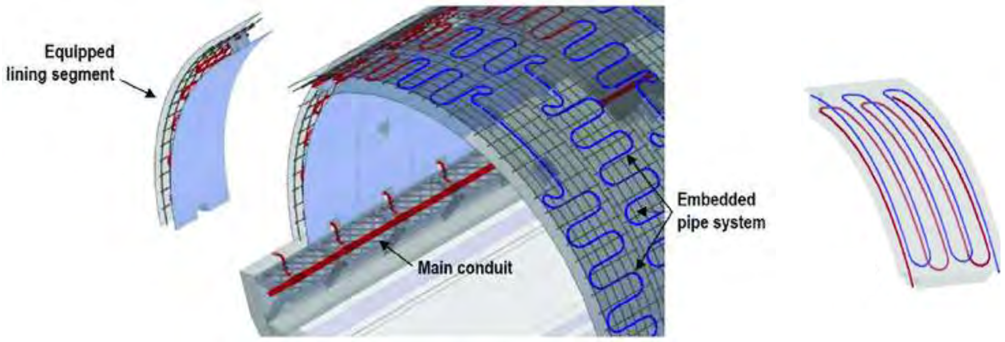

Figure 22 - Energy segmental lining acting as a ground heat exchanger (left), and the improved stacked ground&air pipe system running perpendicular to the tunnel axis(right) (Barla and Di Donna, 2018).

These systems, designed for injection-extraction of water paired to heat pumps, are best suited at low enthalpy. This reduces the effect on the surrounding soil's thermal equilibrium and improves heat pump performance (Barla et al., 2016).

Winter thermal needs extract heat from the tunnel, whereas summer injections store power in the ground mass. For example, Torino's Line 1 extracts 1.67kW during winter, and injects 2.34kW during summer. In Barla et al.'s (2016) study, the optimal difference between the outlet water ($T_{w,o}$) and ground temperature (T_g) is quantified as:

$$Winter\ heating\ extracted\ \Delta T_{winter} = \left(T_o - T_g\right) \in [-11 : -6\ °C]$$

$$Summer\ cooling\ injected\ \ \Delta T_{summer}\ \left(T_o - T_g\right) \in [11 : 16°C]$$

Whereas the heat exchange plant is optimized by maintaining the absorber pipe initial temperature and output between:

$$Input\ and\ output\ water\ difference\ \Delta T_{i-o} \in [3 : 5\ °C]$$

The systems performance is strongly dependant on ground-water flow regimes (Houhou and Laloui, 2022). In the saturated gravel-sands of Torino (1e-3m/s), seasonal cyclic heating-cooling models showed an oscillation and rapid thermal recharge radially around the tunnel (*Figure 23*). In such a mediums, using the ground as an active storage and source is most sustainable.

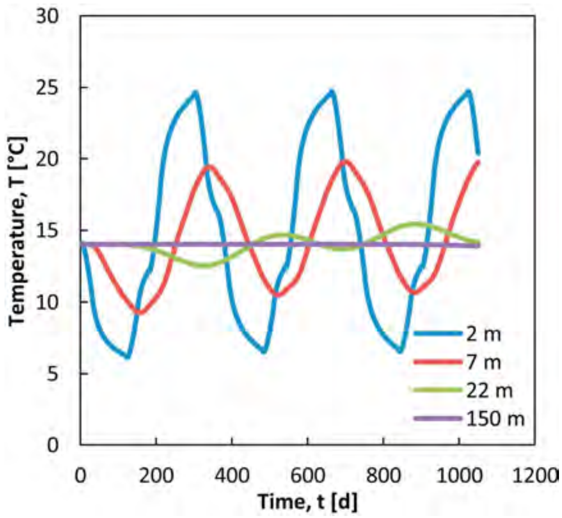

Figure 23 - Temperature model at different distances from the tunnel in a homogeneous isotropic soil. Modelled for 3 years, radially from the Torino Line 1 metro (Barla et al. 2016)

Furthermore, recent modelling developments have spurred a greater fundamental understanding of the convection heat transfer phenomena due to airflow in underground tunnel. In fact EPFL's own LMS has provided insight on specific convection coefficient correlations in non-isothermal tunnels (Peltier et al., 2019). This is crucial in determining the heating-cooling cycles in function of the tunnels inner air temperature, and is currently used to develop the innovative Lausanne M3 metro.

8.3.2 Mountain Region Applicability

Mountain regions usually provide significant potential for low enthalpy systems. The highly efficient closed systems allow for greater distances top due to their rock-mass flow regimes and large overburden (Tinti et al., 2017). Large flow rates in occurring in geotherms rapidly recharge the thermal potential of mountainous areas. Absorber pipes included in the pre-cast concrete segments are a low investment opportunity to harness thermal power when excavating by TBM (Houhou and Laloui, 2022). Furthermore, the thermal dissipation of rubber tyred metros heats the tunnels air, which can also be harnessed by the tunnel liner GHEs.

Two zones along the preliminary VAlp tunnel alignment are expected to yield temperatures of 18-19°C (*see 8.2*). Two zones display predominant potential for geothermal exploitation:

1. The geology along the Villars-Diablerets section (*Figure 20*) guarantees a high hydraulic conductivity, which although being thermally desirable for the GHE, may be cooler than the modelled 18.5°C maxima (rainwater infiltration along preferential flow paths, extensive vertical faulting along the Chamosère, only ~500m overburden). Further refinements of the regional hydro-geothermal model are desirable to reduce the local geotherm's uncertainty.
2. The Niesen formation north of Les Diablerets (*Figure 21*) benefits of the largest overburdens and reduced uncertainty (cooling via preferential flow systems). The greatest temperatures of 19°C are modelled in this section

In both locations, and impermeable pre-cast segmental liner is proposed to reduce maintenance costs while negating negative externalities (depletion of water resources, subsidence by dewatering rocks, etc.). The surrounding soil hydraulic conductivity was modelled and is expected to range from 1e-6 to 1e-9m/s. This implies that the tunnel liner GHE can extract and inject around 10 W/m^2 during summer and winter alike (*Figure 24*).

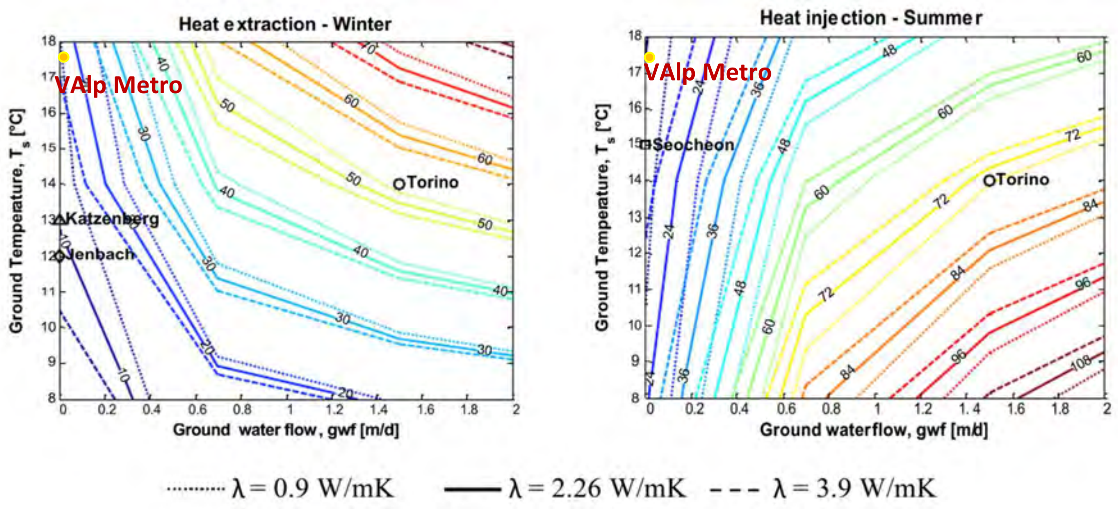

Figure 24 - Heat extraction of tunnel liner GHEs in W/m^2 for varying ground thermal conductivities (dotted line) and hydrothermal regimes (axes) (Barla and Di Donna, 2018).

More precisely, an energy extraction system is envisaged to capture energy out of the surrounding soil (19°C) by injecting and circulating cold water during winter. For example, warm tunnel water from the 34.6km long Lötschberg is used for fish farms and greenhouses (Link and Minning, 2022). In the same way, the VAlp metro can provide heat for limitrophe buildings in the Diablerets region. For example, by relying on the 120m^2 system designed by Barla et al.'s (2016) and the modelled ground temperature:

$$Input\ water\ T_i = 6°C\ ,\quad Optimal\ \ \Delta T_{winter} = -10°C\ ,\qquad \boldsymbol{T_g = 19°C}$$

The temperature gained during winter heat extraction would be:

$$\Delta T_{winter} = T_o - T_g = (T_i + \Delta T_{i-o}) - \boldsymbol{T_g}$$
$$= (6 + \Delta T_{i-o}) - \boldsymbol{19}°C = -10°C$$
$$\Delta T_{i-o} = +3\ °C$$

The GHEs surface area defines what absorber pipe flow rates can be used to reach a desired thermal regime. In this preliminary concept study, the Torino Line 1 absorber pipe flow rates of 0.06m^3/h are used. A greater activated surface area allows for faster flow along the absorber pipes. This equates to a heat extraction of:

$$Q_{winter} = q_w * \rho_w * C_w * \Delta T_{i-o}$$
$$Q_{winte} = 0.0001667\ [m^3/s]\ * 1000[kg/m^3]\ * 4.211 \frac{kJ}{kg\ K} * (+3°)$$
$$\boldsymbol{Q_{winter} = 2.11kW}$$

Meanwhile in summer, warm atmospheric airflow and metro thermal dissipation, allows for injection exploitation of the liner GHE. This implies circulating warm water (30-35°C) in the absorber pipes to heat the ground (19°C) and cool the tunnel. This benefits the tunnel exterior by thermally recharging the ground, while reducing running costs to cool the interior's air.

$$Input\ water\ T_i = 34°C\ ,\quad Optimal\ \ \Delta T_{summer} = +11°C\ ,\qquad \boldsymbol{T_g = 19°C}$$

The temperature gained during summer cooling would be:

$$\Delta T_{summer} = T_o - T_g = (T_i + \Delta T_{i-o}) - \boldsymbol{T_g}$$
$$= (34 + \Delta T_{i-o}) - \boldsymbol{19}°C = 10°C$$

$$\Delta T_{i-o} = -4\ °C$$

Using an absorber pipe flow rates of 0.06m^3/h, a heat injection of:

$$Q_{summer} = q_w * \rho_w * C_w * \Delta T_{i-o}$$

$$Q_{summer} = 0.0001667\ [m^3/s]\ * 1000[kg/m^3]\ * 4.211 \frac{kJ}{kg\ K} * (-4°)$$

$$\boldsymbol{Q_{summer} = 2.81kW}$$

Nonetheless, the complex nature of hydro-thermal-mechanical coupling of the energy tunnel in varying soils types have shown that thermal induced settlement is a non-negligeable risk for the tunnel design (Liu and Zhou, 2022). Since the effect is reduced with large overburden, the 19°C tunnel section residing 3km north of Les Diablerets is assumed to pose a smaller risk of thermal settlement. Additionally, most research currently models the coupled energy processes in shallow soil formations (Ma et al., 2022; Liu and Zhou, 2022). Current state of the art energy segments have however shown that thermally induced stress and deformations remain within acceptable ranges during operation (Ma et al., 2022). It is advisable to gather field samples of Niesen flysch and limestone lithologies to better quantify the coefficients of thermal expansion and elastic moduli of the porous medium.

8.3.3 Future Perspectives

Future modelling work should aim to simulate smaller sites for specific coupled models, rather than the large domain currently studied. By working in detailed three dimensional domains, precise analysis of tunnel liner GHE performance in Niesen flysch and Meilleret conglomerates can be made. This would require precise field characterization and geotechnical parametrization of the two suitable locations.

The current collaboration between UNIL and EPFL provides the necessary know-how. Firstly, Professor Laloui's non-isothermal tunnel airflow models are currently used for Lausanne's M3 metro energy geostructural study (Peltier et al., 2019). Secondly, Professor Jaboyedoff's structural geology exploration allows for precise geotechnical characterization target location (Jaboyedoff et al., 2009). Combining the two, allows for ad-hoc analyses of the low enthalpy potential of VAlp tunnel liner.

Additionally, the potential of deep geothermal exploitation from the tunnel should also be considered. For example, north of Les Diablerets, excavating a 500m borehole would guarantee around 2000m of overburden, potentially reaching deep-seated fluid circulation in hypogenic karsts (Valley and Miller, 2009). Natural fracturing near basement fault zones reduces operational challenges compared to deep hydraulic fracturing of basement rocks by enhanced geothermal systems currently tested in Bedretto, CH (Hertrich et al., 2021). Various examples currently exist and are investigated in Switzerland's chase of the 2050 renewable energy agenda. For example, the Grob geothermal project in Schlattingen (Thurgau, CH) has been extracting 65°C water from the 1000m deep Ober Muschekalk lithology (*Figure 25*). A downsized infrastructure could be envisaged to be constructed in an ad-hoc underground plant along the VAlp metro line.

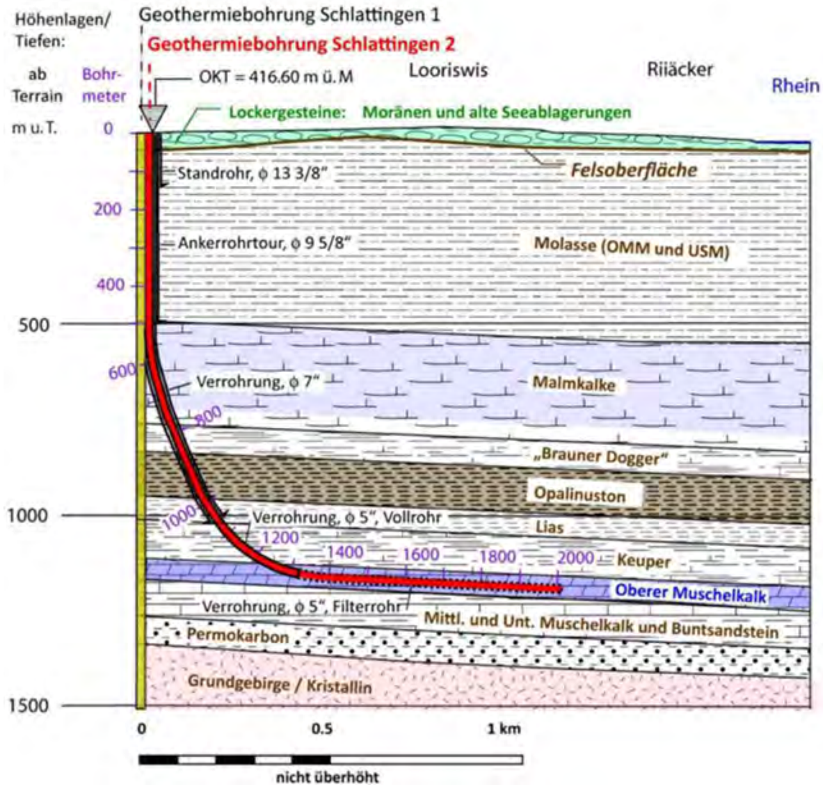

Figure 25 - Deep geothermal exploitation for agricultural and industrial use in canton Thurgau's Grob Gemüse project (Link and Minning, 2022).

9 Tunnel Design

The tunnel and it's cross section are designed to minimize the excavated volume to reduce costs and time. Furthermore, the tunnel is designed to being extremely safe and resistant to reduce maintenance costs in the long run.
In the following chapter, existing metro tunnels are compared, followed by a detailed list of the applicable Swiss safety norms, and concluded by a first cross sectional profile of the high-speed lightweight alpine metro.

9.1 Existing Metro Tunnels

Eight existing metro lines are compared, showing that excavation diameters by TBM vary from 5.5-7.65 meters. The liners are predominantly composed of precast concrete segments. which the expected dimensions of a rapid light-weight VAlp metro are proposed in Table 11.

Table 11 - Tunnel diameter comparison for various metro technologies throughout the world.

Name	Count.	Type	Ø Diam Ext	Ø Diam Int	Liner Type	Max. Velocity	Track guage	Power	Reference
Torino Metro L1	IT	Rail	7.5m EPB	6.88m	Precast concrete	32km/h	1.435m	750V DC	SeA (2011)
Copenhagen M1-4	DK	Rail	5.5m	4.9m	-	90km/h	1.435m	630kW, 750V DC	Metroselskabet I/S (2021)
Berlin U5	DE	Rail	6.65m HDSM	5.7m	Impermeable liner, concrete	60km/h	1.435m	750V DC	Lemke and Poppel (1992)
Syndey NW	AU	Rail	6.7m	6.1m	Precast concrete 6 segm.	100km/h	1.435m	1500V DC	Nievergelt (2023)
Bangkok Orange	TH	Rail	6.4m EPBM	5.7m	Precast concrete 5 segm.	80km/h	1.435m	750V DC	Tunnel-online (2020)
Melbourne	AU	Rail	7.3m	6.3m	Precast concrete 6 segm.	80-110km/h	1.600m	1500V DC	VIC (2023)
Lausanne M2	CH	Rubber-tyred	n.a.	n.a.	Shotcrete anchors	80km/h	1.435m	750V DC	Badoux (2011); Jaccard and Schobinger (2012)
Lille Metro VAL208	FR	Rubber-tyred	7.65m EPBS	-	Neoprene gasket, bolted segments	100km/h	1.000m	750V DC	Midi Mobilites
VAlp Metro	**CH**	**Rubber-tyred**	**6.5-7.5m DS / EPBS**	**f(liner)**	**Precast concrete 6 segm.**	**100km/h**	**1.435m**	**1500V DC**	

9.2 Safety Requirements

Safety requirements for a high-speed, rubber tired metro, running over a length of 34.3km are summarized hereafter in accordance to the latest notified technical rules by the Federal Office of Transport (FOT, 2015). The enforced rules abide by reference European TSI norms, as well as the national Swiss SIA requirements.

9.2.1 Infrastructure Norms

Therefore, the VAlp Metro follows the infrastructural safety requirements of the according to the Swiss Notified national technical rules (NNRTs) of SIA 197/1:2003:

- **Two single-shaft tunnels** are required for very long tunnels (>20km), as per the European railway and passenger transport directives. It is envisaged that crossing tunnels, as per

Figure 26, will be constructed to allow the evacuation of metro vehicles to the parallel shaft.

- **Escape routes** must lead to safe areas. In two single-track tunnels, the safe area is the adjacent parallel tube.
- **Cross passages** must connect both tunnels every 500m, allowing access to the safe area and deployment of emergency services. Cross passages must be minimum 2.2m wide, 2m tall. The doors are to be minimum 1m wide, 2m tall, revolving inwards. Subjected to dynamic pressure loads from passing trains, they must be sufficiently resistant. The internal environment must be pressurized to prevent smoke and combustible inflow.
- **Escape walkways** along the single-track tunnels must have minimum 2.2m of vertical clearance, and have a 1m wide elevated surface with respect to the track level. For tunnels >1km, they must be equipped with handrails, lighting and sign indications. Autonomous power supply is to be guaranteed for the lighting, situated laterally below or built-in the handrail.
- **Emergency communication systems** including radio (train, construction and emergency services) and telephony are to be provided.
- **Fire-water systems** are required for tunnels >1km. Hydrants and fire extinguishers must provide extraction water pressures from 0.6-1.5MPa, and extraction volumes of 20L/s per supply point.
- **Traction energy supply** such as overhead lines for tunnels of >5km must be segmented into maximum 5km sections (SRT TSI (1303/2014/EU)). Additional space must be provided for contact lines at switches and tensioners (SN 505 197/1).
- **Portal maneuvering spaces** of 500m^2 are required for fire-fighting vehicles (SRT TSI (1303/2014/EU)).

9.2.2 Ventilation System

National technical rules from tunnelling ventilation for the initial phase (SIA 31) until the final service instalment (SIA 53) are to be studied ad-hoc. This includes the design of the ventilation system, and anti-smoke systems used to fight potential tunnel fires (as the Lausanne M2 metro ventilation by GESTE Engineering, 2008). The concept design's, dimensions, realisation, testing and finalization can only be performed once the tunnel's cross section and vehicle gauge are finalized.

9.2.3 Overpressure

Aerodynamic modelling of the VAlp Metro tunnel cross section must be performed in parallel with the design of the project specific high speed metro design. Simulations of the aerodynamic fields must be performed, considering the overpressure effect on the vehicles and infrastructure. Special attention must be given to the portals, ensuring that the metro can maintain maximal velocity while entering and exiting the tunnels.

9.2.4 Fire Risk

A risk analysis for the tunnel dimensions, planned walkway geometry and spacing must be designed in view of the 34km long metro tunnel. Then, the infrastructure is to be measured for resistance to a given fire load according to Section 7.4.1.1 of SN 505 197/1, SIA 197/1:2003. This must be done to prevent concrete liner spalling that could endanger passengers.

9.3 Cross-Sectional Profile

The design of the cross-section is constrained by the vehicle dimensions (we propose an ad-hoc design in subsequent project phases), dynamic travel gauge, safety infrastructure layout and power supply requirements.

9.3.1 General Considerations

European rail guidelines for rail travel define safety spaces and escape route requirements independently of the design speed (Maidl et al., 2013). Additionally, the civil protection guideline of the DE-EBA, states that two-way passenger and goods traffic occurring at less than 160km/h, must take place in separate parallel tunnels. The VAlp Metro, must therefore abide to **two single-track tunnels**. Additionally, connecting shafts should be provided to allow vehicles to evacuate from one tunnel into the other in case of fire.

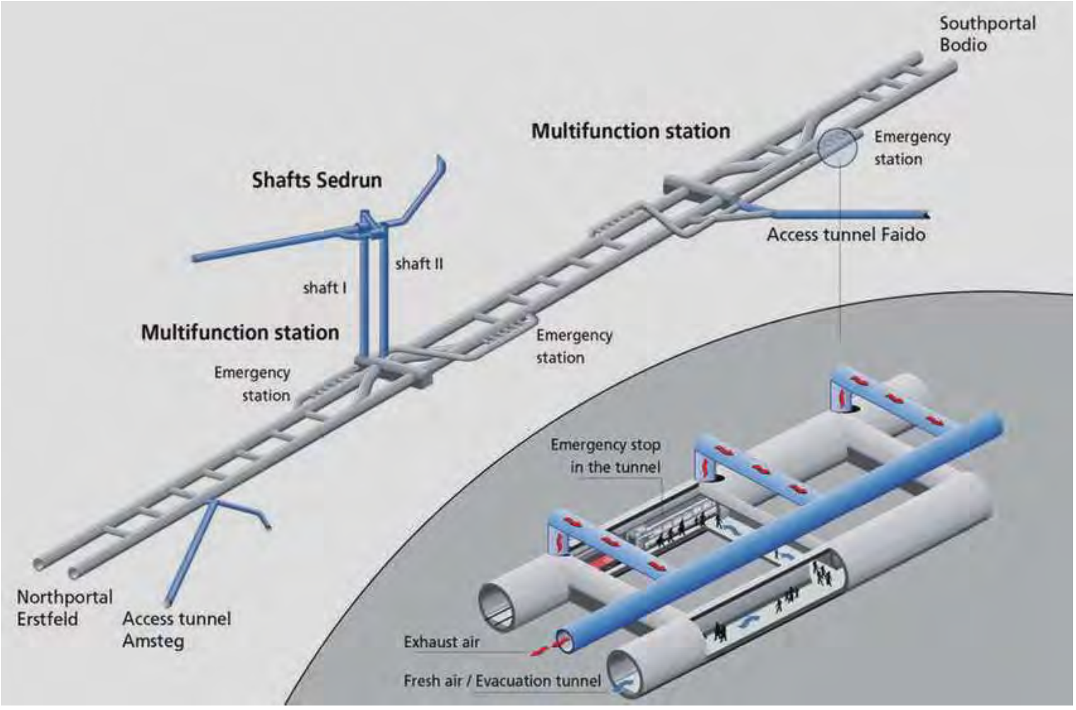

Figure 26 - Gothard base tunnel twin tube system, including cross-passages every 330m and additional emergency stations (AlpTransit Gotthard AG). The VAlp will implement a similar design.

9.3.2 Cross-Sectional Shape

The cross-section shape and metro technology are critical in determining the outline of the loading and structure clearance gauge. In view of reduced tunnelling and running costs, mechanically guided innovative transport systems benefit of small internal tunnel diameters. For example, the circular bus tunnels in Essen benefit from internal diameters of 4.5m (Maidl et al., 2014). Other works, such as the 1.6km long Saas Fee 1984 ski funicular tunnel merely measures 4.2m in diameter. The latter includes safety infrastructure such as escape pathways, lighting, handrails, signalling, power cables, telephone and water pipes. Current metro projects with circular tunnel cross sections were excavated by TBMs with external diameters ranging from 5.5-7.65m. Rounded profiles are optimal for brittle rock with medium strength (Limestone, Marl, Sandstone and Conglomerates crossed along the tunnel alignment).

For tunnels with lifespans greater than 40 years, the design standard for European civil engineering tunnels, suggests the use of segmental precast concrete linings (Brox, 2013).

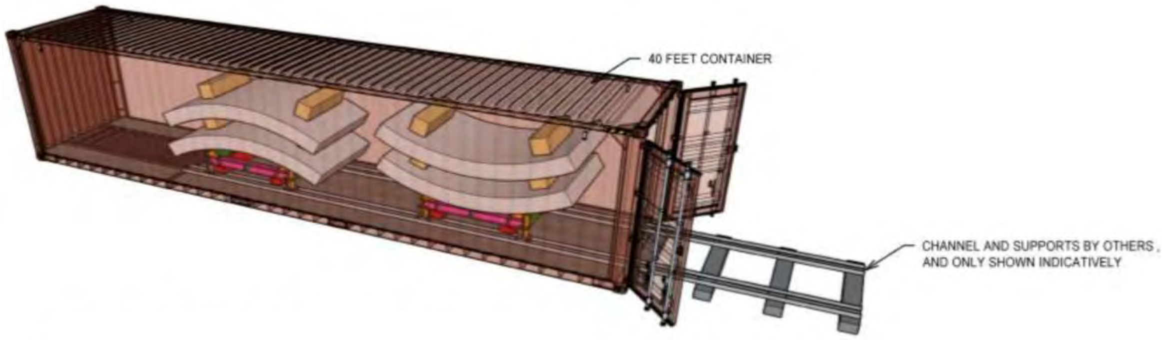

Figure 27 - Concrete liner segments placed behing the TBM cutterhead (Guerrieri et al., 2020)

Therefore, to ensure long term reliability and strength, five/six precast concrete segments (as visualized in Figure 27) are to be installed, fitted with waterproofing EPDM gaskets (water pressure resistance up to 16 bar) and along the TBMs advancement (British Tunnelling Society, 2004). This assures sufficient waterproofing, resistance to swelling and plastic deformations in high primary stress states in low strength Triassic formations. Segmental closure of the invert is therefore imperative in rock susceptible to softening, such as the Bex gypsum, due to its high plasticity and low modulus of subgrade reaction (Maidl, 2013). In fractured and vertically dipping pre-alpine Limestone, the segmental precast concrete liners provide resistance against the stress redistribution failure modes behind the TBM head (Brox, 2013). Lastly, this design allows to minimize the running maintenance costs are along the VAlp metro's lifetime. To save cross-sectional space, inner linings are not foreseen. Furthermore, the waterproofed tunnel will prevent modification of the effective stress field. Doing so should minimize drainage induced surface subsidence, which has occurred in projects such as the Gotthard highway tunnel (Zangerl et al., 2023).

Safety infrastructure – Escape paths, handrails, lighting and signs are included in the cross-section design. For the complete safety requirements, the VAlp metro concept refers to the applicable SIA norms (*see 9.2*).

9.3.3 Clearance requirements

Commercial passenger transport by metro can optimize the clearance profile by relying on power sources between the track gauge, rather than overhead cables. In doing so, the structural gauge is reduced significantly. Future aerodynamic studies must be performed once the aerodynamic light-weight metro cars are designed. According to trans-european TSI norms, the maximum pressure variations between peak positive and negative pressures must not exceed 10 MPa for trains travelling at maximal speeds supported by the single-track infrastructure (TSI Infrastructure, 2008). Aerodynamic studies should seek to optimizing energetic consumption, guarantee pressure confort of passengers and conform to pressure variability norms. For example, the 6.5m tunnel must be designed to prevent overpressure build-up, or provide de-compression ducts along the tunnel trace. Lastly, environmental noise concerns must also be addressed in the vicinity of the tunnel portals near Villars-sur-Ollons and Les Diablerets.

9.3.4 Final Cross Section

Considering the existing metro tunnels, safety requirements, ventilation systems, tunnel liner and communication infrastructure a first cross section is designed for a tunnel boring machine excavating a 6.5m external diameter (Figure 28). This shows sufficient clearance for a rubber-tyred metro in a metro tunnel of standard dimensions. This design shall be further refined and potentially optimized in function of a future detailed geotechnical and geohydrological study of the region (defining the precast segment thickness), a detailed impermeabilization and drainage analysis, and most important the aerodynamic and rolling stock design.

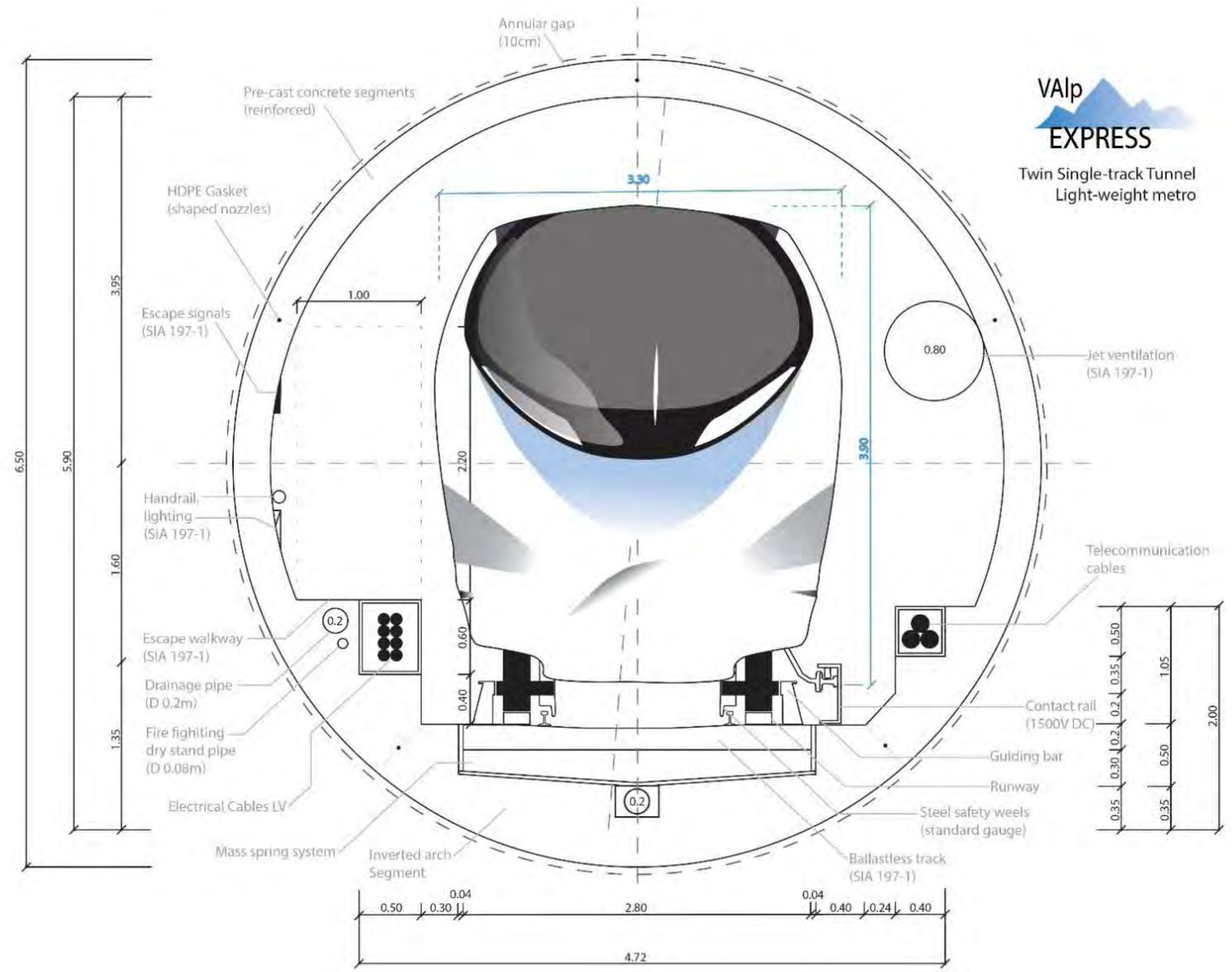

Figure 28 - Considerations and development of the VAlp Metro cross-sectional profile. Cable ducts and drainage facilities are included in the inverse arch concrete segment, as per the Koralm tunnel final cross-sectional design by Harer et al. (2008). A central drainage system minimizes the total length of required drainage pipes to 68km. Future studies should optimize the mass spring system and drainage facilities below the track.

VAlp
EXPRESS

10 Energy

Mobility in mountainous regions remains complex and energy inefficient, and thus provides enormous potential for future innovations. The ambitious VAlp metro concept explores the vision of a new light-weight mobility option. At the core of the proposal lies the challenge to improve green mobility in mountainous regions. To tackle this problem, additional light is shed on the energetic requirements for the execution of the VAlp innovation.

One time energetic needs are specified during the tunnelling excavation phase by TBM, followed by the yearly operational energy requirements of the VAlp Metro operation. Thereafter, a proposed renewable energy production is proposed. This simplified model compares the required energy and the produced energy as per Figure 29.

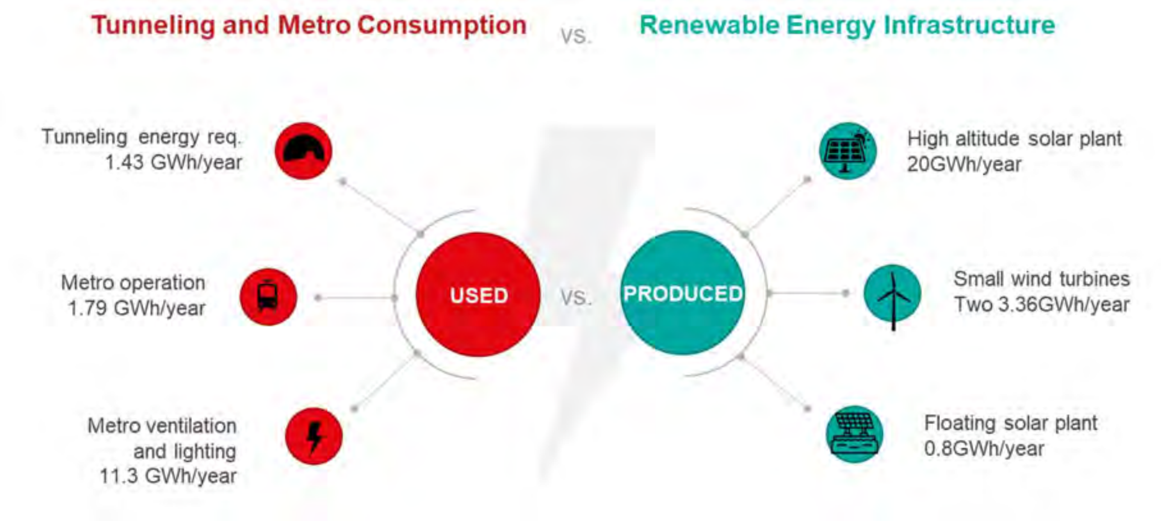

Figure 29 - Energetic consumption during the tunneling and VAlp operation, versus the produced green energy infrastructure included in the project proposal.

10.1 Tunnelling Consumption

10.1.1 TBM Excavation and Construction

State of the art excavation by TBM is driven by electrical engines, reducing noise and emissions. All components such as separation, mixing plants, transfer tanks, pumps and pre-crushing units are all electrically powered. The advance rate, rotary speed and energetic use of the TBM varies greatly based on cross sectional area, rock type and more. To approximate the energy use of double shield or EPBS tunnel boring machines for this study, literature averages are used to approximate electrical needs.

Peeling et al. (2016) have estimated TBM consumption 195.3 kWh / m (Figure 30). This value is used in the energy requirements estimation of the VAlp metro tunnelling project.

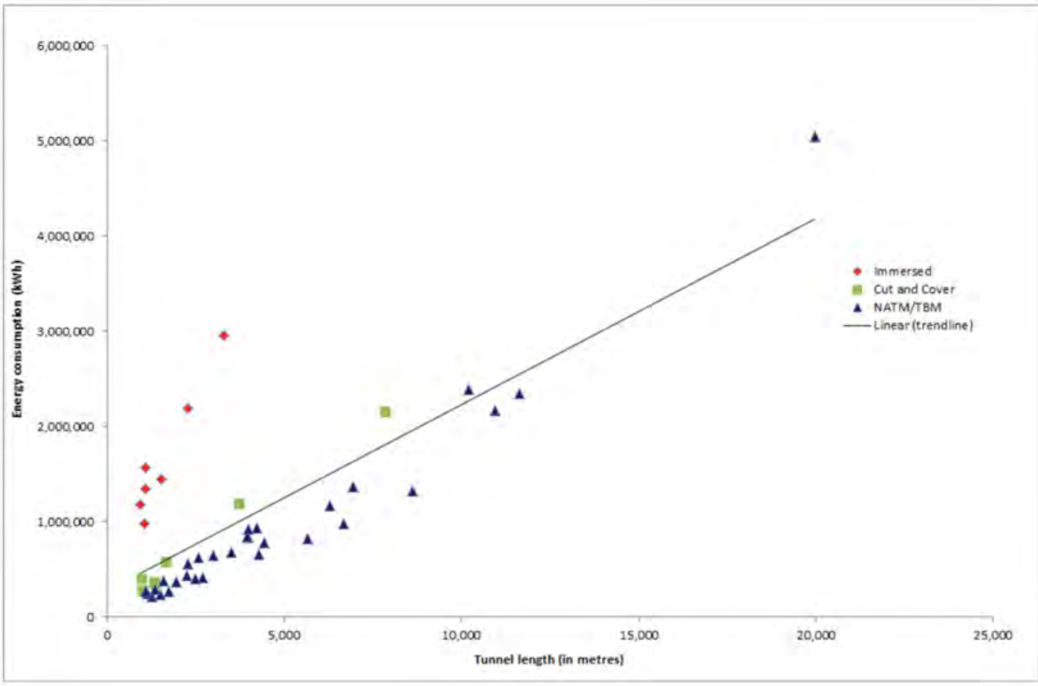

Figure 30 - Total energy consumption of european tunneling projects over varying lengths. Three tunneling technologies are depicted; amonst them the TBM in blue (Peeling et al., 2016)

In the scope of the project, a first order energetic calculation is performed according to the following specifications:

- TBM consumption = 195.3 kWh / m.
- Tunnel length = two tunnels of 34.25 km
- **Total TBM energy consumption** = 2*(195.3kWh/m * 34'250m) = **13.378 GWh**
- **Total TBM energy cost** = 13'378'050kWh/yr * 0.16chf/kWh = **2'140'490.- chf**

Additionally, a key factor in the future project proposal of the VAlp tunnel is to minimize grey energy usage of the TBM. Companies such as the industry leading Herrenknecht (DE) propose various way to do so, reusing large steel components over multiple project cycles. They state that refurbishing individual components saves 80% electricity compared to new elements (*https://www.herrenknecht.com*).

10.2 Operational Consumption

10.2.1 Metro Operation

Energy consumption of mountain metros - Light rail driverless metro systems in mountainous regions are rare, but have shown great potential. For example, the Lausanne rubber tyred metro carries 222 passengers over gradients up to 12%, with an average of 5.7%. Its three rail track system provides 750 V DC current, consuming 150kWh per journey from Ouchy to Croisettes. Similar metros, such as the VAL 208 models by Siemens, climb gradients up to 10% and consume on average 80kWh. Three European metros are compared in Table 12, where the Lausanne M2 is the only one climbing steep gradients.

Table 12 – Average energy consumption of four European rubber tyred metros.

Name	Count.	Type	Max. Velocity	Max Gradient	Avg. Gradient	Power	Mean Consumption	Reference
Copenhagen M3	DK	Rubber - tyred	90km/h	n.a.	n.a.	630kW, 750V DC	102kWh	Metroselskabet I/S (2021)
Lausanne M2	CH	Rubber - tyred	80km/h	12%	5.7%	750V DC	150kWh	Jaccard and Schobinger (2012)
Lille Metro VAL208	FR	Rubber - tyred	100km/h	10%	n.a.	750V DC	80kWh	Midi Mobilites
VAlp Metro	**CH**	**Rubber-tyred**	**100km/h**	**11%**	**3.8%**	**750/1500V DC**	**80-140kWh (?)**	

Steep gradients equal recycled energy - Electrical braking energy can be recycled by an inverter system. New mobility relies on this technology to reduced energetic consumption. For example, the rail London metro's braking systems leads to annual savings of up to 5% (re-collection of 1MWh) (CEC CREW, 2015). Others, such as the Melbourne metro have reached energy savings of 27% per kilometer (Lo Monaco et al., 2016). These systems can reach a highest recovery efficiency of ~85%, as seen in Figure 31 (Ruigang et al., 2017).

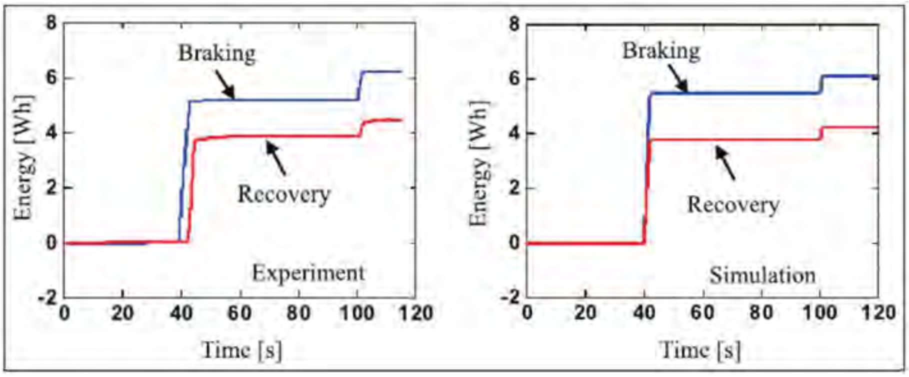

Figure 31 - Braking and recovery experiments for rail vehicles using a new DC/DC converter and supercapacitors (Ruigang et al., 2017).

In the scope of the project, a first order energetic calculation is performed according to the following specifications:

- Light-weight rubber tyred vehicle = 140kWh (Jaccard and Schobinger, 2012)
- Travel time Aigle - Chateau d'Oex = 35 minutes
- One two-way trip = 2*(140kWh (0.35h/0.6h)) = 163.3 kWh
- Every hour, doubled during peak hours = 30 runs per day
- **Total metro energy consumption** = 4'900 kWh/d = **1.788 GWh/year**
- **Total metro cost** = 1'788'500kWh/yr * 0.16chf/kWh = **286'160.- chf/year**

10.2.2 Ventilation and Lighting

Rail Ventilation Systems – Railway tunnels have less ventilation equipment than highway road tunnels, leading to reduced operational costs between tunnels of varying traffic type. On average, swiss motorway tunnels consume on average 0.54GWh/km of road (Riess, 2022), whereas long railway tunnels consume only 0.21GWh/km of rail (Guo et al., 2016).

The 57km long Gothard (CH) base rail tunnel is ventilated by 24 jet fans located at the portals, with additional fresh air vertical shafts in three locations. The fans have 3.5m diameter providing a **maximum power of 15.6MW** (ABB, 2016).

These values remain five times higher than actual energetic consumption of such systems, which are reduced by optimizing ventilation modes. For example, the 27.8km long Taihangshan Tunnel along Shi-Tai Railway (CI) has a yearly **energetic consumption of 3.04MW**, amounting to operational costs of 1.43 million dollars (Guo et al., 2016).

Jet Fan System – Longitudinal tunnel ventilation is requried to satisfy airglow regulation and smoke control in case of a fire. Recent developments in jet fan systems allow an energy efficient, compact and 100% reversible airflow solution (Tarada, 2015). Their improved performance over conventional axial flow fans allows for optimized usage of the cross-sectional space, which is desired in the scope of this project. For example, the ventilation optimization study of various long tunnels ranging from 4.2km to 18km by Guo et al. (2016), resulted in 26.8% energy savings when implementing jet fan ventilation. With energy costs of 0.24 $/kWh, the tunnel operating costs were reduced by 84-678 million dollars per year.

Additionally, jet fans with shaped nozzles (Figure 32) further reduce energy consumption and noise. MoJet® models lead to 7dB reduction in noise emissions while requiring 30% less power (Tarada, 2018).

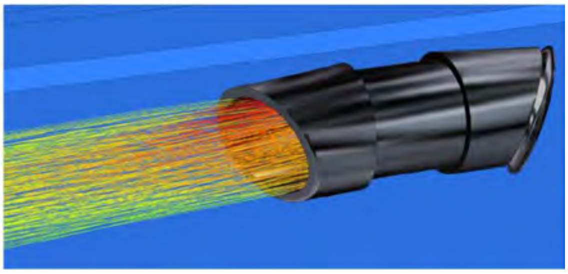

Figure 32 - Efficient ventilation via jet fans with shaped nozzles to direct flow away from the tunnel walls (Tarada, 2015).

In the scope of the project, a first order energetic calculation is performed according to the following specifications:

- Jetfan Diameter = 800mm
- Power requirement per jetfan = 37 kW (Tarada, 2018)
- Fan operating time, speed controlled = 1’800 h *(assumed ~20% of the year)*
- Two Single-tunnel shaft = Two single jet fan ventilation *(see cross section design)*
- Fan every placed every = 480m *(must conform SIA 197-1 Appendix H)*
- Number of fans = 2*(34km) / 0.48km = 142
- Total ventilation power = 37kW * 142 = 5.254 MW
- **Total ventilation energy consumption** = 5.254 MW * 1800h **= 9.46 GWh/year**
- **Total ventilation cost** = 9’457’000kWh/yr * 0.16chf/kWh = **1’513’150.- chf/year**

Lighting Requirements - As specified by SIA 197-1-2004, rail traffic does not require lighting. Nonetheless, it is noted that high speed single track railway lighting optimization field studies have shown maximal efficiency when using 25W LED lights every 20m, along one side of the tunnel (Zang, 2014). Maintenance workers, for example, provide their own mobile sources. It is further specified that the emergency lighting must be designed in 500m sectors.

In the scope of the project, a first order energetic calculation is performed according to the following specifications:

- Emergency light power = 2W *(for example EVAC by Sammode©)*

- Number of emergency lights = 34km / 0.02km = 1700
- **Total light power** = 2W * 1700 lights = 3.4 kW
- **Total light energy consumption** = 3.4 kW * (24h * 365 days) = **29.8 MWh/year**
- **Total light cost** = 29'784kWh/yr * 0.16chf/kWh = **4'765.- chf/year**

10.2.3 Total Operational Energy per Year

The total operational energy consumption amounts to 11.275 GWh per year, for a cost of 1'803'000.- chf/year. Most energy is used to ventilate the tunnel, indicating a likely source of optimization in future studies. We propose vertical shafts in tunnel areas proximal to the surface, which along with the moving pressure shifts of the metro, should be studied as an alternative to decrease energetic needs and running costs of jet fans.

Overall, the VAlp metro energetic consumption prediction amounts to 0.33 GWh/km of rubber metro rail. This estimate is 39.9% less than the average Swiss road tunnel (Riess, 2022) and 57.1% more than the longest Chinese rail tunnel (Guo et al., 2016).

10.3 Wind and Solar Production

Swiss renewable energy production has lagged behind other European countries. Assuring solar and wind power production is key in assuring a greater energetic autonomy of region. The VAlp tunnelling and operational energy needs shall be met with the construction of permanent renewable energy power stations.

10.3.1 National Interest

In 2022, Swiss wind farms have produced a total effective of 185GWh (Keystone-SDA/jc, 2022). Additionally, regional parliaments have been pushing the development of large solar parks in high mountain regions, in an attempt to increase the current production to projections of 16TWh nationally (Keystone-SDA/RTS/sb, 2023). Swiss aeolian production increases in winter, whereas solar and hydropower increases in summer. The two energy sources therefore display a large synergistic potential.

While renewables account for 29% of the nation's total energy consumption, Switzerland remains well below the front running Sweden (60%) and Denmark (44%). In the current domestic renewable energy production, hydro-electric plants account for 60% of Swiss output. Meanwhile, the largest un-tapped potential remains in high-altitude solar and wind farms (Presence Switzerland, 2023).

10.3.2 Regional Study

To optimize the synergy of renewable energy infrastructure for the Vaud Alps, a future study in synergy with EPFL's Laboratory of Cryospheric Sciences (CRYOS) could use the new tool by Dujardin et al. (2021). The tool is used to guide planning and siting of the infrastructure. It has shown great potential in a Swiss nation-wide case study, and could be used to analyse and optimizing the VAlp's energy production contribution to Swissgrid. This would serve as a quantifiable model of impact in the canton de Vaud in securing Swiss energetic needs.

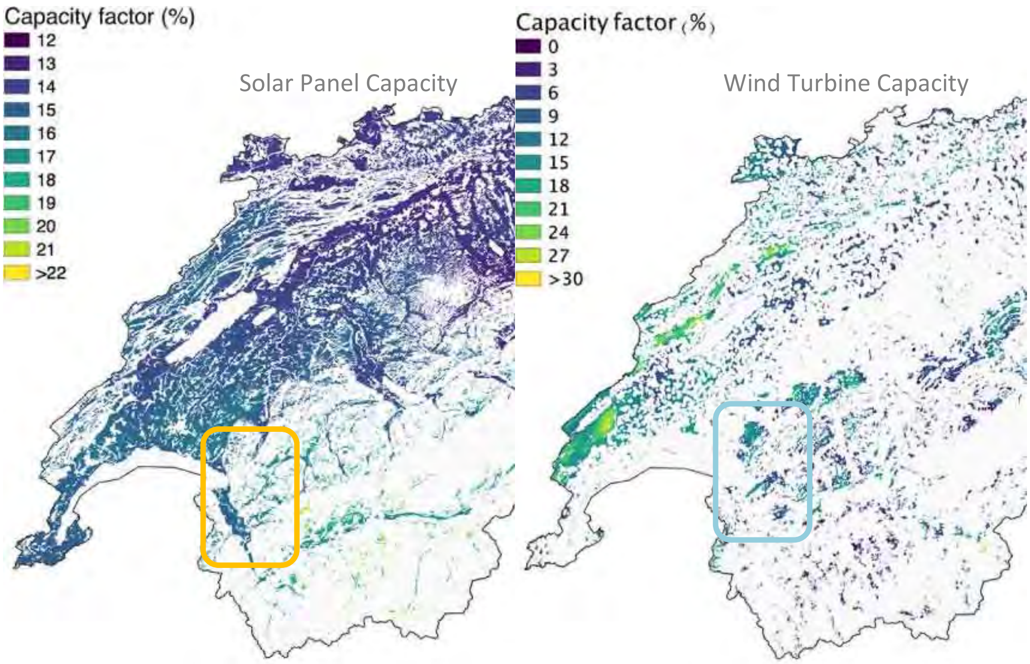

Figure 33 – Potential locations of photovoltaic infrastructure (left) and wind turbines (right). Extract of the Switzerland case study by Dujardin et al. (2021).

The Vaud Alps show promise in contributing as an innovator of renewable energy production (Figure 33). Photovoltaic installations show greater promise at altitude and towards the south-west Villars-Aigle region. Meanwhile, wind turbines are best suited farther along the metro tunnel, near Les Diablerets and Chateau d'Oex. Alongside existing hydro-power plants, the new renewable energy infrastructure can ensure a secure national energy supply once connected to the Swissgrid.

10.3.3 Project Specific Design

The current study proposes a first order estimate of the tunnelling and operations energetic needs. Using this data, a list of strategies is proposed for to develop innovative renewable energy installations in the Vaud Alps. They are ordered by decreasing scale, providing a broad toolbox for spatial optimization in a future stage.

- **High-altitude solar plant** – A large facility of bifacial panels such as the Valais based Grengiols solar project is proposed, capable of providing up to 600GWh annually (Ivanova, 2023). Located between 2000-2500m, the projected 6.6km^2 infrastructure benefits of 1'500h of sunshine per year. Downscaled versions of the project (likely reducing opposition by environmental activists) are proposed, such as the Gondosolar pilot which aims to produce 23.3GWh per year using solar panels covering 10 hectares (Bradley, 2022). In fact, large solar plants in the Alps producing more than 10GWh annually can benefit from federal funding of up to 60% investment costs (Bradley, 2022).
  For the VAlp metro a similar structure is envisioned **producing 20GWh per year** of electricity. This would require **0.1-0.22km^2 of space** in the Vaud Alps. The increase in winter effective output may be further increased by albedo effects (Fritzsch et al., 2022).

Figure 34 – Grengiols-Solar originally projected at 600GWh over a surface of 6.6km2 (Ivanova, 2023)

- **Floating solar farm in the Lac de l'Hongrin** – Floating high-altitude solar farms have a higher energetic yield, especially during high albedo winter months . A pilot project by Romande Energie covering **2'240m^2** of the Lac de Toules in Valais yields an **effective 800'000 kWh annually** (Huszno, 2021). With a cost of 2.35 million francs, the innovation has won the Watt d'Or award and is at the forefront of the Swiss energy transition. The environmental concerns are minimized when located behind dams in artificial lakes.

Figure 35 - Potential location for high floating photo-voltaic infrastructure in the Vaud Alps, as the pilot project located in Valais (Huszno, 2021).

Following this innovation the canton Vaud can evaluate the potential of deploying a similar technology in the Lac de l'Hongrin.

- **Wind turbines** – Swiss renewable energy production in 2022 relied on wind 41 turbines, producing a total of 146GWh. To achieve the 4.3TWh goal set for 2050 by Switzerland's energy strategy, a total of 760 turbines must be installed. To harness sufficient power, ETHZ studied the distribution of wind turbines. They suggest "…smaller ones (100 metres high, 39 metres rotor radius) for the Alps, medium-sized ones (125 metres high, 67 metres rotor radius) for the foothills of the Alps and the Jura Mountains, and the largest and most powerful wind turbines (150 metres high, 73 metres rotor radius) for the plains of the Swiss Plateau" (Elhardt, 2023).

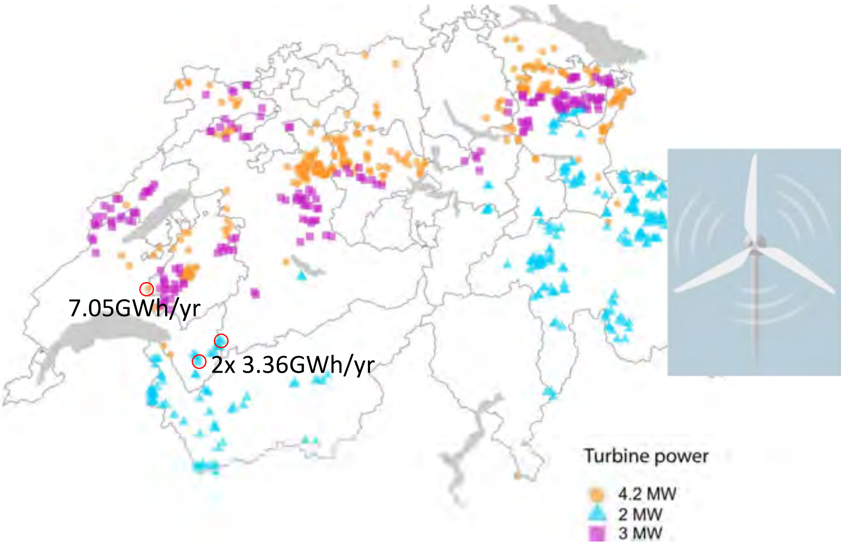

Figure 36 - Optimal distribution of wind turbines needed to meet the national 2050 renewable energy strategy (Spielhofer et al., 2023). Circled in red the two windiest areas in Vaud, conveniently located along the tunnel alignment.

Small scale, low visibility turbines are proposed as optimal solutions placed along the VAlp study location. Light infrastructure with an installed capacity of 2MW (39m rotor radius) would likely produce **3.36 GWh annually**, whereas large turbines (installed capacity 2MW, 73m rotor radius) would likely produce 7.05 GWh annually (Jorjio, 2023). In the scope of the project, **two small turbines** are suggested in the canton's windiest areas of the study region (red circles, Figure 36). If required, an additional large turbine can be constructed between Moudon and Oron.

- **Solar panels on existing infrastructure** – To minimize the visual impact and cluttering in alpine terrain, solar panels can be placed on existing infrastructure such as avalanche protection. This is beneficial in the public's view alongside environmentalist campaigns against large infrastructure at altitude.

Figure 37 - Photovoltaic installation upon existing mountain infrastructure, such as avalanche protection (Keystone-SDA/RTS/sb, 2023), dams and road infrastructure.

Thanks to the hydroelectric infrastructure near Aigle, a connection line will be developed to connect new electrical production to the Swissgrid extra-high voltage grid and the strategic grid.

10.4 Result

The proposed technology is downscaled compared to the state of the art projects currently being constructed to achieve Switzerland’s 2050 energetic agenda. For this reason, the energy production and consumption plan is deemed realistic for an interdisciplinary project such as the current study.

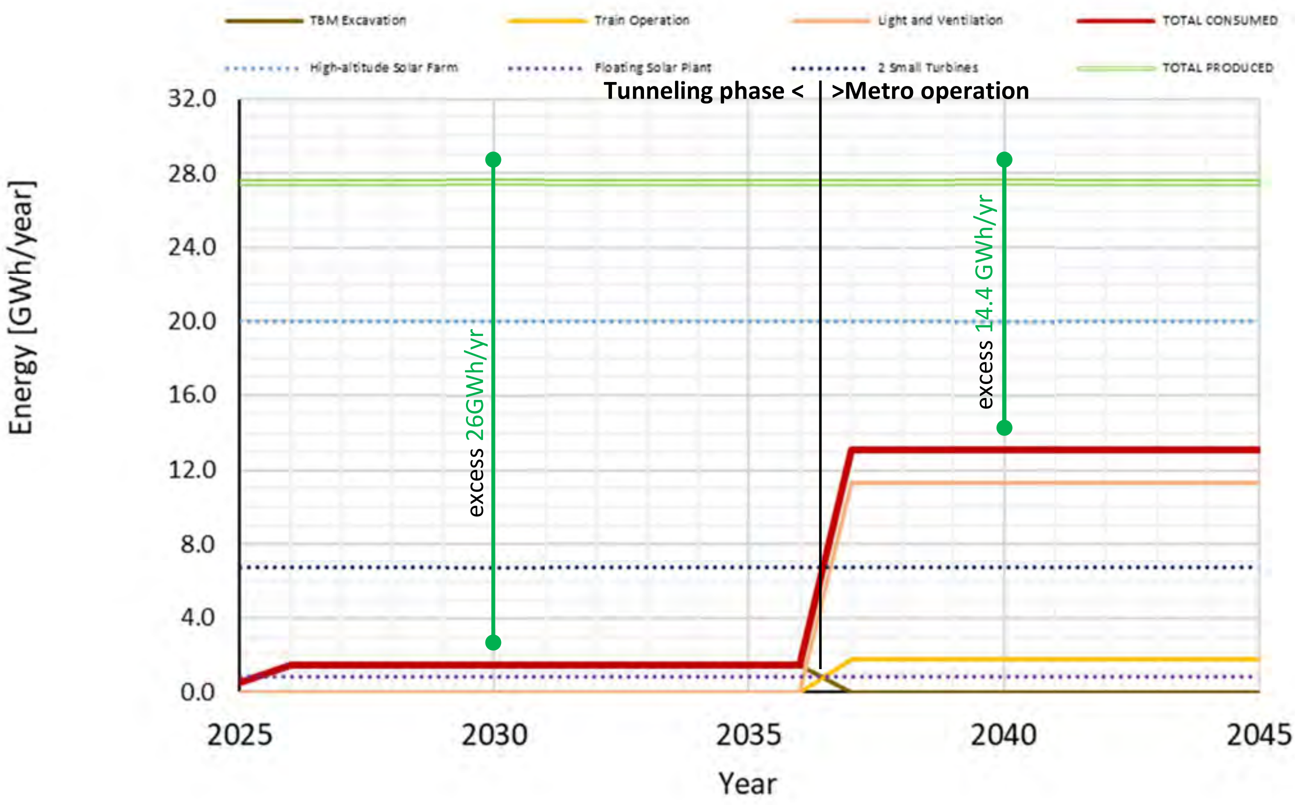

Figure 38 - Energy plan for the VAlp metro project, showing the electrical consumption during tunneling and operation of the high-speed metro. The use of light and non invasive renewable energy infrastructure would lead to an excess production, which shall be connected to the Swissgrid by .

Comparing the consumption and production shows that integrating innovative renewable energy production, the target study shows excess electrical at both tunnelling and operational phases of the VAlp high-speed metro. During tunnelling operations, the excess energy for fully functional renewable energy infrastructure is of 26GWh/year, whereas during normal metro operation the canton and Swissgrid will benefit from 14.4GWh/year.

The logistics of installing and connecting 390KV powerlines can take 10-15 years, and therefore an optimized two-phase construction process could also be implemented. For example:

- <u>Tunnelling Phase</u> = rapid instalment of **2 small wind turbines** (39m radius, installed capacity 2MW) and the **1 floating solar farm** (2’240m2, 0.8GWh/year)
- <u>Metro Operation and Long Term</u> = completion of the renewable energy infrastructure by construction the **high altitude solar plant** (0.22km^2, 20GWh/year)

11 Environmental Impact

A CO_2 assessment is performed to investigate the environmental impact of the VAlp metro project. The situation is evaluated for a horizon of 2080. First, the methodology is explained. After, the results of the current analysis are presented.

11.1 Methodology

A traffic analysis was performed to analyze the impact of the creation of the metro line in terms of CO_2 emissions. The calculation is performed assuming two TBM's excavating the twin-tunnel over the predicted course of 11 years.
Thereafter, the impact is quantified three different evaluation steps:

1. Analyzing existing traffic data for the region
2. Estimation of the current CO_2 emissions from motorized traffic
3. Estimating the CO2 impact of tunneling and metro's operation
4. Predicting CO_2 emissions from motorized traffic with the VAlp metro

The impact of a high-speed VAlp metro is therefore accounts for the scenarios:

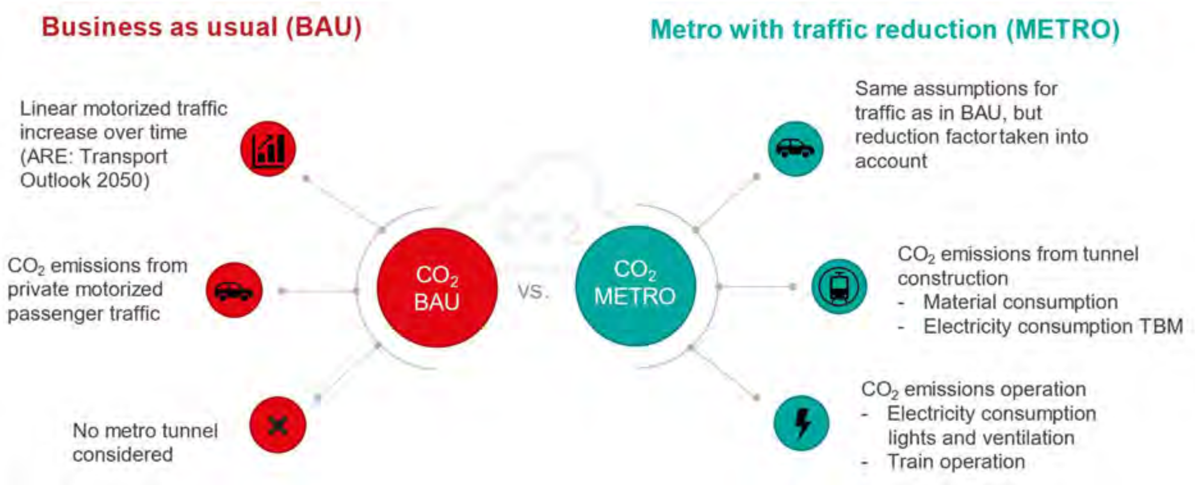

Figure 39 - Overview of the most important assumptions and considerations for the analysis of the carbon dioxide calculation.

11.1.1 Regional traffic overview

The Federal Office of Topography Swisstopo provides traffic data for the Swiss road network. For different road sections, the average daily traffic (ADT) and the average weekday daily traffic (AWDT) are indicated on the map as average over the year 2017. The data, which is of interest in the scope of this feasibility study, is highlighted in Figure 18.

	Average Daily Traffic		Average Weekday Daily Traffic	
	Cars	Lorry & delivery	Cars	Lorry & delivery
1	4694	659	5169	780
2	1801	238	1996	280
3	1391	190	1579	227
4	54	5	65	6
5	1443	197	1643	235
6	187	6	21	8
7	2978	1091	3334	1256
8	4270	390	4905	461

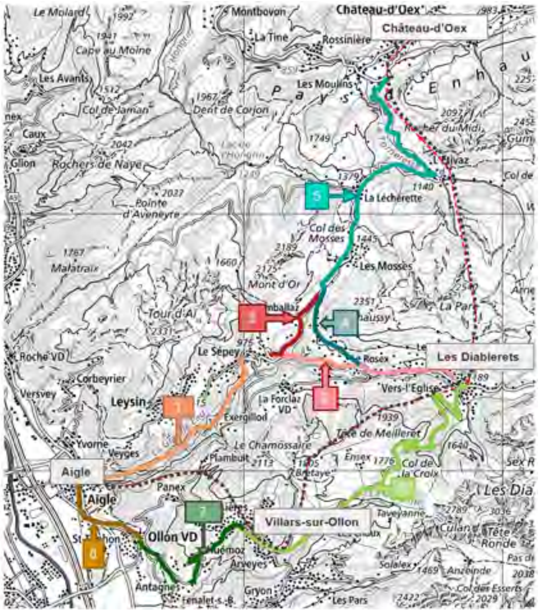

Figure 40- Traffic data from 2017 in the region of interest (Swisstopo)

A traffic prediction for 2050 is done by considering the data of 2017 multiplied by an increasing or decreasing factor. The Federal Department of Environment, Transport, Energy, and Communication has published a report about the transport outlook for 2050 in 2020. The traffic prediction is thereby based on four different scenarios: basis, sustainable society, individual society, and business-as-usual (ARE, 2022).

In the case of the current CO_2 analysis, the business-as-usual is of main interest, since it predicts the transportation and traffic based on a situation, which considers a continuation of the present habits, behavior, and legislation. Slow integration of technological developments into mobility and a similar volume of traffic characterize this scenario. At the same time factors like population growth and population ageing are included in this prediction.

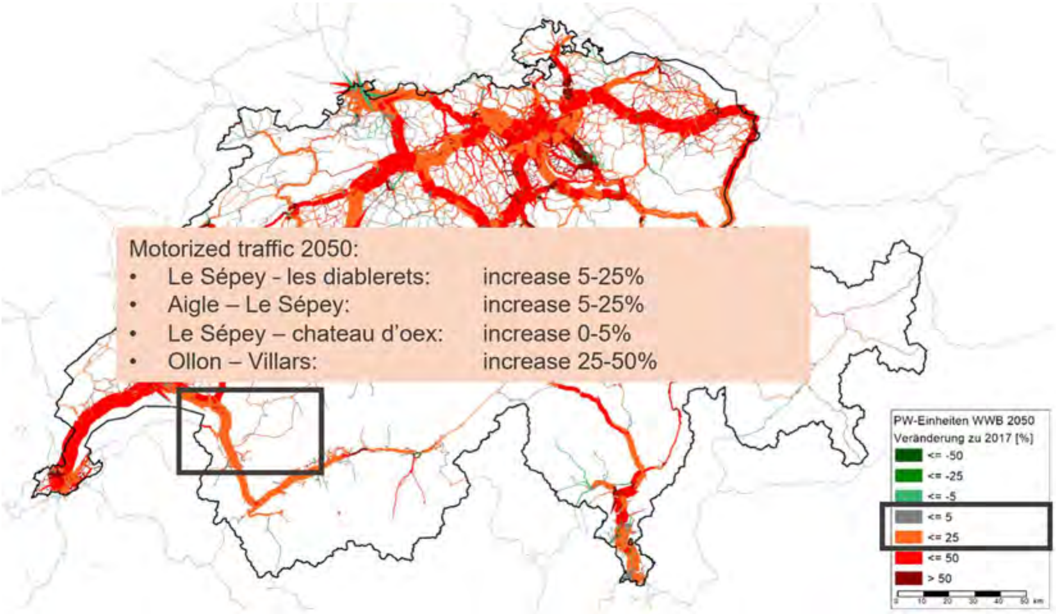

Figure 41, Motorized traffic increase in 2050 compared to 2017 illustrated on the swissmap (federal department of environment, transport, Energy and communication: transport outlook 2050)

	Average Day Traffic 2050		Passengers 2050	
	Prediction factor (max)	cars	Occupancy (commuters)	Total passengers
1	1.25	5868	1.07	6278
2	1.25	2251	1.07	2409
3	1.05	1461	1.07	1563
4	1.25	68	1.07	72
5	1.05	1515	1.07	1621
6	1.00	187	1.07	200
7	1.50	4467	1.07	4780
8	1.25	5338	1.07	5711

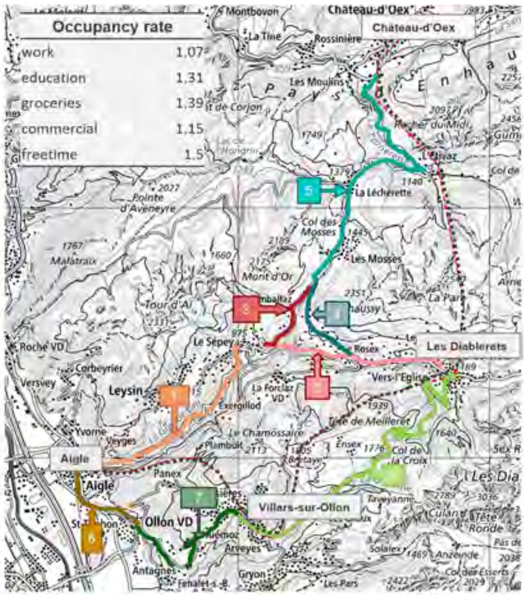

Figure 42 - Car passenger prediction throughout the study location's roads for 2050

11.1.2 CO_2 emissions of motorized traffic

According to a report about passenger commuting behavior from the Federal Statistical Office in 2019, the average traveled distance with motorized private vehicles in Canton Vaud is 27.8 km. The average car emissions are fixed at 153 gCO_2/km (Dings, 2009), which is used to estimate the impact of motorized traffic in 2017. Passenger transport emissions are calculated as per Figure 43.

Section		Average daily traffic 2017 (ADT)		Average workday traffic 2017 (AWDT)		Business as usual - 2017						
		cars	Lorry & delivery	cars	Lorry & delivery	Passengers occupancy[1]	total	Goods	Average distance car [km/(car*day)][2]	Distance reduction factor[4] (used to be 0.7)	gCO2/km[3]	CO2 emissions per section [tCO2/day]
Aigle-Villars	8	4270	659	4905	780	1.07	4569		27.8	1	153	20.9
Villars-Diablerets-Chateau d'Oex	1-5	9383	390	10452	461	1.07	10040		27.8	1	153	44.5

Figure 43 - Overview of the traffic calculation for the current situation (2017 representative)

Based on the predicted car passenger number in 2050, a linear yearly percentage increase in motorized traffic is defined. With 25% increase between 2017-2050, the yearly traffic increases by 0.76%/year on the target region's roads.

The total prediction for the 2050 Business as usual (BAU) scenario is shown in Figure 44.

Buiness as usual - prediction 2050											
factor 2050	ADT 2050		AWDT 2050		Passengers		Goods	distance car	reduction factor[4] (used to be 0.7)	gCO2/km[3]	emissions
	cars	lorry & delivery	cars	lorry & delivery	occupancy[1]	total					
1.25	5338	824	6131	975	1.07	5711		27.8	1	153	26.1
1.25	11729	488	13065	576	1.07	12550		27.8	1	153	55.6

Figure 44 - Business as usual (BAU) prediction for 2050 using the traffic increase as presented before

These assumptions lead to a linear increase in the traffic CO_2 predictions over time.

11.1.3 CO_2 emissions of tunneling and metro operation

To estimate the project's CO_2 impact during the development and operations, first order estimation of the impact of the tunnel is calculated by taking into account the tunneling and operational requirements.

- *Tunneling:* Electricity consumption of the TBM, concrete liner manufacturing and annulus grout
- *Operation:* Electricity consumption due to metro operation, tunnel ventilation and lighting

For each of these components, the calculation is implemented as a function of time, whereby the 11 year (average) VAlp tunneling time predicted by the DAT is used.

11.1.4 Predicted CO_2 emissions with the VAlp metro

A switching factor α is defined as the percent of passengers switching from motorized commuting to the VAlp metro. Once the tunnel is complete, the number of passengers switching to the new metro system is hypothesized as being 30-50% of current commuters. This is an input variable with immediate effect, allowing the evaluation of the influence of a high speed metro on CO_2 emissions.

Thereafter, the metro is hypothesized to reduce the yearly increase of motorized traffic in the region. Once the tunnel is in operation, the traffic increase of 0.76%/year is reduced by 30-50% (factor α).

11.2 Results

Using the previously calculated data a comparison was made between the business as usual scenario and the scenario with the VAlp construction and consequently a reduction factor in the considered traffic in the region. An overview of all the input in this comparison is given in *Figure 39*. Further construction and operational considerations are detailed in the annexed *Table 14* and *Table 15*.

The comparison of yearly CO_2 emissions is shown in Figure 45 for an optimistic (fifty-per-cent) and pessimistic (thirty-per-cent) traffic reduction scenario.

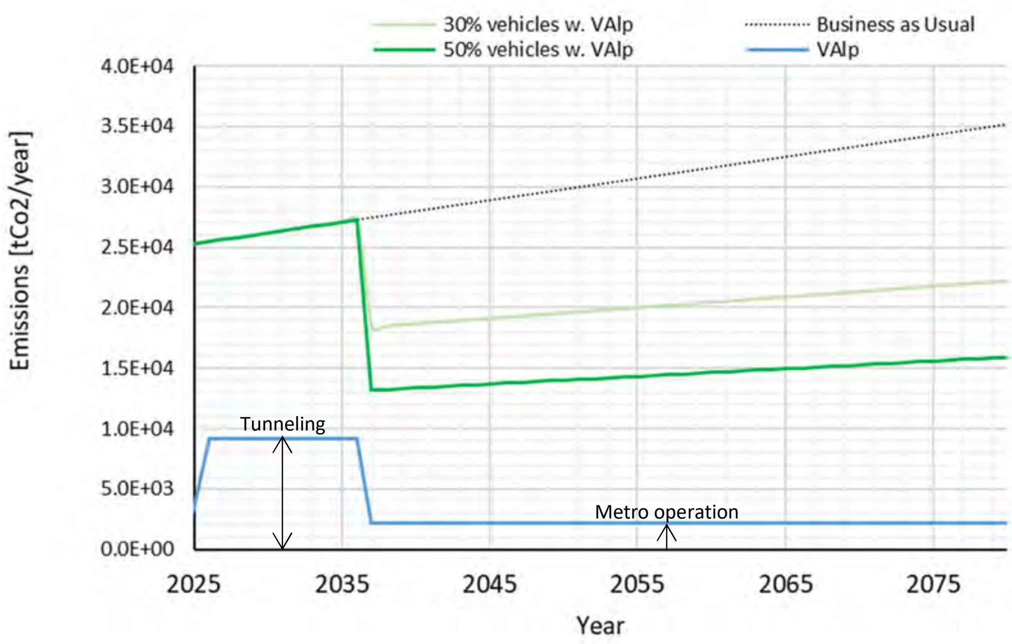

Figure 45 - Yearly carbon dioxide emissions in the Vaud Alps due to motorized commuting, and the effect of a high speed metro.

During the tunnel construction time period the CO2-eq emissions of the VAlp scenario are higher than the reference situation. However, after the completion of the metro station the yearly CO2 emissions are reduced compared to the reference scenario. The point where VAlp metro leads to a reduction on CO2 emissions depends heavily on the factor α, the switching factor, that accounts for the number of people that switch to taking the metro.

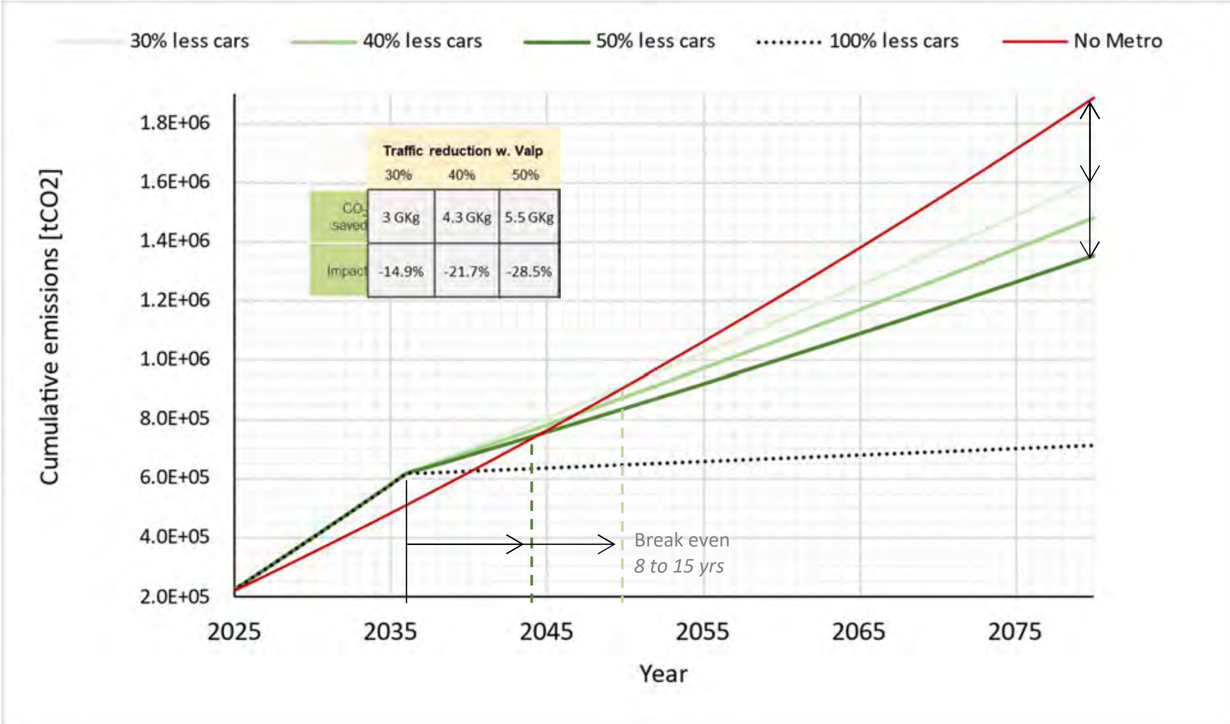

Figure 46 – Cumulative CO_2 over time, considering the impact of the VAlp metro reducing motorized commuting

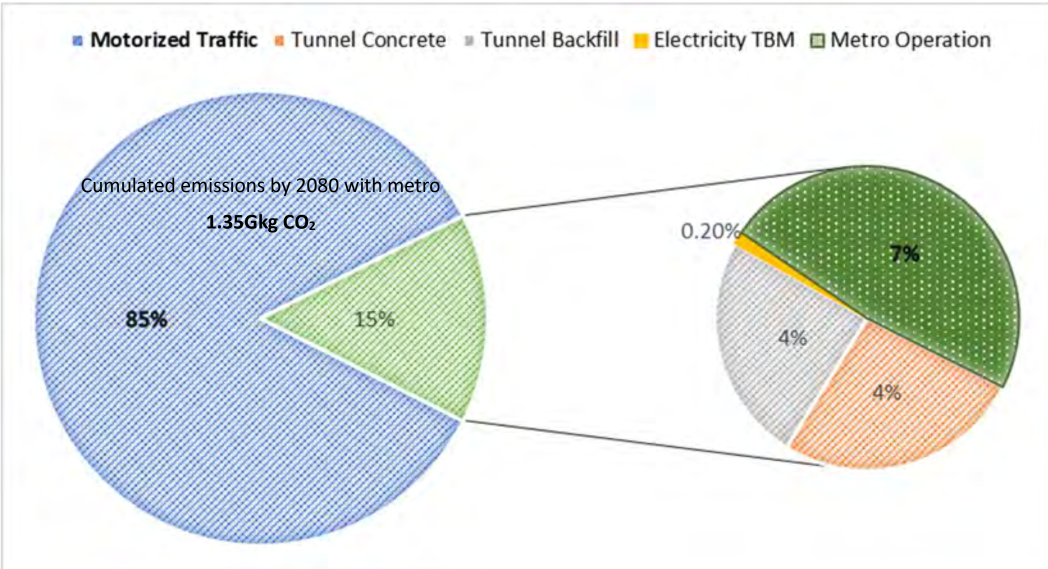

Figure 47 - Breakdown of the constituents of all the cumulated CO_2 until 2080 if 50% of daily commuters take the high speed metro.

The current projection does not take into account the further reduction of emissions if daily cargo metro vehicles are implemented, providing daily transport of goods. Additionally, the service can be provided earlier, and provide an earlier impact if four TBM's excavate simultaneously from adjacent portals (instead of two used in the prediction).

12 Economic Evaluation

A first order financial calculation is executed as part of the pre-feasibility study. It builds upon the considerations made in the previous chapters; notably the tunnel alignment, cross sectional design, energy infrastructure and operational needs.

12.1 Financial Overview

The total cost of creating a metro tunnel of 6.5m in diameter is estimated in Figure 48. An average of 25Mchf/km is assumed in the financial overview. Ergo, the tunnel infrastructure's cost is calculated as the aforementioned average, minus the cost prediction of a twin-tube tunnel calculated with the DAT tool of Einstein (2018).

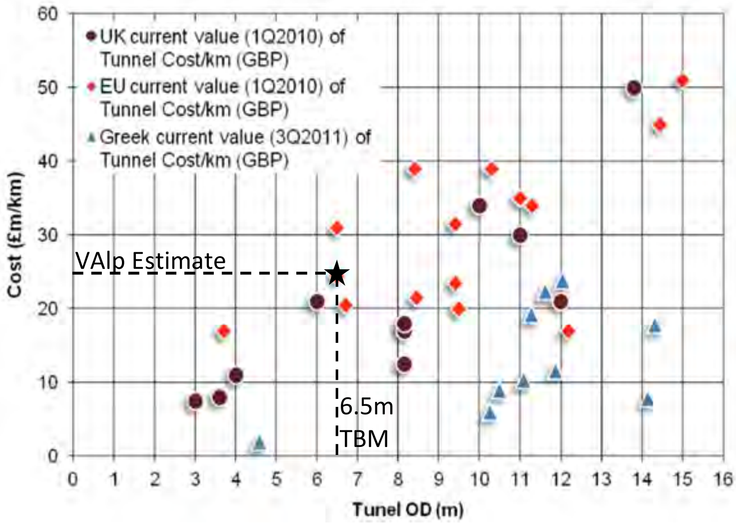

Figure 48 - Total cost analysis including the planning phases, pre-construction phases, tunneling over specified lengths, and with varying liner types (Benardos et al., 2013)

The calculated overview depends on various assumptions. Firstly, the projects energy needs are covered by the projects renewable energy infrastructure. Therefore the tunnel cost per kilometre are estimated as the European total cost for a 6.5m TBM (Figure 48) minus the energy requirements of the TBM (Figure 30Figure 28). This means that the planning, pre-construction and liner costs are estimated as the total cost per kilometre minus the TBM operation-advancement costs calculated with the DAT tool (Chapter 7.2). Secondly, four additional infrastructural expenditures are considered; three renewable energy sources provide green electricity, while infiltration zones secure regional water resources while recycling tunnel spoil. Thirdly, ten new school lightweright rubber tyred metro vehicles by Alstom are purchased during year one. Lastly, the running costs and revenue are split between the VAlp operation, infrastructure maintenance, ticket sales and excess electricity sales.

More specifically, the costs are broken down under the classes listed in Table 13.

Table 13 - Cost and revenue overview showing primary classes and descriptions. Tunneling operations are estimated to take 11 years.

Expense Class	Expense ID	Description	Value	Unit	Number	One time cost (chf)	Running Cost (chf/yr)	Total Costs 2080 (chf)	Reference
Tunnel	TBM Vehicle	Double Shield TBM (6.5m) by industry leader Herrenknec	CHF 8'000'000.00	chf	2	**CHF 16'000'000.00**		CHF 16'000'000.00	https://www.herr
	TBM electricity	Cost of energy for TBM excavation	3906	kWh/day	365		**CHF 228'110.40**	CHF 2'559'398.69	
	Tunnelling	Excavation cost 1 tunnel estimate by DAT tool	CHF 19'416'058.39	chf/km	6.2		**CHF 120'909'090.91**	CHF 1'356'600'000.00	
	Tunnelling additions	Planning phase, tunnel infrastructure, etc	CHF 5'583'941.61	chf/km	6.2		**CHF 34'544'616.87**	CHF 387'590'601.31	(Benardos et al.,
Infiltration Zones	RIBS	Water table rapid refill deisnged for 378m3/day	CHF 619'000.00	chf	4	**CHF 2'476'000.00**	**CHF 40'000.00**	CHF 4'720'000.00	https://www3.epa
Renewable Energy	Infrastructure	Permanent field of solar panels, two 2MW wind turbines	CHF 43'861'871.24	chf		**CHF 43'861'871.24**	**CHF 80'000.00**	CHF 48'349'871.24	https://www.swiss
	Geothermal	Energy geostructures, heat exchange stations	to be decided						https://www.railw
Metro	VAlp metro	New rolling stock of Alstom. Fully automated six-car met	CHF 6'240'000.00	chf	10	**CHF 62'400'000.00**		CHF 62'400'000.00	https://pedestrian
	VAlp electricity	Yearly consumption	1788135	kWh/yr			**CHF 286'101.60**	CHF 16'050'299.76	
	VAlp operation-maintena	12 personnes	CHF 2'000'000.00	chf	1		**CHF 2'000'000.00**	CHF 112'200'000.00	
	Tunnel ventilation	Jet fan operation	9460000	kWh/yr			**CHF 1'513'600.00**	CHF 84'912'960.00	
	Tunnel lighting	Emergency lighting	29800	kWh/yr			**CHF 4'768.00**	CHF 267'484.80	
						Tunnel and Infrastr.	**Yearly Operation**	**CHF 2'091'650'615.80**	
							CHF 2'120'000.00		
					TOTAL	**CHF 1'834'728'656.84**	**CHF 2'120'000.00**		

Revenue Class	Revenue ID	Description	Value	Unit	Number	One time revenue (chf)	Running Income (chf/yr)	Total Revenue 2080 (chf)	
Operation	Tickets	Daily tickets and number of daily users (f(alpha factor))	CHF 20.00	chf	15357		**CHF 5'605'305.00**	CHF 314'457'610.50	
	Tourism Package	Weekly passes in collaboration with mountain resorts, si	CHF 45.00	chf	5000		**CHF 225'000.00**	CHF 225'000.00	https://www.saas
Renewable Energy	Geothermal	Heat sold to heat houses	to be decided						
	Excess electricity tunneli	Permanent field of solar panels, 2 small wind turbines, flo	2.61E+07	kWh/yr			**CHF 4'175'089.60**	CHF 287'037'410.00	see energy calcu
	Excess electricity operati	Permanent field of solar panels, 2 small wind turbines, flo	1.44E+07	kWh/yr			**CHF 2'308'698.40**	CHF 634'892'060.00	see energy calcu
Tunnel Spoil	Crude gypsum	For cement and plaster production (2km section)	CHF 12.00	chf/ton	89594.3	**CHF 1'075'131.55**		CHF 1'075'131.55	https://www.statis
	Crude limestone/dolomi	For aggregates, backfill, infiltration zones (5km)	CHF 14.00	chf/ton	348422.3	**CHF 4'877'911.64**		CHF 4'877'911.64	https://www.statis
						One time	**Yearly Operation**	**CHF 1'242'565'123.69**	
							CHF 12'314'093.00		
					TOTAL	**CHF 5'953'043**	**CHF 12'314'093.00**		

VAlp EXPRESS

12.2 Results

12.2.1 Fixed Costs

The fixed costs include two tunnel boring machines and their manned operation over the predicted 11 year excavation period. Then, the renewable energy infrastructure defined in the Energy chapter, the purchase of ten Alstom rubber-tyred metro vehicles, and four infiltration basins are shown:

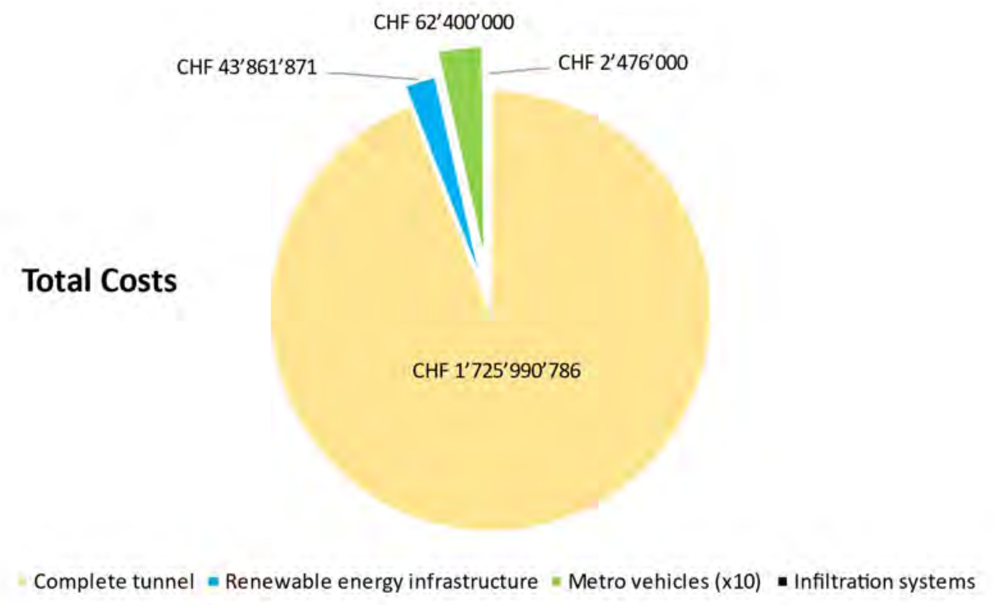

Figure 49 - Total one time investments projected for the high-speed metro connection of the Vaud alps.

Recycling of geological material to produce geo-materials capable of grouting the annular volume outside the precast tunnel concrete segments will further reduce the costs (Zhang et al., 2022). This has not been taken into account in this first order financial overview.

12.2.2 Fixed Revenue

The sale of spoils due to the excavation of crude gypsum and limestone-dolomite generates a one time revenue of 5'953'054.- CHF due to them having a market value of 12chf/ton and 14chf/ton respectively (Statista, 2022).

12.2.3 Yearly Costs and Revenue

Assuming an excavation of 11 years with two tunnel boring machines, and the production of green energy from year two onwards, the following yearly costs and revenues are predicted.

Between 2025 to 2036 the tunnel is being excavated, leading to yearly operational costs of 150Mchf for the TBM. In year one and two all investments to purchase the metro vehicles renewable energy infrastructure for the Vaud alps are made. During this time, 26GWh/year of excess electricity are sold as running revenue.

Once the metro is operational, the operational VAlp costs amount to 2Mchf per year, whereas the yearly revenue of almoMchf per year is split between ticket sales, tourism packages and excess electricity sales of 14.4GWh/year.

Figure 50 - Yearly costs and revenue for a 20year prediction of the VAlp Express.

13 Conclusion

The high speed mountain metro provides both regional and global economic interests. Firstly, the rapid connection with the Vaud valley will increase tourism year-round. Operating below the surface implies reliable mobility for the region; the service is not hampered by snow, ice, rock-falls and more. The rapid underground metro system will not compete with the current customer base of slower panoramic trains. Secondly, the improved connection will incentivize primary residencies and alleviate parking shortages, increasing the local housing economic valuation. Thirdly, the integrated project proposes energetic self-sufficiency, improving the electrical security of the Vaud alps. Additional heat exchange in the tunnel liner (injection-extraction) reduces both heating and cooling costs year-round. This is aligned with the renewable energy 2050 agenda voted by the Swiss population. Lastly, improved green mobility means less traffic and valorised landscapes.

13.1 Summary

A driverless lightweight high-speed metro is envisaged as an innovative solution to connect mountain regions of the Vaud alps. The rubber tire traction technology allows for the VAlp metro to climb 11% maximal gradients from Aigle to Villars-sur-Ollon. Thereafter, the sub planar tunnel alignment allows the rolling-stock to reach maximal speeds of around 100km/h. With this technology the Aigle – Villars-sur-Ollon is reached in 10 minutes, Villars – Les Diablerets in 10 minutes, and Les Diablerets – Chateau d'Oex in 15 minutes.

The current geological 3D model provides a suitable optimized tunnel alignment for the VAlp Metro concept. For the current state of the feasibility study, the level of detail is deemed suitable. Future data such as deep boreholes and geophysical exploration will improve the 3D geological model.

Using the DAT tool, the geotechnical estimates and ground classes attributed to the target location allowed for realistic (albeit slightly optimistic) cost and advance rate estimates for a TBM tunnel. The two single-shaft tunnel is estimated to take 9-15 years and cost 1-1.5 billion francs. Additional infrastructure and telecommunication is likely to require a similar investment. This is in line with current projects of this magnitude. Future DAT simulations should evaluate the cost-time impact of multiple TBMs operating simultaneously, as well as including rock laboratory and field characterized geotechnical parameters (allowing precise RMR rating for refined ground classes).

Regional scale hydro geothermal models indicate the potential for low-enthalpy thermal exploitation. With two tunnel locations reaching 18.5-19°C, liners containing absorber pipes connected to heat pumps, can provide injection-extraction to cool-heat buildings, agriculture etc.

The cross sectional design shows how a rapid rubber-tyred lightweight metro can operate in small diameter tunnels. A 6.5m wide TBM with 30cm wide pre-cast concrete segments is sufficient to guarantee clearance requirements according to the SIA norms. The twin tube design and cross passages guarantee passenger safety and vehicle extraction in case of a fire.

A aeolian and solar renewable energy plant is envisioned as part of the integrated project design. The proposed permanent infrastructure covers both the excavation and operational phase of the VAlp mountain metro. In both phases the excess renewable energy is injected into the high-voltage swissgrid. While serving the high-speed mobility in the Vaud alps, this also contributes to the national 2050 renewable energy target.

The environmental impact study shows the beneficial effect of reducing traffic emissions before 2050. Tunneling and concrete production is the main CO_2 emitter of the VAlp Express concept. The increased impact during the 11 year construction phase is compensated by low operational emissions. If 30-50% of daily car commuters switch to the metro, the CO_2 balance breaks even over 8-15 years of operation. Once operating, 3-5.5Gkg of carbon dioxide are saved over 40 years.

A first-order cost analysis is provided in this study. Fixed costs including renewable energy infrastructure, metro vehicles, tunneling requirements and tunnel spoil recycling infiltration zones amount to 1.83 billion CHF. A one-time revenue by crude gypsum and limestone-dolomite is envisioned to generate 6 million CHF. Finally once operating, VAlp yearly costs amount to 2 million CHF whereas revenues reach 12 million CHF.

13.2 Future Perspectives

The current report shows the integrated potential of the VAlp Express. Geological and engineering are paired with regional mobility and energetical interests, all while envisioning virtuous societal changes. The next steps are detailed in *Figure 51*.

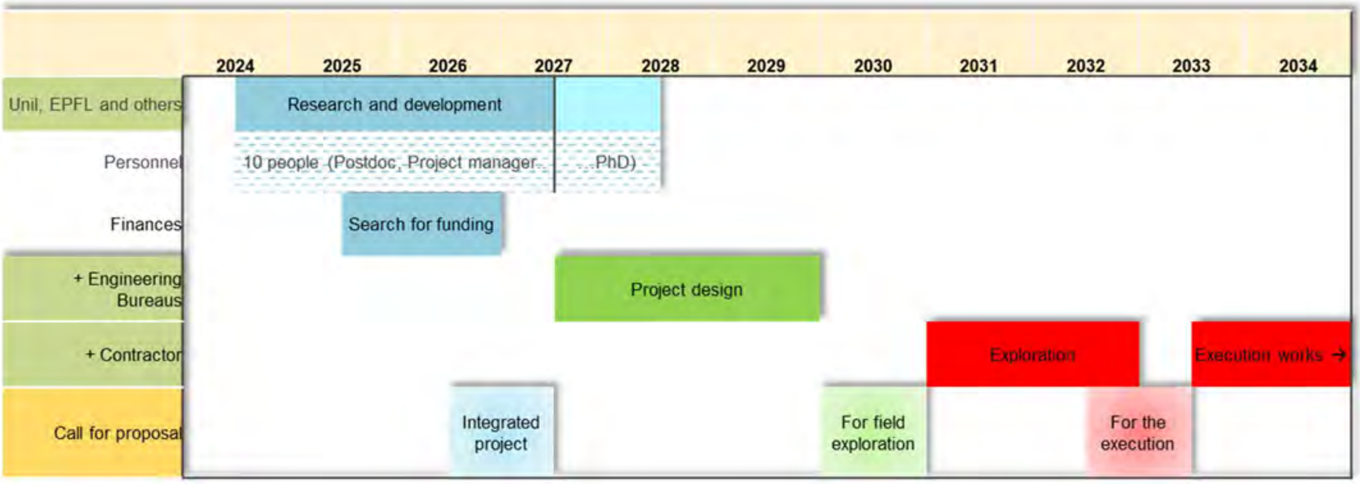

Figure 51 - Next steps to reach an integrated design, field exploration and execution phase.

More specifically the Research and Development should expand upon the following topics over the span of four years:

Tunnel

- Subsurface models (with field and lab data)
    - *Geological 3D*
    - *Geotechnical (characterization, updated DAT)*
    - *Hydro geothermal 3D*
- Low-impact concrete
- Pre-cast liner as a ground heat exchanger
- Tunneling technology

Metro

- Traction
- Aerodynamics
- Vehicle design
- Technical requirements

Society

- Demography and migration
- Mobility (general evolution, metro scenario analysis, new behaviors)
- Tourism (current tendency, new summer-winter opportunities, paradigm shift)

- Impact of rapid valley connection (Geneva-Lausanne axis)

Energy

- Renewable infrastructure design (societal and political behaviour, impact study, cost analysis, electrical grid connections)
    - *Construction*
    - *Operation*
- Source of energy (excavation by TBM, metro operation, excess electricity)

Additionally, the safety and reliability must be a key target of the VAlp high speed metro. The driverless metro must be developed with an integrated approach, aiming to respond to public needs and national targets. Finally if successful, the VAlp metro will become an Swiss exportable concept in global mountainous regions!

14 References

A new metro line will transform Lausanne. (2021, April 8). *BG Magazine*.

ABB. (2016). *Fresh Air for the Gotthard Base Tunnel: Successful completion of the commissioning of the world's most powerful ventilation system*. https://new.abb.com/ch/en/gottardo-english/fresh-air-for-the-gotthard-base-tunnel

ABC News. (2023, April 21). 'Significant moment': First driverless metro train travels under Sydney Harbour. *ABC News*. https://www.abc.net.au/news/2023-04-21/sydney-metro-train-travels-under-harbour/102252872

Alstom unveils 52m rubber-tyre metro trains. (2019, November 18). *Railway Technology*. https://www.railway-technology.com/news/alstom-52m-rubber-tyre-metro-trains/

Andres, A. S., Walther, E. F., He, C., & Turkmen, M. (2013). *Evaluation of Rapid Infiltration Basin Systems (RIBS) | The Delaware Geological Survey*. https://www.dgs.udel.edu/projects/evaluation-rapid-infiltration-basin-systems-ribs

Architecture 2030. (2020). *GYPSUM BOARD – Carbon Smart Materials Palette*. https://materialspalette.org/gypsum-board/

Badoux, M. (2011, October 31). Growth through innovation – Lausanne's new driverless metro. *Intelligent Transport*, *Issue 5*.

Barton, N. (2000). *TBM tunnelling in jointed and faulted rock*. Balkema.

BEC CREW. (2015, September 28). London Is Now Recycling Energy From Train Brakes to Power Their Stations. *Science Alert*.

Benardos, A., Paraskevopoulou, C., & Diederichs, M. (n.d.). *Assessing and benchmarking the construction cost of tunnels*.

British Tunnelling Society, & Institution of Civil Engineers (Eds.). (2004). *Tunnel lining design guide*. Thomas Telford ; Distributed in the USA by ASCE Press.

Brox, D. (2013). *Technical considerations for TBM tunneling for mining projects*. https://www.semanticscholar.org/paper/Technical-considerations-for-TBM-tunneling-for-Brox/67af34b7a6574e095d81262cf6b84ab3b891696e#citing-papers

Bufalini, M., Dati, G., Rocca, M., & Scevaroli, R. (2017). The Mont Cenis Base Tunnel. *Geomechanics and Tunnelling*, *10*(3), 246–255. https://doi.org/10.1002/geot.201700009

Chapman, D. N., Metje, N., & Stärk, A. (2010). *Introduction to tunnel construction*. Spon Press.

Chen, J., Cheng, X., Qi, S., Feng, H., Ma, L., & Gong, L. (2017). Optimal Sections of Tunnels' Cross Sections with Different Overburdens. *The Open Civil Engineering Journal*, *11*(1), 714–725. https://doi.org/10.2174/1874149501711010714

Crude gypsum price in U.S. 2022. (n.d.). Statista. Retrieved 24 May 2023, from https://www.statista.com/statistics/219363/wallboard-products-crude-price-in-the-us/

Dujardin, J., Kahl, A., & Lehning, M. (2021). Synergistic optimization of renewable energy installations through evolution strategy. *Environmental Research Letters*, *16*(6), 064016. https://doi.org/10.1088/1748-9326/abfc75

Ehrbar, H. (2016). Long Railway Tunnels System choice—Review for the future. *GeoResources Journal*, *2*, 30.

Einstein, H. H. (2018). *Decision Aids for Tunneling*. 83–86. https://doi.org/10.1061/9780784415139.ch07

Elhardt, C. (2023, March 20). *Where should wind turbines be constructed in Switzerland?* [ETH News]. https://ethz.ch/en/news-and-events/eth-news/news/2023/03/where-should-wind-turbines-be-constructed-in-switzerland.html

Fritzsch, J., Jacquod, P., & Pagnier, L. (2022). *The Grengiols-Saflischtal Photovoltaic Solar Farm: An Independent Analysis*. https://doi.org/10.13140/RG.2.2.16850.43207

Garcia, G. R., Michau, G., Einstein, H. H., & Fink, O. (2021). Decision support system for an intelligent operator of utility tunnel boring machines. *Automation in Construction*, *131*, 103880. https://doi.org/10.1016/j.autcon.2021.103880

Guerrieri, M., Sanabria, C., Lee, W. M., Pazmino, E., & Patel, R. (2020). Design of the metro tunnel project tunnel linings for fire testing. *Structural Concrete*, *21*(6), 2452–2480. https://doi.org/10.1002/suco.202000140

Guo, C., Wang, M., Yang, L., Sun, Z., Zhang, Y., & Xu, J. (2016). A review of energy consumption and saving in extra-long tunnel operation ventilation in China. *Renewable and Sustainable Energy Reviews*, *53*, 1558–1569. https://doi.org/10.1016/j.rser.2015.09.094

Guo, H. (2019). A Review of Metro Tunnel Construction Methods. *IOP Conference Series: Earth and Environmental Science*, *218*, 012110. https://doi.org/10.1088/1755-1315/218/1/012110

Harer, G., Mussger, K., Hochgatterer, B., & Bopp, R. (2008). Considerations for Development of the Typical Cross Section for the Koralm Tunnel. *Geomechanik Und Tunnelbau*, *1*(4), 257–263. https://doi.org/10.1002/geot.200800031

Harran, R. (2018). *Decision Aids for Tunneling—A CATALOGUE FOR APPLICATION TO SMALL TUNNELS* [Master's Thesis]. EPFL.

Hilar, M., & Srb, M. (2009). Long railway tunnels–comparison of major projects. *Safe Tunneling for the City and for the Environment*. ITA-AITES World Tunnel.

HM Treasury. (2010). *Infrastructure Cost Review: Technical Report* (Infrastructure UK).

Huszno, L. (2021, January 27). *World's first high-altitude floating solar farm – in the Swiss Alps*. House of Switzerland. https://houseofswitzerland.org/swissstories/environment/worlds-first-high-altitude-floating-solar-farm-swiss-alps

Ivanova, A. (2023). *Solar park in Swiss Alps could supply 600 GWh annually, study says*. Renewablesnow.Com. https://renewablesnow.com/news/solar-park-in-swiss-alps-could-supply-600-gwh-annually-study-says-817670/

Jaboyedoff, M., Couture, R., & Locat, P. (2009). Structural analysis of Turtle Mountain (Alberta) using digital elevation model: Toward a progressive failure. *Geomorphology*, *103*(1), 5–16.

Jaccard, L., & Schobinger, M. (2008). *M2: Le défi*. Editions Favre.

Jorjio, L. (2023, April 18). *Will the Swiss countryside soon be dotted with wind turbines?* SWI Swissinfo.Ch. https://www.swissinfo.ch/eng/business/will-the-swiss-countryside-soon-be-dotted-with-wind-turbines-/48422614

Kaehler, C., & Belitz, K. (2003). *Tracing Reclaimed Water in the Menifee, Winchester, and Perris-South Ground-Water Subbasins, Riverside County, California*.

Keystone-SDA/jc. (2023, February 28). *Wind power production increases slightly in Switzerland*. SWI Swissinfo.Ch. https://www.swissinfo.ch/eng/business/wind-power-production-increases-in-switzerland/48322036

Keystone-SDA/RTS/sb. (2023, May 17). *Alpine solar farms set for public vote in canton Valais*. SWI Swissinfo.Ch. https://www.swissinfo.ch/eng/sci-tech/alpine-solar-farms-set-for-public-vote-in-canton-valais/48521118

Lemke, U., & Poppel, U. (1992). *Berliner U-Bahn* (3., überarb. Aufl). Alba.

Leung, S. H. M. (2012). LED Lighting Application in Long Railway Tunnels. *HKIE Transactions*, *19*(4), 42–46. https://doi.org/10.1080/1023697X.2012.10669004

Lo Monaco, M., Kitchen, T., & Ryan. (2016). *Greenhouse Gas Impact Assessment*. Melbourne Metro Rail Authority. https://bigbuild.vic.gov.au/__data/assets/pdf_file/0016/51091/MT-Technical-Appendix-V-Greenhouse-Gas.pdf

Maidl, B., Thewes, M., & Maidl, U. (2014). General Principles for the Design of the Cross-Section. In B. Maidl, M. Thewes, & U. Maidl, *Handbook of Tunnel Engineering II* (pp. 1–20). Wiley-VCH Verlag GmbH. https://doi.org/10.1002/9783433603536.ch1

Maidl, B., Thewes, M., Maidl, U., & Sturge, D. (2013). *Handbook of tunnel engineering*. Ernst & Sohn.

Maximum power for excavating uphill tunnels. (n.d.). Retrieved 17 May 2023, from https://www.danfoss.com/en/service-and-support/case-stories/dds/cogeis-tbm-maximum-power-for-excavating-uphill-tunnels/

Merlini, D., Stocker, D., Falanesca, M., & Schuerch, R. (2018). The Ceneri Base Tunnel: Construction Experience with the Southern Portion of the Flat Railway Line Crossing the Swiss Alps. *Engineering*, *4*(2), 235–248. https://doi.org/10.1016/j.eng.2017.09.004

Metroselskabet I/S. (2021). *Annual Report 2021*. Metroselskabet I/S. https://m.dk/media/4904/en-ms-%C3%A5rsrapport-2021.pdf

Midi Mobilites. (n.d.). *Https://www.midimobilites.fr/siemens-siemens-matra/*. Retrieved 31 May 2023, from https://www.midimobilites.fr/siemens-siemens-matra/

Moret, Y., & Einstein, H. H. (2016). Construction Cost and Duration Uncertainty Model: Application to High-Speed Rail Line Project. *Journal of Construction Engineering and Management*, *142*(10), 05016010. https://doi.org/10.1061/(ASCE)CO.1943-7862.0001161

Muir Wood, A. M. (2000). *Tunnelling: Management by design*. E & FN Spon.

Nievergelt, R. (2023). *Sydney Metro Northwest: Tunnels & Stations Contract—The APP Group*. https://www.app.com.au/our-work/sydney-metro-northwest-tunnels-stations-contract

Orange Line Metro Project Bangkok: Breakthrough of the Westbound Tunnel on Contract E3 - tunnel. (2020). Tunnel-Online. https://www.tunnel-online.info/en/artikel/tunnel_Orange_Line_Metro_Project_Bangkok_Breakthrough_of_the_Westbound_Tunnel_on-3526287.html

Paraskevopoulou, C., & Benardos, A. (2013). Assessing the construction cost of Greek transportation tunnel projects. *Tunnelling and Underground Space Technology*, *38*, 497–505. https://doi.org/10.1016/j.tust.2013.08.005

Peeling, J., Wayman, M., Mocanu, I., Nitsche, P., Rands, J., & Potter, J. (2016). Energy Efficient Tunnel Solutions. *Transportation Research Procedia*, *14*, 1472–1481. https://doi.org/10.1016/j.trpro.2016.05.221

Presence Switzerland. (2023). *Renewable Energy*. https://www.eda.admin.ch/aboutswitzerland/en/home/wirtschaft/energie/die-erneuerbaren-energien.html

Rahimzadeh, A., Sher, W., Davis, P., & Tang, W. (2018, January 10). *Management of Excavated Material in Infrastructure Construction-A Critical Review of Literature*.

Riess, I. (2022). *Improving the Energy Efficiency of Road Tunnels*.

Rubli, S. (2014). *Substance dossier for gypsum recovery from waste compared to primary production* [Fact Sheet]. Swiss Geotechnical Comission. https://www.zh.ch/content/dam/zhweb/bilder-dokumente/themen/umwelt-tiere/abfall-rohstoffe/abfallwirtschaft/publikationen/urban-mining-potentialbetrachtung/ump_en_gypsum_2014.pdf

Ruigang, S., Tianchen, Y., Jian, Y., & Hao, H. (2017). Simulation of braking energy recovery for the metro vehicles based on the traction experiment system. *SIMULATION*, *93*(12), 1099–1112. https://doi.org/10.1177/0037549717726146

SeA, R. (2022, March 9). *Il prolungamento della Linea 1 della metro di Torino – prima parte*. Strade & Autostrade Online. https://www.stradeeautostrade.it/ferrovie-e-metropolitane/il-prolungamento-della-linea-1-della-metro-di-torino-prima-parte/

Second tube Gotthard Tunnel: First tunnel boring machine 'Carla' at target. (2023, May 8). https://implenia.com/en/media/news-article/tbm-carla/

Sissins, S., & Paraskevopoulou, C. (2021). Assessing TBM performance in heterogeneous rock masses. *Bulletin of Engineering Geology and the Environment*, *80*(8), 6177–6203. https://doi.org/10.1007/s10064-021-02209-2

Sommer, C., Malz, P., Seehaus, T. C., Lippl, S., Zemp, M., & Braun, M. H. (2020). Rapid glacier retreat and downwasting throughout the European Alps in the early 21st century. *Nature Communications*, *11*(1), Article 1. https://doi.org/10.1038/s41467-020-16818-0

Spielhofer, R., Schwaab, J., & Grêt-Regamey, A. (2023). How spatial policies can leverage energy transitions − Finding Pareto-optimal solutions for wind turbine locations with evolutionary multiobjective optimization. *Environmental Science & Policy*, *142*, 220–232. https://doi.org/10.1016/j.envsci.2023.02.016

Sun, W., Wang, X., Lintao, W., & Song 宋学官, X. (2016). Multidisciplinary design optimization of tunnel boring machine considering both structure and control parameters under complex geological conditions. *Structural and Multidisciplinary Optimization*, *54*. https://doi.org/10.1007/s00158-016-1455-9

Swiss Tunnelling Society. (n.d.). *Banque de données des tunnels suisses—FGU - Fachgruppe für Untertagbau*. Retrieved 31 May 2023, from https://www.swisstunnel.ch/fr/tunnels-en-suisse/banque-de-donnees-des-tunnels-suisses/?tx_xrtunnel_pi1%5BshowUid%5D=905&cHash=942d8f3919f3cea7aed0b1c1190a400b

Tarada, F. (n.d.). *TECHNOLOGIES FOR THE IMPROVEMENT OF JETFAN INSTALLATION FACTORS*. 9th International Conference 'Tunnel Safety and Ventilation', Graz.

Tarada, F. (2015). Energy-Efficient Tunnel Ventilation. *Ansys Advantage*, *Volume IX*(Issue 1). https://www.researchgate.net/publication/287223897_Energy-Efficient_Tunnel_Ventilation

Tatiya, R. (2005). *Civil excavations and tunnelling: A practical guide*. Thomas Telford ; Distributed in the USA by ASCE Press.

The Doha Metro – Tunnelling in special Dimensions. (2012). *Tunnel*, *05*. https://www.tunnel-online.info/en/artikel/tunnel_2012-05_The_Doha_Metro_Tunnelling_in_special_Dimensions-1459895.html

The European Metropolitan Area of Lille and Alstom present the future metro and its 52-metre trains | Alstom. (2019, November 14). [Press-release]. https://www.alstom.com/press-releases-news/2019/11/european-metropolitan-area-lille-and-alstom-present-future-metro-and

TL. (2022). *2021 En Chiffres* (p. 26) [Activity report]. https://rapportannuel.t-l.ch/wp-content/uploads/2022/06/Rapport_annuel_2021_TL.pdf

TSI Infrastructure. (n.d.). Concerning the technical specification of interoperability relating to the operation subsystem of the trans-European high-speed rail system adopted referred to in Article

6(1) of Council Directive 96/48/EC and repealing Commission Decision 2002/734/EC of 30 May 2002. *Official Journal of the European Union*, *2008/231/CE*.

VIC. (2023, May 31). *Metro Tunnel Project* (Victoria) [Text]. Victoria's Big Build. https://bigbuild.vic.gov.au/projects/metro-tunnel

Yang, J. (2014). *Optimization research on the high-speed railway tunnel illumination plan based on field measurement data*. *31*, 72–76.

Zhang, C., Yang, J., Xie, Y., Fu, J., Wang, S., & Yin, J. (2022). Utilization of tunnel spoils as a lightweight filling material for the voids behind tunnel excavation contour. *Journal of Cleaner Production*, *372*, 133559. https://doi.org/10.1016/j.jclepro.2022.133559

Zhang, Y., Chen, J., Han, S., & Li, B. (2022). Big Data-Based Performance Analysis of Tunnel Boring Machine Tunneling Using Deep Learning. *Buildings*, *12*(10), 1567. https://doi.org/10.3390/buildings12101567

15 Annexes

15.1 Hydro-Geothermal Models

15.1.1 Governing Equations

The hydrological governing equation revolves around Darcy's equation. The intrinsic properties of the porous media and the fluid's physical properties dictate the permeability of soil. A highly permeable soil will allow rapid flow, whereas a highly viscous fluid in an impermeable medium will be characterized by little to no flow.

In a hydrostatic system the total hydraulic head [m] is the sum of gravitational and pressure potential. Therefore, the total head equals the elevation head from a reference point plus the pressure head (due to isotropic water pressure).

$$\boldsymbol{h_{tot}} = \boldsymbol{z} + \boldsymbol{h_w} = z + \frac{P}{\gamma_w} \quad in\ [m]$$

Assuming laminar, non-turbulent and non-viscous flow, Darcy's law quantifies the discharge due to a hydraulic gradient in a soil. In is important to note that a pressure gradient alone does not guarantee flow. The increasing pore pressure in a hydrostatic system is evidence of the latter. According to Darcy's law the fluid flow occurs from high to low potential. This is quantified by the total hydraulic head difference *dh [m]* over a length *dL [m].* Furthermore, the difference in potential is also known as the hydraulic gradient *i [-]*, such that the specific discharge *q* is:

$$\boldsymbol{q_f} = -K_{sat}\frac{dh}{dL} = -K_{sat} * i \quad in\ [m/s]$$

The thermal governing equations describe the flow of heat in the porous media induced by a temperature gradient, whereby flux moves hot to cold areas. The homogeneous and isotropic medium is simplified to two dimensions, meaning the out of plane dimension is a assigned a value of one (d_z). The effective thermal conductivity of the porous medium (k_{eff}) and the divergence of temperature (*T*) are used to calculate Fourrier's heat flux in space.

$$\boldsymbol{q_h} = -\,k_{eff}\nabla T \quad [W/m^2]$$

The conservation equation governing thermal transport in the porous media is comprised of temporal diffusive term, a fluid advection term in space (coupled to Darcy's velocity field) and the dispersive term (including both the hydrodynamic dispersion tensor of the fluid and the isotropic thermal conductivity tensor of the solid). Additional heat sources are grouped in the *Q* term, which in this model is only comprised of the inward boundary heat flux.

$$(\rho C_p)_{eff}\frac{\partial T}{\partial t} + \rho_f C_{p,f} u \cdot \nabla T + \nabla \cdot \boldsymbol{q_h} = Q$$

Additionally, the interfacial thermal resistance of heat transfer between solid-liquid and solid-solid is modelled according to an effective thermal conductivity of the porous media (composite material). Rayleigh's spherical formulation yields better results when the solid matrix exceeds 75% of the pore space (Pietrak and Wiśniewski, 2015). Furthermore, the model's assumption of isotropic material properties is well represented by averaging models such as

“Solid spherical inclusions (Rayleigh’s model)” and “Equivalent thermal conductivity” model (COMSOL, 2023).

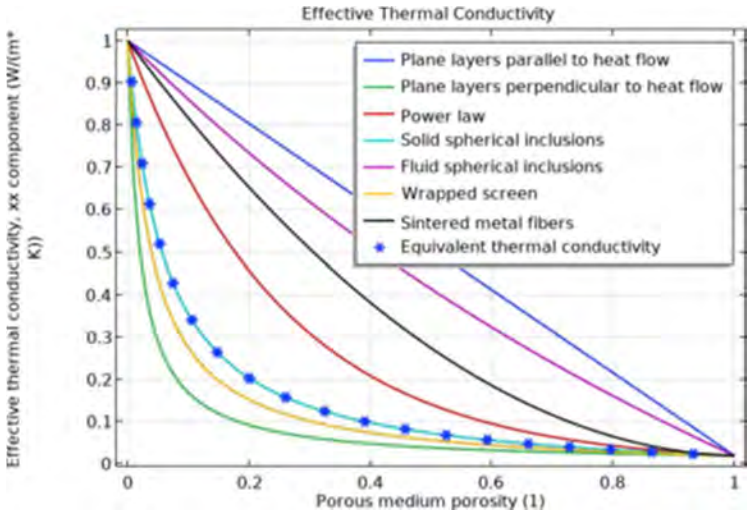

Figure 52 - Averaging models for effective thermal conductivity in porous media implemented in COMSOL. Thermal resistance increases for media containing a large share of isotropic solids, such as the spherical solid particle and equivalent thermal conductivity (used) models.

Finally, the solid spherical inclusion model is used, meaning the effective thermal conductivity of the porous medium is calculated as a function of the solid (k_f) and fluid (k_f) thermal conductivity, the volume of solids (θ_s), and the dispersive thermal conductivity tensor (k_{disp}). The latter is derived in the software “…based on the method of volume averaging of the velocity and temperature deviations in the pores” (Hsu and Cheng, 1990).

$$k_{eff} = k_f \frac{2k_f + k_s - 2(k_f - k_s)\theta_s}{2k_f + k_s + (k_f - k_s)\theta_s} + k_{disp}$$

Furthermore, a linear reduction in thermal conductivity is accounted at increasing temperatures. The temperature dependency of water and air is included in the program’s material library. The solid’s thermal conductivity is manually coupled to the temperature variable as per Selvadurai and Rezaei Niya’s (2020) experiments on intact heterogeneous limestone.

$$k_s = k_{273K} - \frac{373[K] - \boldsymbol{T}}{100\ [K]} * \Delta k_{per100K}$$

Lastly, a wall distance equation is solved to establish the distance from the surface topography. In the absence of subsurface thermal data, this variable is used to calculate the initial geothermal gradient conditions. The domains initial temperature is computed from the atmospheric temperature, a 0.03°C/m gradient, and the distance to the surface (*D=1/G*). To do so, the modified Eikodal equation is calculated as the divergence of the reciprocal distance (*G*) from the topographic boundary of the model. The smoothing parameter σ_w is taken as 0.1, and l_{ref} fixed at 1[m]. The distance from the topography (D_w) is computed over the domain as:

$$\nabla G \cdot \nabla G + \sigma_w G(\nabla \cdot \nabla G) = (1 + 2\sigma_w)G^4$$

$$G = G_0 = 2/l_{ref}$$

$$D_w = \frac{1}{G} - \frac{1}{G_0}$$

To prevent nested computational errors, the distance is computed and exported for each node of the model's mesh. It is then imported as linearly interpolated function variable in COMSOL. Doing so prevents re-calculation at each hydro geothermal iteration.

15.1.2 Isotropic domains, no faulting

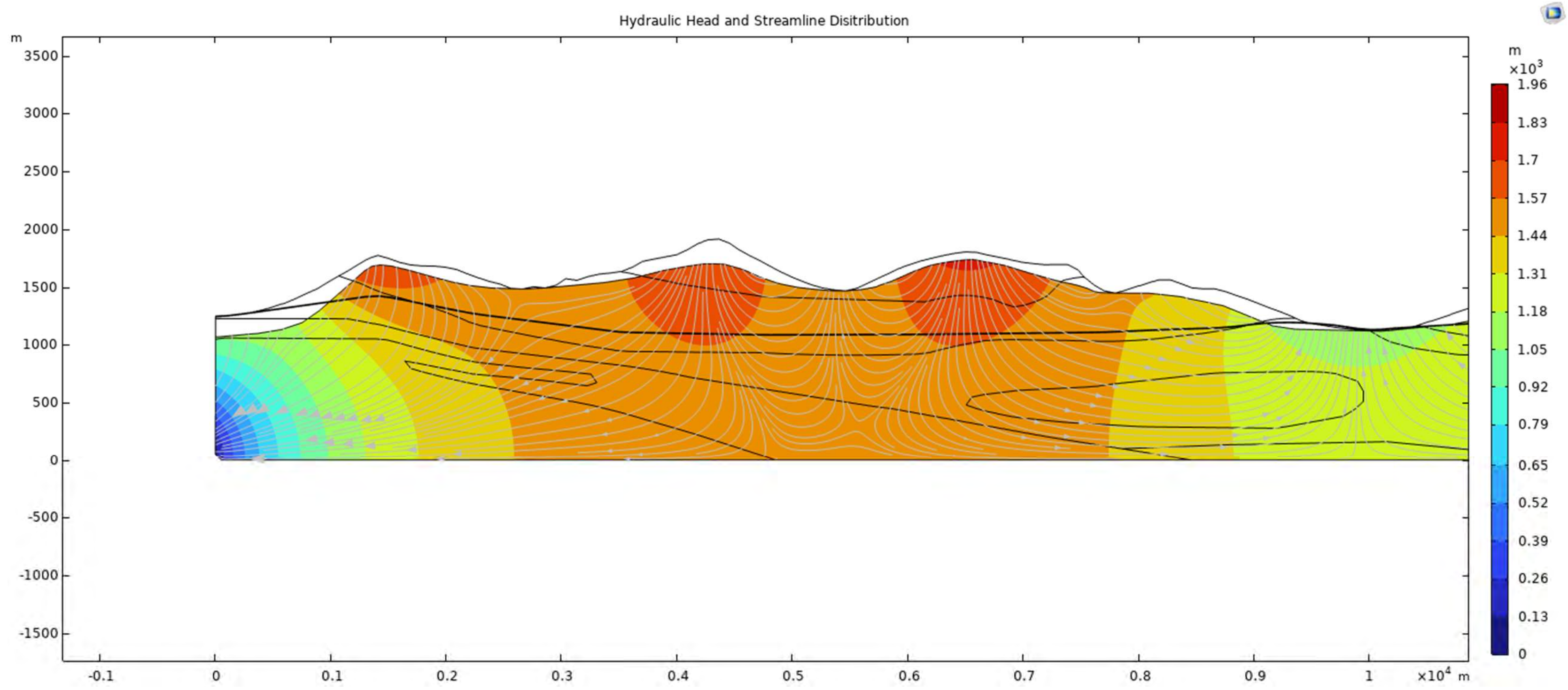

Figure 53 - Hydrological model without faults, Villars to Diablerets.

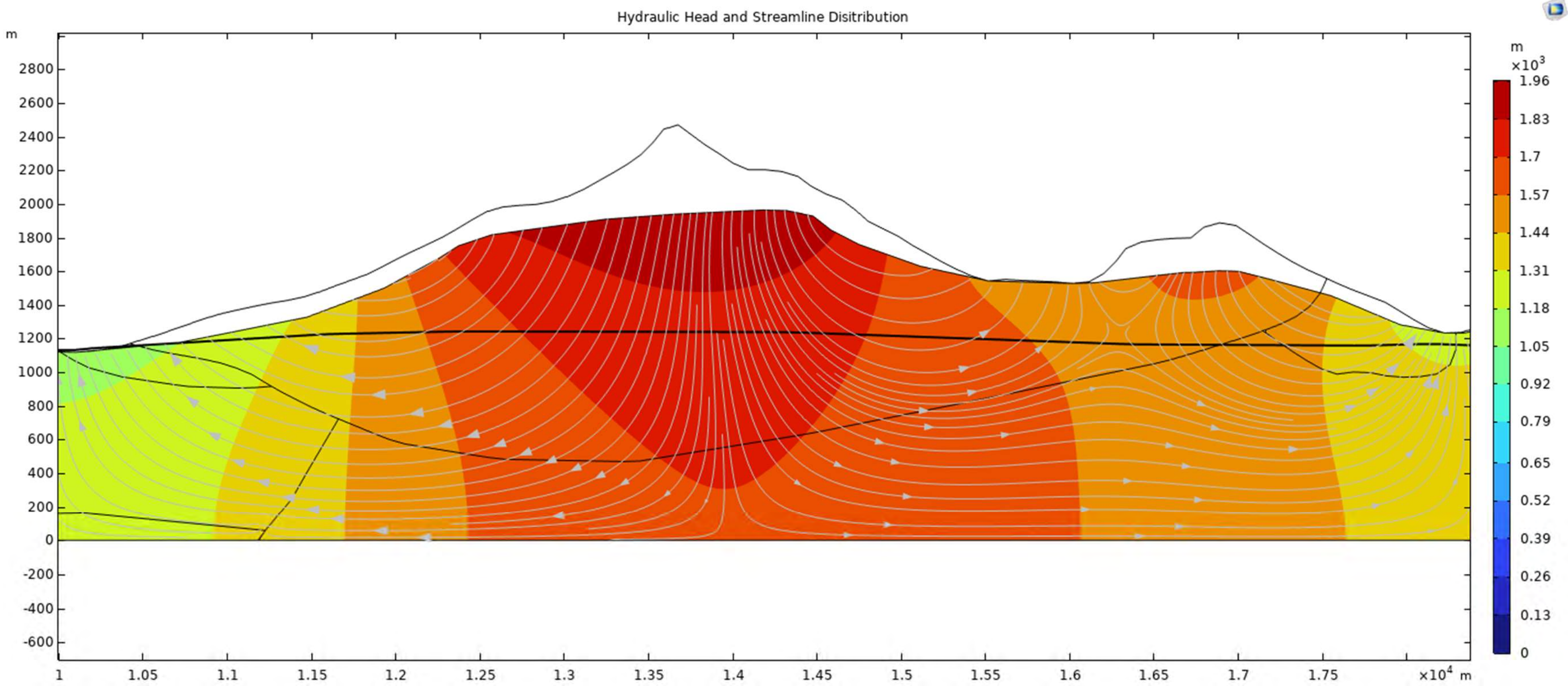

Figure 54- Hydrological model without faults, Diablerets to CHateau d'Oex.

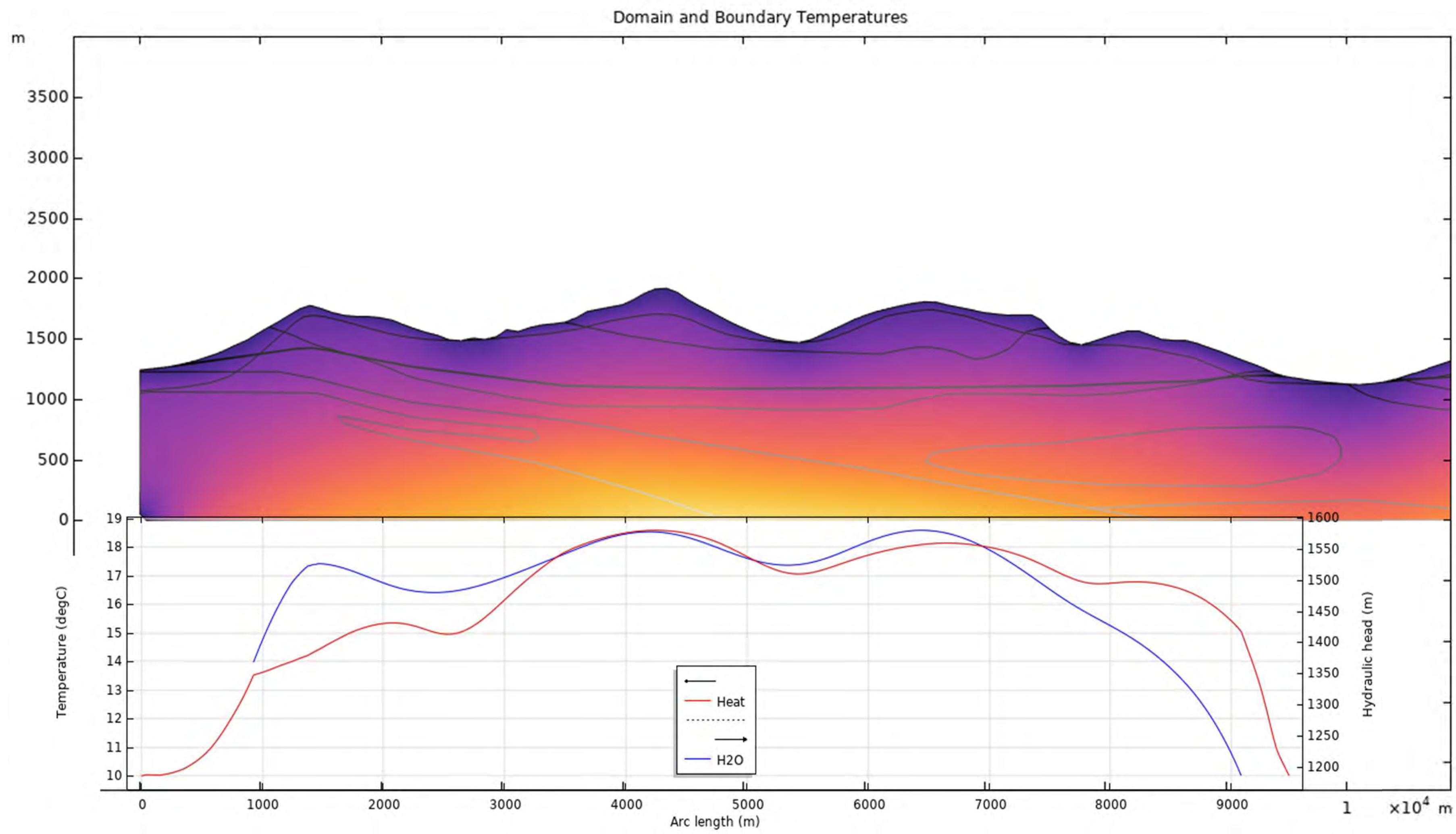

Figure 55 - Geothermal distribution between Villars to Les Diablerets.

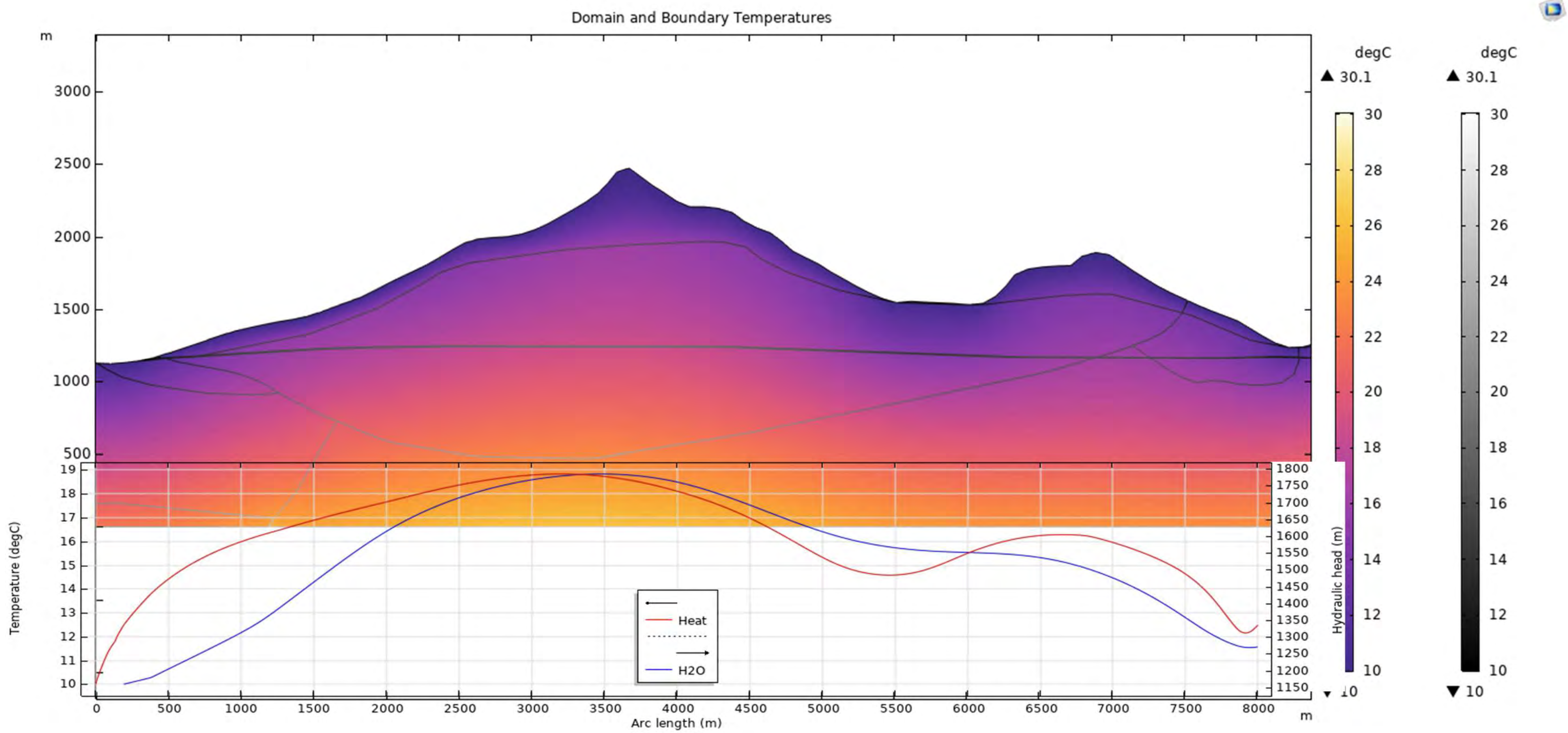

Figure 56 - Geothermal distribution Les Diablerets to Château d'Oex.

15.1.3 *Isotropic domain, with faults*

The initial model is highly sensitive to the permeability and void ratio of the geological formations. For this reason, a second iteration of the model analyzes the inclusion of highly porous, fast flowing regions. The inclusion of faulted and karstic domains (taken from *Figure 16*, implemented as in *Figure 57*) lead to drastical modification of the hydrological regime. Regional cooling is drastically recorded, with geotherm reductions of up to 6°C noted along the tunnel trace.

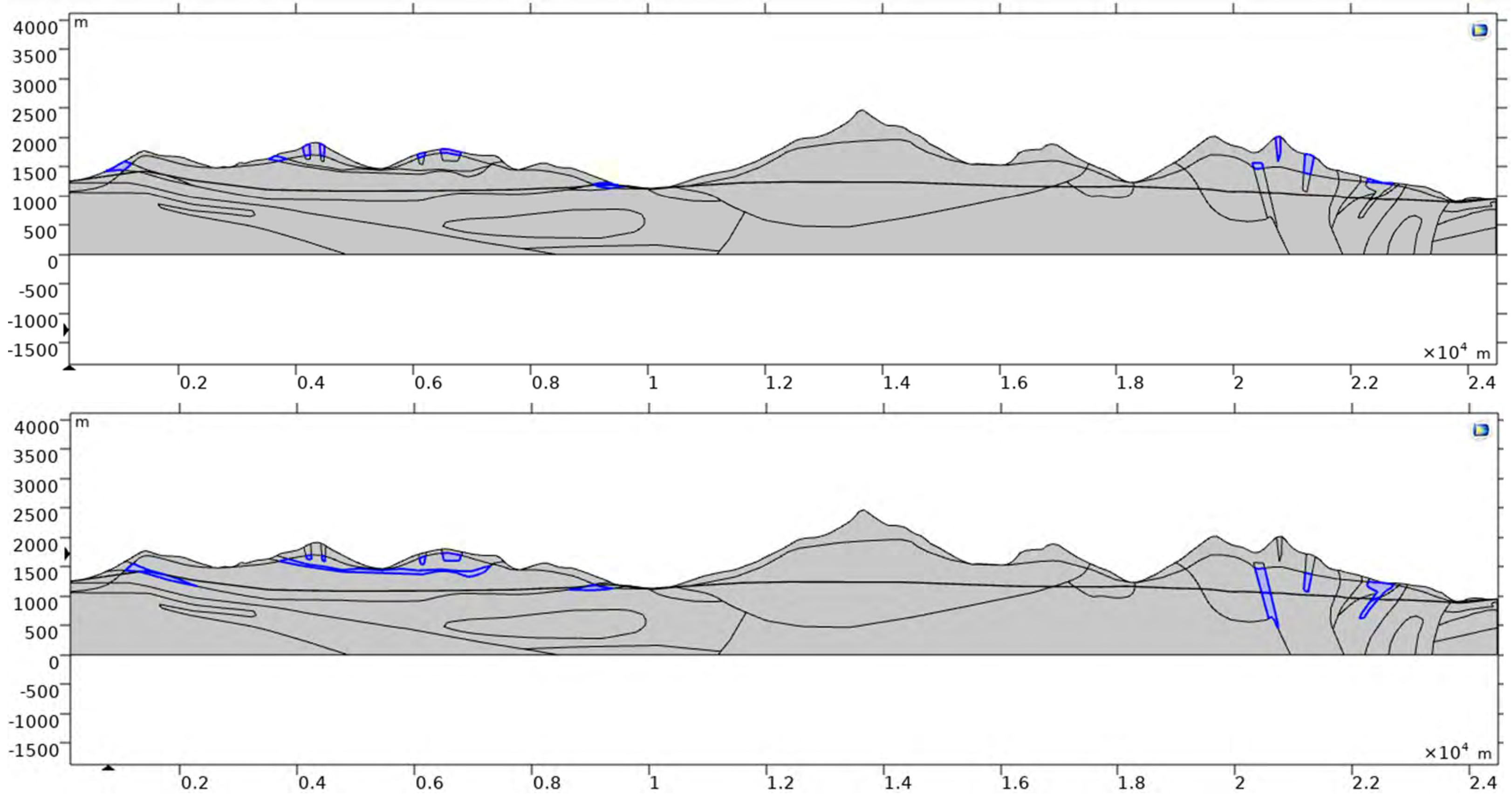

Figure 57 - Geometry of the fractured domains, showing the polygons above the aquifer (top) and the saturated areas (bottom).

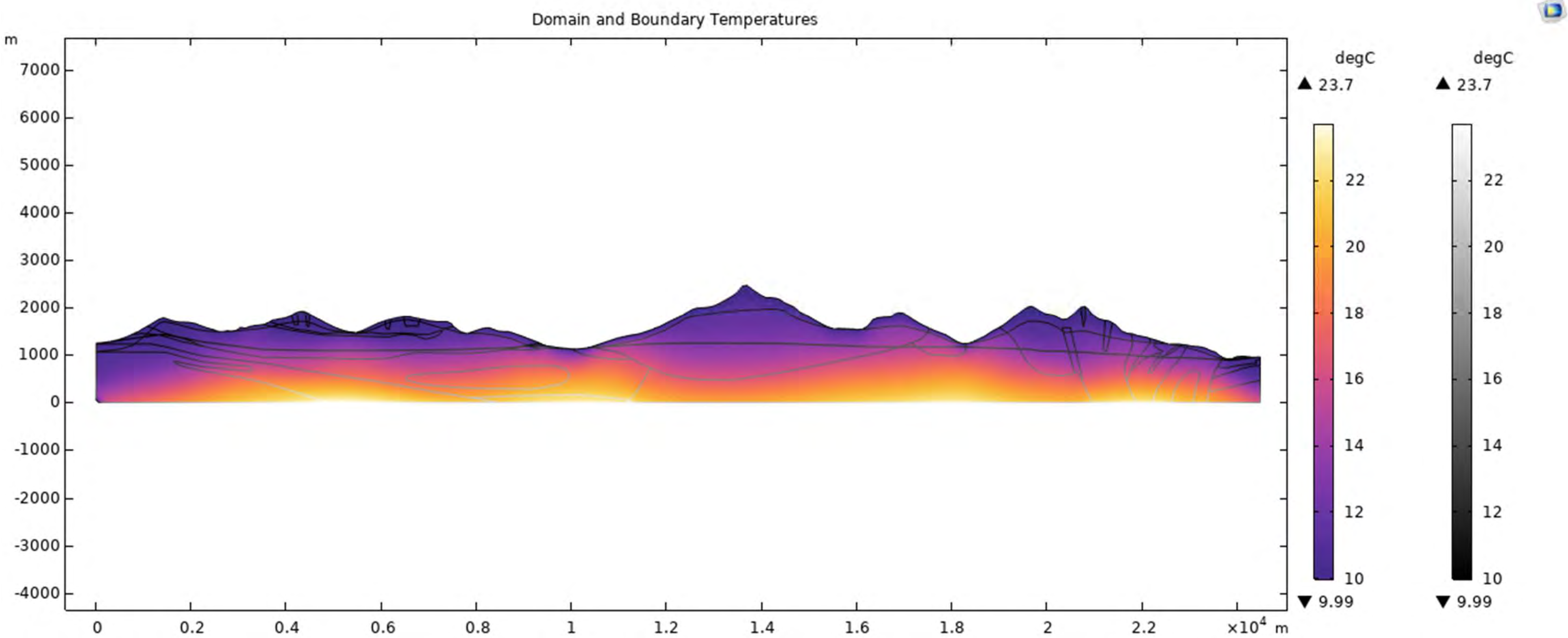

Figure 58 – Fractured cooling effect on the geothermal field along the tunnel alignment between Villars and Chateau d'Oex. The grayscale indicates the temperature at geological, aquifer and tunnel geometrical boundaries.

Fluid flow dominates the thermal regime when including the highly permeable fractured domains. In fact, the once coldest upwelling regions in *Figure 19* become the warmest near-surface regions in *Figure 58*. As an example, the difference in thermal profiles north of Les Diablerets are compared in *Figure 59*. The main model shows a 19°C maxima along the tunnel. However, when resolving the steady state model with highly permeable faulted domains, a drastic cooling effect of the flysch geology occurs. The same zone is cooled to 13°C.

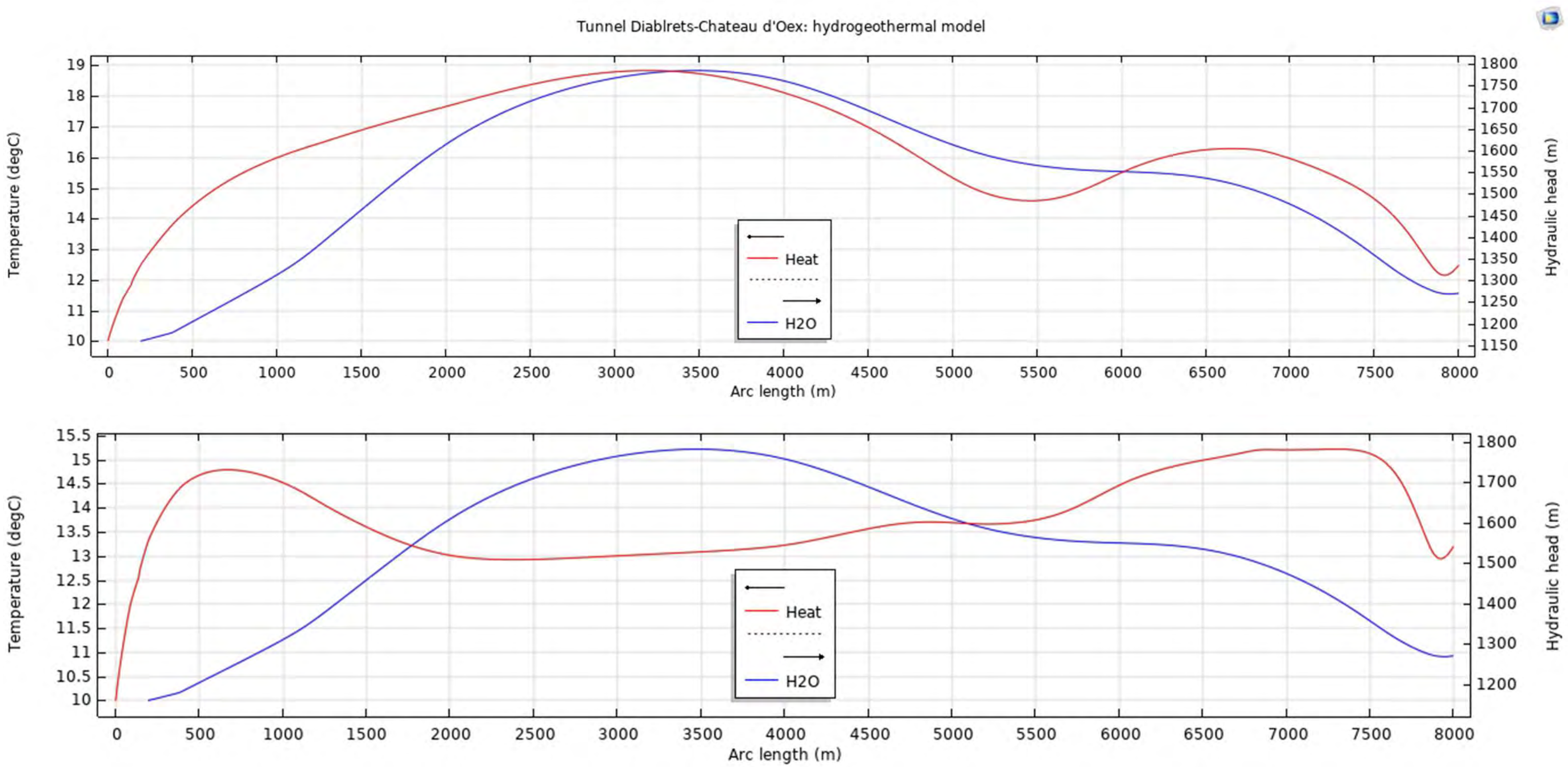

Figure 59 – Comparison of hydro-geothermal gradients along the VAlp tunnel's outer liner: Large overburdens and slow water flow generate 18-19degC temperatures (top, initial model). Regional cooling induced by faulted domains (25% porosity, high hydraulic conductivity) drastically reduce geotherms along the tunnel to maximum 15degC (bottom, fractured model).

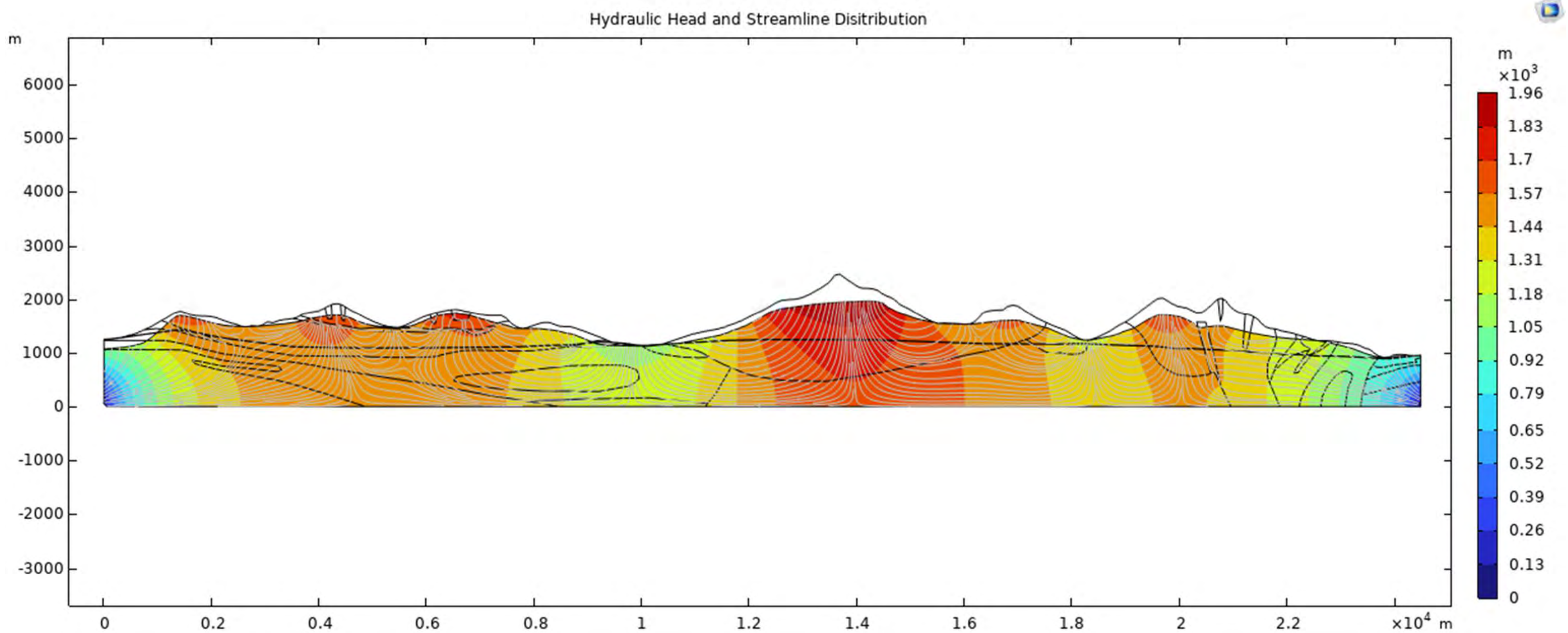

Figure 60 - Hydrological model with faults, Villars to Chateau d'Oex.

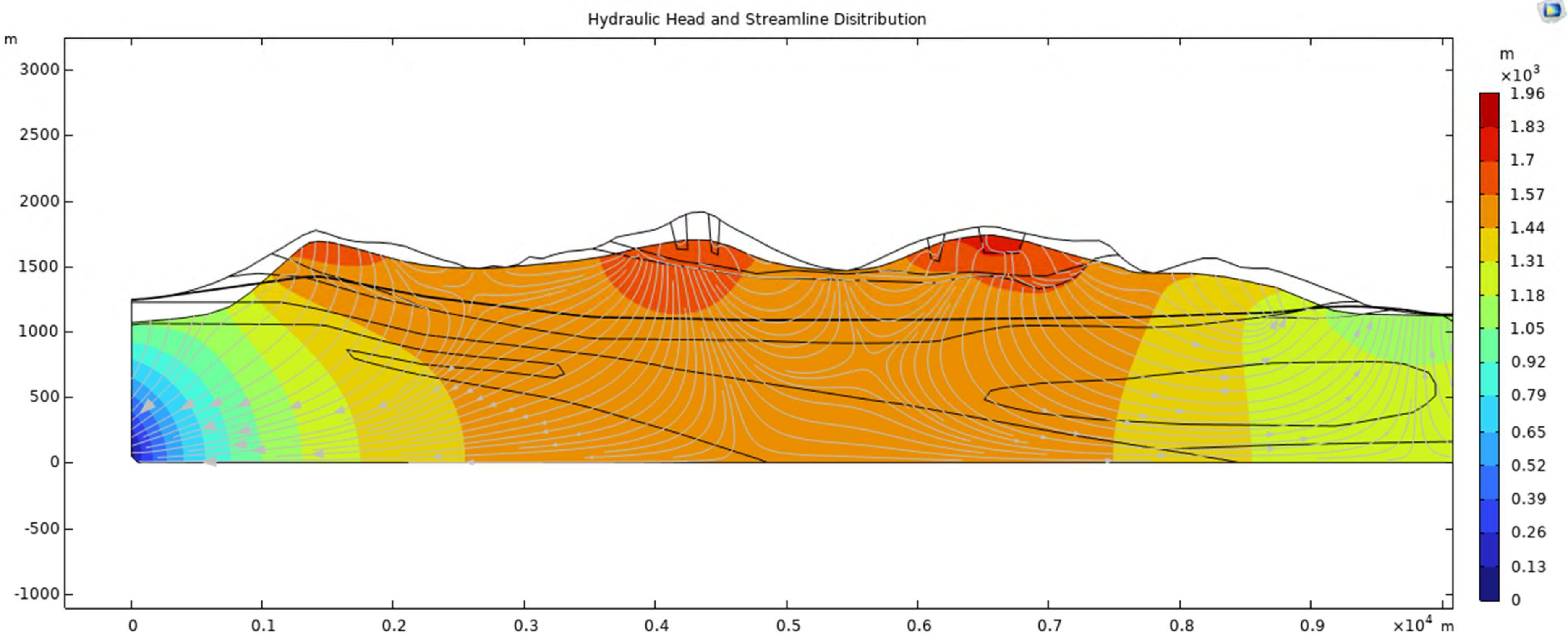

Figure 61- Hydrological model with faults, Villars to Diablerets.

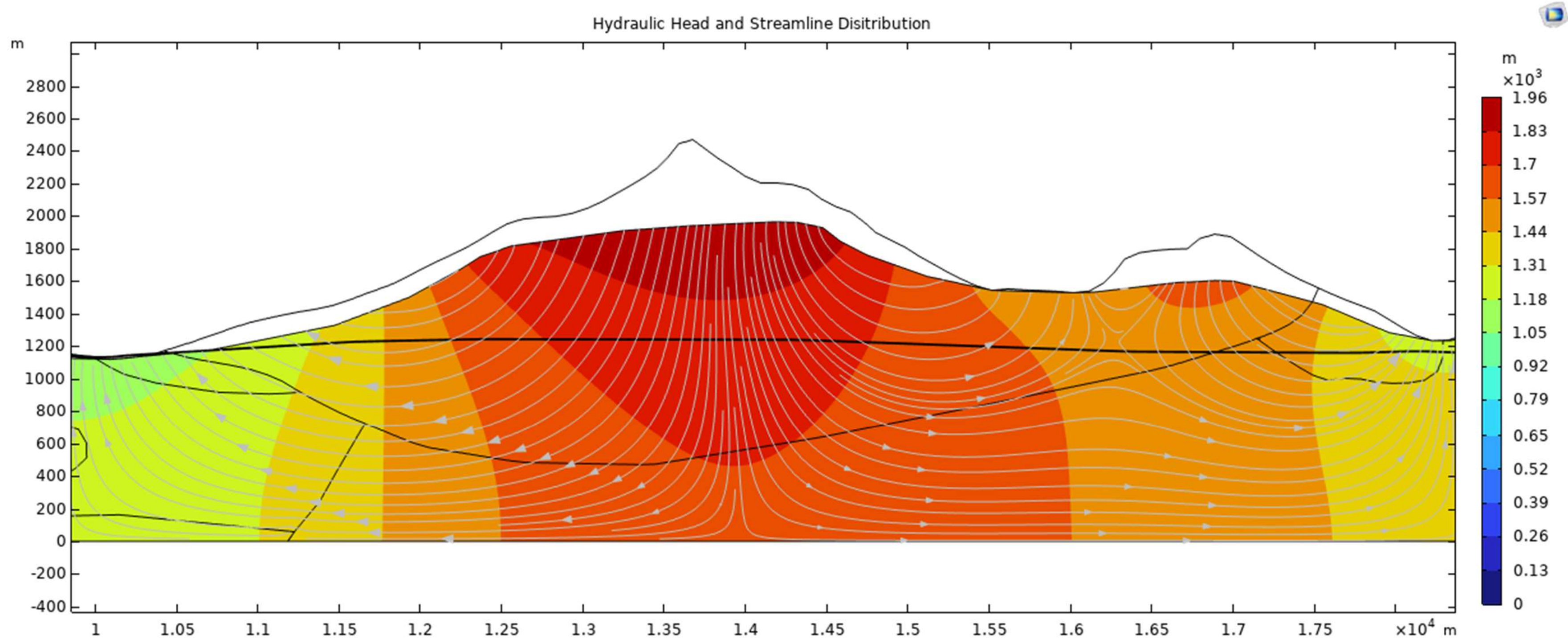

Figure 62- Hydrological model with faults, Diablerets to Chateau d'Oex.

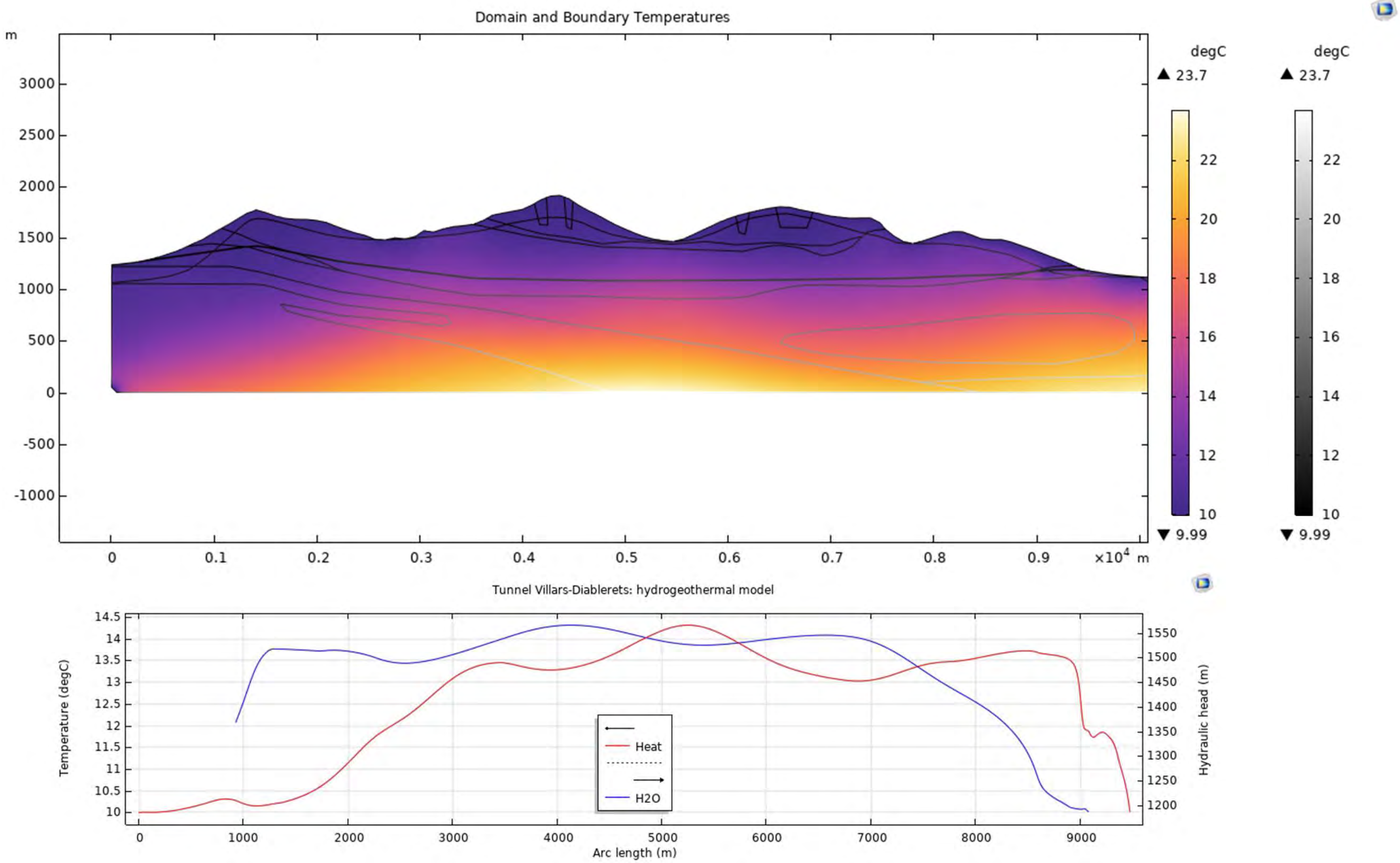

Figure 63- Fracture effect on geothermal distribution from Villars to Les Diablerets.

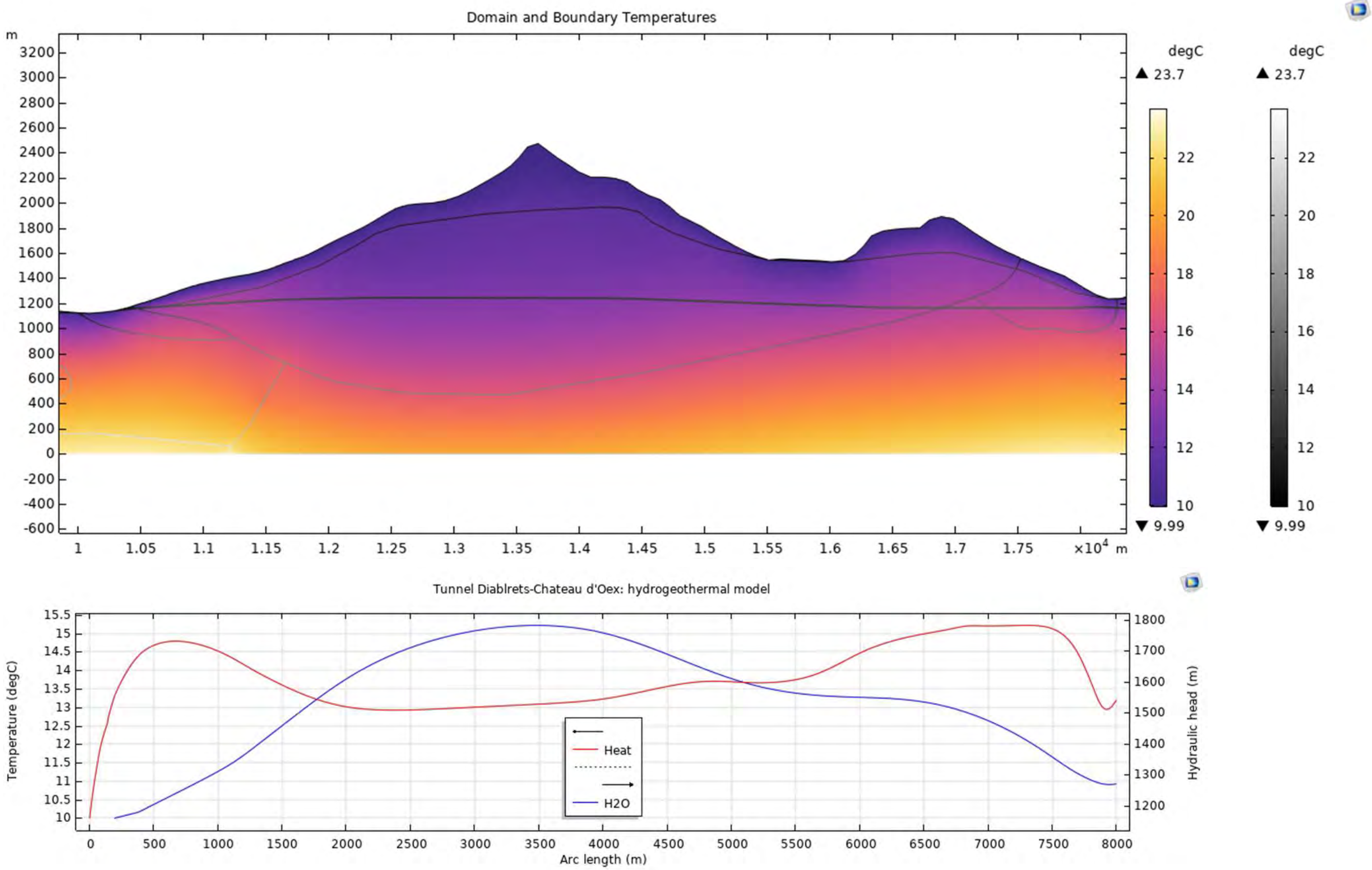

Figure 64- Fracture effect on geothermal distribution from Les Diablerets northward.

15.2 CO2 Input

Table 14 - General input parameters and legend of the CO2 calculation.

Tunnel construction

to validate the range of CO2 emissions: https://civils.ai/carbon

	data input
	given data
	calculation
	(intermediate) result

General parameters

Tunnel length	34.25	km
Tunnel excavation diameter	6.5	m
Tunnel cross-section	33.2	m2
Advance rate	10	m/day

Tunneling

End if 9yr tunnel	2034

Table 15 - CO2 emissions due to material use, electrical needs and tunnel operation.

CO2 emissions: Materials

Concrete			**Backfilling grout**		
Concrete lining width	0.3	m		0.1	m
concrete lining volume per day	64.1	m3		20.7	m3
density reinforced concrete	2.5	t/m3	density bentonite grout***	1.35	t/m3
CO2 emission factor concrete**	80.2	kCO2/t	CO2 emission factor bentonite grout****	422	kCO2/t
CO2 eq from concrete lining per day	13	tCO2/day		12	tCO2/day

***reference: https://www.sustainableconcrete.org.uk/Sustainable-Concrete/Performance-Indic* ****https://www.bentonitems.co.uk/wp-content/uploads/2020/08/Bentonite-MS-Ltd.pdf*

*****Carbon Emission Factors Identification and MeasurementModel Construction for Railway Construction Projects, Hu et al (2022)*

CO2 emissions: Electricity

TBM			
Excavated kWh/m	195.3	m	Peeling et al. (2016)
Daily consumption of 2 TBM	3906	kWh/day	
CO2 emission factor swiss electricity*	168	gCO2eq/kWh	https://app.electricitymaps.com/zone/CH
CO2 eq from TBM per day	0.7	tCO2eq/day	

Tunnel operation			
Electricity consumption tunnel operation	330	kWh/(m*year)	See chapter 10 Energy, 11.3GWh/year (Peeling et al., 2016; Tarada, 2018;)
CO2 emission factor swiss electricity*	168	gCO2eq/kWh	
	1899	tCO2eq/year	

Train operation		
E VAlp	163.3	kWh/run
Daily E Valp	4899	kWh/d
Yearly E Valp	1788135	kWh/yr
	300	tCO2eq/year